A Comparison of CAD Models and Experimental Results for Some Passive Microwave Circuits

Elias Ghafari

A Thesis

in

The Department

of

Electrical and Computer Engineering

Presented in Partial Fulfillment of the Requirements
For the Degree of Master of Applied Science in Electrical Engineering at
Concordia University
Montreal, Quebec, Canada

August 2006

Your file Votre référence
ISBN: 978-0-494-20745-1
Our file Notre référence
ISBN: 978-0-494-20745-1

Abstract

A Comparison of CAD Models and Experimental Results for Some Passive Microwave Circuits

Elias Ghafari. M.A.Sc.

Concordia University, 2006

Passive RF and microwave components printed on microstrip circuit boards are essential elements of microwave circuits. Creating approximate closed-form solutions for the electrical characteristics in terms of S-parameters for these components and finding the appropriate microwave simulator to produce reasonably accurate results can be a challenge. In this thesis, we go through the design, simulation and S-parameters bench measurements of four commonly used passive microwave components and compare their simulation results to their laboratory measurements results. The four circuits studied in this work are: Stepped-Impedance (*hi-Z, low-Z)* low pass filter, edge coupled-line band pass filter, 3-dB 90° hybrid and a rectangular patch antenna. The two simulation packages used to design these components are PUFF (from California Institute of Technology), and the student version of Serenade (from Ansoft). The results of the study conducted on all four components show that unlike PUFF, Serenade predicted more reasonable and comparable results to the bench measurements. It is worth mentioning that there are slight differences between the Serenade simulation results and their corresponding bench results, such as frequency shift, insertion loss and return loss, but are less significant than those obtained from PUFF.

ACKNOWLEDGMENT

I would like to thank my Supervisor Dr. Robert Paknys for his guidance throughout this work. I would also like to take the opportunity and thank Randy Snoeyink, my supervisor at Delphi Electronics and Safety and Dr. Korkut Yegin and Daniel Morris, my colleagues at Delphi for their support and help in making this work possible.

Elias Ghafari

TABLE OF CONTENTS

LIST OF FIGURES

LIST OF TABLES

CHAPTER 5:

1. INTRODUCTION

Wireless communications systems are essential nowadays and are commonly used in the vast majority of today's world communications networks. RF and microwave engineers are always faced with challenges in designing and modeling the RF and microwave components that make up the wireless communications systems. These components can be categorized into two major groups: the active components group which consists of low noise amplifiers (LNA), power amplifiers (PA), mixers, active attenuators, switches and active filters, and the passive components group which consists of couplers, transmission lines, filters, impedance matching networks and printed antennas. The design of microwave passive components often requires full electromagnetic modeling which can be time consuming and costly during the design stage. Therefore, rapid simulation methods and models that utilize closed-form approximations are preferred over full electromagnetic field solvers.

Often, electrical engineers go through multiple design cycles assuming that any available microwave simulation software can be used and will produce accurate results, not realizing that these tools have limited capabilities. The design of microwave components is challenging and requires an iterative process of simulations and bench measurements. The key factor in minimizing the number of iterations is to understand the capabilities and limitations of the simulation tools used in the design stage.

The most accessible simulation packages that are available to students and engineers are PUFF (developed by California Institute of Technology), and the student version of Serenade from Ansoft. The purpose of this thesis is to compare the ability of PUFF and

Serenade to match measured results and to gain experience in the design and fabrication of selected passive microwave circuits. In this thesis, we go through the design, simulation and bench measurements of four commonly used passive microwave components and compare their simulation results to their laboratory measurements results. The four circuits studied in this work are: Stepped-Impedance *(hi-Z, low-Z)* low pass filter, edge coupled-line band pass filter, 3-dB 90° hybrid, and a rectangular patch antenna. The circuits are fabricated on MCL-LX-67Y microstrip dielectric material with dielectric constant of ε_r=3.38, loss tangent of tanδ=0.0009 and material thickness of 0.787mm from Hitachi Chemical Co. In addition to designing these commonly used circuits, a comparative study of PUFF and Serenade is also presented.

Except for the patch antenna, two versions of each circuit were fabricated. In the "Serenade" version, transmission line parameters such as characteristic impedance and electrical length were converted to physical microstrip dimensions by using the appropriate design formulas. The dimensions were then used to fabricate the device, and as input data to the Serenade program. In contrast, the PUFF program is able to directly calculate the dimensional information from the electrical transmission line parameters. The "PUFF" versions of the circuits were fabricated by using this dimensional information directly. PUFF cannot model radiating structures so it was not used for the patch antenna design.

1.1 Literature Review

Microstrip transmission lines are essential elements of RF and microwave circuits. Analysis, modeling and design of microstrip transmission lines are important and critical

for any component development. Accounting for the parasitic effects from discontinuities in transmission lines is important and critical in obtaining accurate results. These discontinuities occur at open-ended transmission lines, a T-junction, a bend and a cross junction.

The analysis of microstrip transmission lines begins with quasi-TEM approximation. Yamashita [1] used variational methods to derive line capacitance and guide wavelengths for shielded microstrip lines. Numerical approximations and procedures of transmission lines properties of strip lines were first presented by Wheeler [2] and accurate models (closed-form approximations) were derived by Hammerstad and Jensen [3]. Also, a microstrip dispersion model was proposed and corroborated with measurements by Getsinger [4]. Microstrip line end effects and discontinuities were also studied [5–7].

The quasi-TEM approximations and dispersion analysis of microstrip lines as presented by G. Gonzalez [8] are reviewed in Chapter 2. Although the quasi-TEM analysis is simple, it is not rigorously accurate as the operating frequency of the microstrip line is increased. This is mainly because the quasi-TEM analysis neglects the hybrid nature of the guided modes in the microstrip transmission line which is also discussed in Chapter 2. To study the validity of those closed-form approximations, PUFF [9] and Serenade [10] are used to simulate the four passive components presented in this work. Learning to use microwave simulators involves extensive study and requires expensive resources in their making which make them substantially costly for students and engineers. PUFF and the student version of Serenade are two of the very few software tools that were made available for students and engineers. PUFF was originally developed for Caltech's microwave circuits course students and Ansoft made a *limited* version of Serenade

available for students. RF and microwave simulators are used to design these components and the accuracy of their models is extremely critical in ensuring realistic and accurate results. These two software tools are discussed in Chapter 3.

Although the simulation tools are vital in the design of microwave components, the physical characteristics of such components can only be determined by bench measurements. These measurements are usually done using a network analyzer. In this work, a network analyzer (8720ES) from Agilent Technologies is used to measure the characteristics of these components. The full 2-port calibration procedure of the Network Analyzer is presented in Chapter 4 [11].

The first component studied and designed in this thesis is the *stepped-impedance* low pass filter which is also known as *hi-Z, low-Z filter*. Consisting of alternating sections of high and low characteristic impedance lines, this form of filter is popular because of its relatively simple design. The filter's elements values and the attenuation values were obtained from the tables presented by Matthaei, Young and Jones [12]. The theory, design, simulation and measurements of the stepped-impedance low pass filter are presented and discussed in Chapter 5.

The second component studied and designed in this thesis is the edge-coupled band pass filter. This type of filter consists of coupled lines structures which are two identical transmission lines used as a coupled pair. When this type of structure is used, two orthogonal dominant modes are supported which are referred to as *even-* and *odd-* modes. Akhtarzad, Rowbotham and Johns [13] presented a design procedure which allows for the geometry of the coupled microstrip lines to be obtained from the even- and odd-mode impedances and uses single microstrip line geometry as an intermediate step. Garg and

Bahl [14] presented semi-empirical design equations for the even- and odd- mode characteristics such as capacitance and effective dielectric constant impedance and losses. Also, formulas derived from the computations of the even- and odd- mode capacitances and impedances, which are extremely useful for computer aided design (CAD) tools and optimization, are presented by Ramadan and Westgate [15]. The theory, design, simulation and measurements of the edge-coupled band pass filter are presented and discussed in Chapter 6.

The third component studied and designed in this thesis is the 3dB 90° hybrid which is also known as quadrature hybrid or branch-line coupler. This coupler is 3dB directional coupler that has 90° phase difference between the "through" and "coupled" ports. Reed and Wheeler [16] presented an analysis of four arm symmetrical networks such as branch-line couplers and hybrid rings. This analysis involves breaking an input wave into an even- and an odd- mode and the vector amplitude out to be computed from the sums and differences of the reflection or transmission coefficients for the two modes. The theory, design, simulation and measurements of the 3dB 90° hybrid are presented and discussed in Chapter 7.

The last component studied and designed in this thesis is the patch antenna, also known as the microstrip antenna. Patch antennas are rugged, lightweight, and low-cost antennas that are widely used in applications where size and weight are of prime concern. An accurate and numerically efficient transmission line model for the rectangular microstrip antenna was presented by Pues and Capelle [17]. Hammerstad [18] presented popular and practical approximate relations for the normalized extension of the length as a function of effective dielectric constant and width to length ratio. The theory, as

presented by Balanis [19], design, simulation and measurements of the microstrip rectangular patch antenna are presented and discussed in Chapter 8.

2. MICROSTRIP TRANSMISSION LINE THEORY

A microstrip line consists of a conductor of given width printed on a grounded dielectric substrate of relative permittivity ε_r as shown in Figure 2.1 [19].

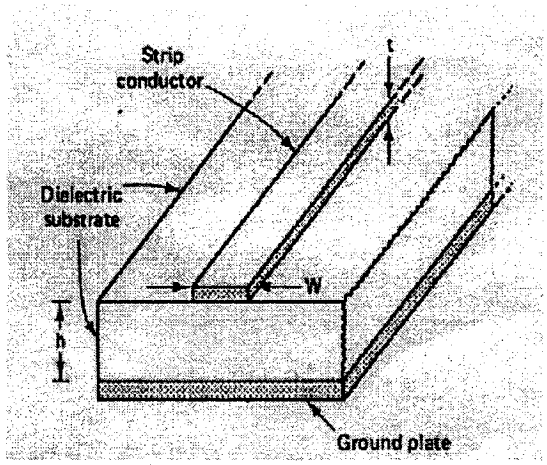

Figure 2.1: Microstrip geometry.

The quantities W and t are the width and thickness of the conductor strip, respectively; h is the thickness of the substrate.

As can be seen in Figure 2.2 [20], the dielectric material does not surround the conductor strip. Therefore, a microstrip line cannot sustain a pure transverse electromagnetic mode (TEM) of propagation, since the field lines are not entirely confined within the substrate.

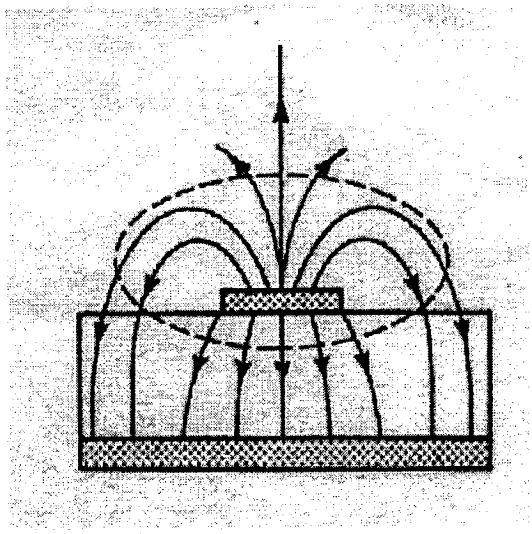

Figure 2.2: Field line geometry.

The field actually behaves as a hybrid TE-TM wave, and an exact analysis would prove irritably cumbersome and would yield little practical benefit compared to an approximate solution. Indeed, more often than not, the substrate is electrically thin (i.e., $h << \lambda$; in particular, $t/h < 0.005$) and most of the field lines are confined within the substrate, with only a few extending beyond it; thus, for all intents and purposes, a quasi-TEM approximation of the field lines is a satisfactory one, and relatively tractable static-TEM solutions can be readily applied. Nonetheless, the quasi-TEM approximation has limitations; in particular, the approximation is valid for lower microwave frequencies; operation at higher microwave frequencies would require a more exact approach. Since many practical applications satisfy the conditions for the quasi-TEM assumption, the approximate solutions are presented next.

2.1 The Quasi-TEM Model

In the vein of the static and quasi-static solutions, the phase velocity, propagation constant, line wavelength, and characteristic impedance as presented are expressed as [21]:

$$v_p = \frac{c}{\sqrt{\varepsilon_{eff}}} \tag{2.1.1a}$$

$$\beta = k_0\sqrt{\varepsilon_{eff}} \tag{2.1.1b}$$

$$\lambda = \frac{v_p}{f} = \frac{c}{f\sqrt{\varepsilon_{eff}}} = \frac{\lambda_0}{\sqrt{\varepsilon_{eff}}} \tag{2.1.1c}$$

$$Z_0 = \frac{1}{v_p C} \tag{2.1.1d}$$

where c is the speed of light and C is the capacitance per unit length.

In the instance of a conductor of negligible thickness (t/h < 0.005; unless otherwise specified, all results herein assume negligible thickness), the following set of relations may be used to determine the characteristic impedance:

$$Z_0 = \frac{60}{\sqrt{\varepsilon_{eff}}}\ln\left(8\frac{h}{W} + 0.25\frac{W}{h}\right),\ W/h \le 1 \tag{2.1.2a}$$

where

$$\varepsilon_{eff} = \frac{\varepsilon_r + 1}{2} + \frac{\varepsilon_r - 1}{2}\left[\left(1 + 12\frac{h}{W}\right)^{-1/2} + 0.04\left(1 - \frac{W}{h}\right)^2\right] \tag{2.1.2b}$$

and

$$Z_0 = \frac{120\pi / \sqrt{\varepsilon_{eff}}}{W/h + 1.393 + 0.667 \ln(W/h + 1.444)}, \quad W/h \geq 1 \tag{2.1.3a}$$

$$\varepsilon_{eff} = \frac{\varepsilon_r + 1}{2} + \frac{\varepsilon_r - 1}{2}\left(1 + 12\frac{h}{W}\right)^{-1/2}. \tag{2.1.3b}$$

Figure 2.3 [22] below is a plot of the characteristic impedance as a function of the aspect ratio.

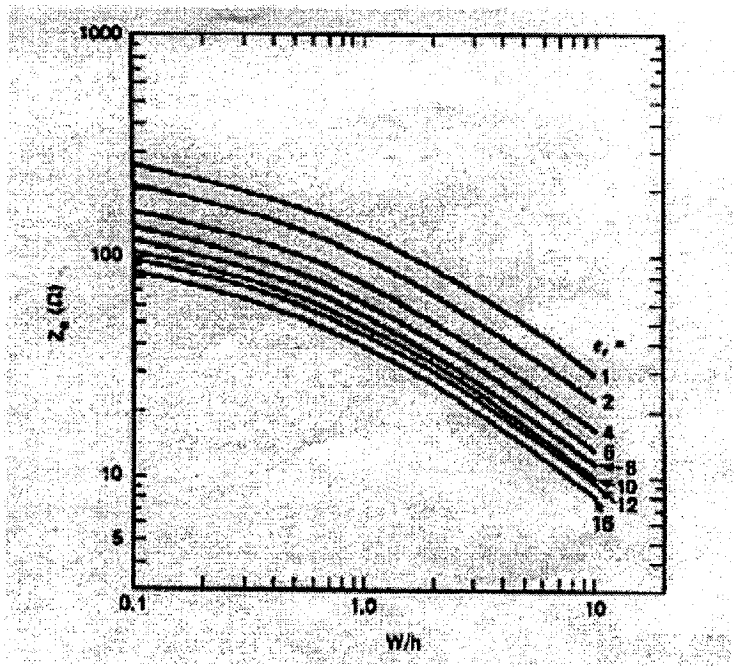

Figure 2.3: Characteristic impedance Z_0 in Ω, as a function of aspect ratio W/h. The dielectric constant ε_r is a parameter.

Further, it has been shown experimentally by Sobol [23] that the line wavelength is given within excellent approximation by the following expressions:

$$\lambda = \frac{\lambda_0}{\sqrt{\varepsilon_r}}\left[\frac{\varepsilon_r}{1+0.6(\varepsilon_r-1)(W/h)^{0.0297}}\right]^{1/2}, \; W/h < 0.6 \qquad (2.1.4a)$$

$$\lambda = \frac{\lambda_0}{\sqrt{\varepsilon_r}}\left[\frac{\varepsilon_r}{1+0.63(\varepsilon_r-1)(W/h)^{0.1255}}\right]^{1/2}, \; W/h \geq 0.6. \qquad (2.1.4b)$$

Figure 2.4 [24] is a plot of the normalized wavelength as a function of the aspect ratio.

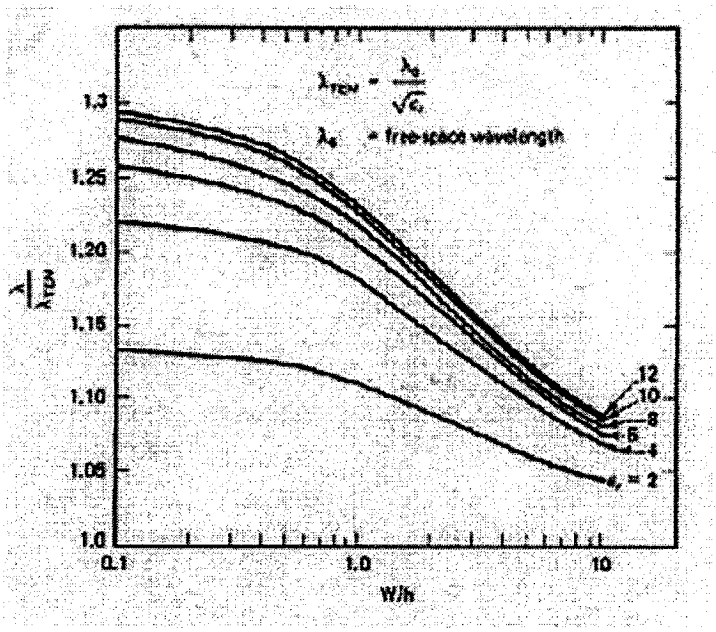

Figure 2.4: Normalized wavelength λ/λ_{TEM} as a function of aspect ratio W/h

Here, $\lambda_{TEM} = \lambda_0 / \sqrt{\varepsilon_r}$ where λ_0 is the free space wavelength.

The following expressions listed below can be used to determine the aspect ratio, given characteristic impedance and relative dielectric constant. These expressions are useful for design purposes:

$$\frac{W}{h} = \frac{8e^A}{e^{2A}-2}, \; W/h \leq 2 \qquad (2.1.5a)$$

$$\frac{W}{h}=\frac{2}{\pi}\left\{B-1-\ln(2B-1)+\frac{\varepsilon_r-1}{2\varepsilon_r}\left[\ln(B-1)+0.39-\frac{0.61}{\varepsilon_r}\right]\right\},\ W/h\geq 2 \qquad (2.1.5b)$$

where

$$A=\frac{Z_0}{60}\sqrt{\frac{\varepsilon_r+1}{2}}+\frac{\varepsilon_r-1}{\varepsilon_r+1}\left(0.23+\frac{0.11}{\varepsilon_r}\right) \qquad (2.1.6a)$$

$$B=\frac{377\pi}{2Z_0\sqrt{\varepsilon_r}}. \qquad (2.1.6b)$$

If more accurate design results are desired, equations 2.1.5 can be modified to take the strip conductor's thickness into consideration. The modified expressions are:

$$\frac{W_{eff}}{h}=\frac{W}{h}+\frac{t}{\pi h}\left(1+\ln\frac{4\pi W}{t}\right),\ \frac{W}{h}\leq\frac{1}{2\pi} \qquad (2.1.7a)$$

$$\frac{W_{eff}}{h}=\frac{W}{h}+\frac{t}{\pi h}\left(1+\ln\frac{2h}{t}\right),\ \frac{W}{h}\geq\frac{1}{2\pi}. \qquad (2.1.7b)$$

In the above equations, the aspect ratio *W/h* is obtained using equations 2.1.5, and then "corrected" for the effects of the conductor thickness through expressions 2.1.7; the corrected aspect ratio is expressed as W_{eff}/h, where W_{eff} is the *effective conductor width.* It should be noted that (2.1.7) could be employed only under these restrictions $t < h$ and $t < W/2$.

The attenuation resulting from dielectric loss is given by:

$$\alpha_d=\frac{k_0\varepsilon_r(\varepsilon_{eff}-1)\tan\delta}{2\sqrt{\varepsilon_{eff}}(\varepsilon_r-1)}Np/m \qquad (2.1.8)$$

where $\tan\delta$ is the dielectric loss tangent, and k_0 is the free-space wave number. The attenuation resulting from conductor loss is given by:

$$\alpha_c = \frac{R_S}{Z_0 W} Np/m \tag{2.1.9}$$

where $R_S = \sqrt{\omega\mu_0/2\sigma}$ is the conductor surface resistivity. By far, conductor loss outweighs dielectric loss for most choices of substrate.

2.2 Failure of the Quasi-TEM Model: The Effects of Higher Frequencies

As discussed earlier, operation at lower frequencies is one of the assumptions upon which the quasi-TEM model rests. At higher frequencies, the effective dielectric constant and the characteristic impedance become functions of frequency, as the microstrip line becomes dispersive.

Thus far, the terms "lower frequencies" and "higher frequencies" have been used to make the distinction between dispersive and non-dispersive behavior in the line; apart from the intuitive understanding they provide, however, they are of no quantitative value. The following expression provides the numerical equivalent to the above two terms; it specifies the threshold frequency, below which dispersion may be disregarded:

$$f_0(GHz) = 0.3\sqrt{\frac{Z_0}{h\sqrt{\varepsilon_r} - 1}} \tag{2.2.1}$$

where h is expressed in centimeters.

For the effective dielectric constant, the effects of dispersion are taken into account in the following expression:

$$\varepsilon_{eff}(f) = \varepsilon_r - \frac{\varepsilon_r - \varepsilon_{eff}}{1 + G(f/f_p)^2} \tag{2.2.2}$$

where f is expressed in GHz, and f_p and G are determined from

$$f_p = \frac{Z_0}{8\pi h} \tag{2.2.3a}$$

$$G = 0.6 + 0.009 Z_0 . \tag{2.2.3b}$$

Lastly, dispersion can be accounted for in the characteristic impedance via the following:

$$Z_0(f) = \frac{377h}{W_{eff}(f)\sqrt{\varepsilon_{eff}}} \tag{2.2.4}$$

where

$$W_{eff}(f) = W + \frac{W_{eff}(0) - W}{1 + (f / f_p)^2} \tag{2.2.5a}$$

with

$$W_{eff}(0) = \frac{377h}{Z_0(0)\sqrt{\varepsilon_{eff}(0)}} . \tag{2.2.5b}$$

The physical reason for dispersion is that at higher frequencies it is possible for the wave to zig-zag between the two conductors and behaves as a waveguide rather than a TEM transmission line.

3. SIMULATORS

3.1 Introduction

We will discuss in this chapter the two computer aided design (CAD) tools used in this thesis, PUFF developed by California Institute of Technology and the student version of Serenade offered by Ansoft.

3.2 PUFF

PUFF was originally created for the microwave course students at California Institute of Technology as an inexpensive and easy-to-use teaching tool. It was created as an alternative to expensive and hardly available to students software packages. PUFF is a scattering parameters and layout calculator which uses a relatively simple interactive schematic-capture type environment. PUFF computes the circuit's scattering parameters using a relatively fast and memory efficient algorithm called "*subnetwork growth*" [25]. It involves dividing the network under analysis to be solved into sub-circuits to further simplify the analysis and calculations. This technique was first described by Murray-Lasso [26] in 1969 and applied to scattering matrices by Monaco and Tiberio [27] in 1970. The calculations use small and dense scattering parameters and conversions to impedance or admittance matrices are unnecessary. Since microwave networks are characterized by scattering parameters, and if we want to analyze a microwave circuit in terms of an admittance matrix, we must first convert the s-parameters of the components to admittance matrices, then calculate for the admittance matrix of the entire network, and finally convert back to s-parameters. This entire matrix will have to be solved by

Gaussian elimination. This approach has an advantage of being easy to program, but it is relatively slow for microwave circuits analysis. Also, a matrix that represents a microwave circuit is fairly large and in some cases (such as branch-line couplers) contains a large number of zeroes (sparse matrix). In Gaussian elimination, most of the time would be spent multiplying, adding and storing zeroes, which is somewhat inefficient.

PUFF uses synthesis formulas to determine the circuit dimensions on the screen and in the artwork. The width W for the microstrip transmission line (*tline & qline*) is calculated in PUFF using Wheeler's equations [28, 29]. The width W for the stripline (*tline & qline*) is calculated using the equations given by Cohn's equations [30].

The width and separation of the coupled transmission lines (clines) are obtained by solving for the even and odd impedances Z^e and Z^o equations given by Akhtarzad, Rowbotham and Johns [31]. PUFF's main screen is shown in Figure 3.1 [32].

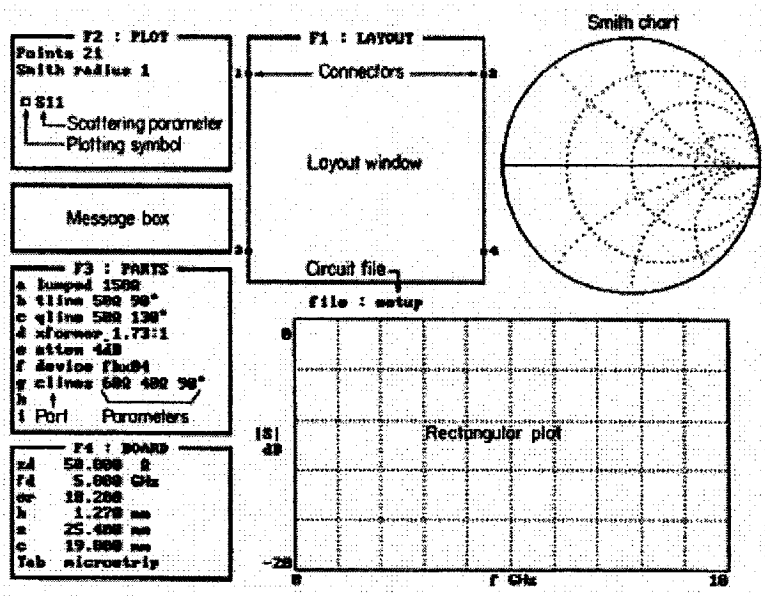

Figure 3.1: PUFF's main screen.

As can be seen in Figure 3.1, PUFF's main screen is divided into 3 groups of windows. The first group consists of 4 windows numbered F1 through F4. These windows are accessible by pressing the F1 through F4 computer keys and are used to create the circuit. These keys are always active. The second group of windows consists of the "Smith Chart" plot and the rectangular plot windows. These windows are used to plot the circuit's response. The third group of windows consists of the "Message" box, which is the command window used to save and read PUFF files. The first step of creating a circuit in PUFF is to define the circuit board parameters such as the design frequency, dielectric constant (εr), and height and PCB dimensions in the "**Board**" window (F4). The second step is to create the parts in the "**Parts**" window (F3). Once the parts are defined, the circuit can be created in the "**Layout**" window (F1) using the computer cursor keys. Then the plot parameters should be defined in the "**plot**" window (F2). Once all these steps are performed, the circuit is ready to be simulated and plotted in either time or frequency domain. In summary, the input parameters into PUFF are the electrical lengths and characteristic impedance of the transmission lines, and the output parameters are the physical width and length dimensions of these lines. Also, a full S-parameters (Sij) file can be obtained from PUFF.

3.3 Serenade

Serenade is a general purpose CAD package for performing high frequency circuits and system simulation and optimization. Super-Compact was the original company that developed Harmonica in the late 1970s. Ansoft purchased Super-Compact in the late 1990s and changed the name to Serenade for the RF circuit tool and Symphony for the

System tool. It is a powerful tool for synthesizing, analyzing and optimizing systems and circuits ranging from audio through microwave frequencies. Serenade's linear simulator uses highly efficient techniques such as sparse matrix methods, full nodal analysis and powerful modeling algorithms. It allows the user to simulate and analyze circuits composed of models from an extensive parts library. Serenade's schematic editor provides a graphical tool for creating schematic drawings, which are then converted into netlists and simulated with Harmonica for linear simulation. Serenade does not use any arbitrary solvers such as 2D, 2.5Dor 3D for the distributed components used in the RF circuit tool. The distributed elements are modeled using closed form equations. The microstrip transmission lines models use the frequency dependent solutions for microstrip lines as presented by Denlinger [33]. The theory enables one to obtain the frequency dependence of phase velocity and characteristic impedance and also to obtain the electromagnetic field quantities around the microstrip line. This theory utilizes a Fourier transform method in which the hybrid-mode solutions for the surface current at the substrate-air interface are summed to represent the fields caused by the current distribution that is finite only over the region occupied by the conducting strip.

Also, for the analysis of coplanar-type and microstrip-type structures, the Serenade models use a higher order solution of the spectral-domain approach as introduced by Mirshekar-Syahkal and Davies [34]. This approach uses Legendre polynomials as basis functions for fields having singularities near the edges which lead to fast convergence to the exact solution.

Serenade uses expressions derived and presented by Pucel, Masse and Hartwig [35] for the conductor loss in microstrip transmission lines. The formulas take into account the finite thickness of the strip conductor and apply to the mixed dielectric system.

The coupled microstrip lines models in Serenade use the quasi-static expressions and theory presented by Bryant and Weiss [36]. These models use a Fourier transform method to determine the dependence of the transmission parameters of the coupled microstrip lines on frequency. The difference between Serenade's student version and the full version is that the student version is limited to the number of components (30 components) that can be used in the schematic editor. The accuracy is the same however. In summary, the input parameters into Serenade are the electrical or physical lengths and widths of the transmission lines, and the output parameters are the S-parameters. The physical dimensions, coupling and characteristic impedance of these lines are not calculated by Serenade.

4. MEASUREMENTS OF S-PARAMETERS

The network analyzer used to measure the circuits studied in this thesis is the S-Parameter Network Analyzer model 8720ES by Agilent Technologies, which covers a wide frequency range from 50MHz to 20GHz. The Network Analyzer has to be calibrated to the proper frequency range before it can be used for measurements. Also, calibration is required to compensate for (*calibrate out*) the losses and phase delays introduced by the cables and connectors/adapters used in the setup. These losses, if not accounted for (in calibration), will introduce extra losses and phase delay to the real measurements values. Presented next is a detailed Network Analyzer full 2-port calibration procedure required before it can be used for measurements [37]. The Agilent documentation contains the information on calibration, but not in a step-by-step fashion. For convenience, the full 2-port calibration procedure is presented next.

4.1 Network Analyzer (8720ES series) Full 2-Port Calibration Procedure

Performing a full 2-port calibration procedure using a 3.5 mm Agilent Calibration Kit (model 85052D) is as follows:

1) Switch the Network Analyzer power switch on
2) Perform the Preset function (green button)
3) Under the Stimulus Menu, select the Sweep Setup function and perform the following steps:
    a. Select the Sweep Type Menu from the Sweep Setup menu
        i. Select the Sweep Time function and set to Auto

b. Select the Lin Freq Swept (Linear Frequency)

c. Select the Start Frequency function (Start button) and set the frequency to 50 MHz

d. Select the Stop Frequency function (Stop button) and set the frequency to 4.0 GHz.

e. Select the Number of Points function and set to 801 points

f. Select the Coupled Ch function and set to On

g. Select the Power menu and perform the following steps:

   i. Set the Power Range to Manual

   ii. Select the Power Ranges menu

   iii. Select the –15dBm to +5dBm function

   iv. Set the power level to 0dBm

Note: If –15dBm to +5dBm power level option is not available, choose the largest range available from the Network Analyzer and set the value output power value to the largest value available without going UNLEVELED

4) Select the Marker Menu

   a. Select Marker1 and set it's value to the desired frequency (3.0 GHz in this application)

5) Select the Marker Function Menu

   a. Select the Marker Mode Menu

   b. Select Continuous function (should be underlined after it is selected)

   c. Select Markers Coupled function (should be underlined after it is selected)

d. Select Smith Mkr Menu

i. Select R + jX Mkr (should be underlined after it is selected)

6) Perform the following steps under the Display / Display menu:

a. Select the Display Data function

b. Select the Dual/Quad setup mode

i. Under the Split Display function, select the 4X option (to get the quad display on Network Analyzer screen)

ii. Set Dual channel to On mode

iii. Set Aux Cannel to On mode

NOTE: At this stage, if you do not obtain a quad display, toggle the Channel buttons between all 4 channels in the Active Channel menu located near the top right side of the screen until the quad display is achieved. The quad display shows all 4 S-parameters graphs.

7) Under the Measure Menu, select the S-Parameter Menu and perform the following steps:

a. Select Channel 1 from the Active Channel Menu

i. From the Measure menu, select S11.

ii. From the Format Menu, select the Smith Chart format.

b. Select Channel 2 from the Active Channel Menu

i. From the Measure menu, select S22.

ii. From the Format Menu, select the Smith Chart format.

c. Select Channel 3 from the Active Channel Menu

i. From the Measure menu, select S21.

ii. From the Format Menu, select the Log/Mag format.

d. Select Channel 4 from the Active Channel Menu

i. From the Measure Menu, select S12

ii. From the Format Menu, select the Log/Mag format

8) Select Ch 3 (Channel 3) from the Active Channel Menu

9) Connect the N-Type connector (with the female 3.5mm connector on the other end) of the "short" high frequency coaxial cable to Network Analyzer Port 1

10) Connect the N-Type connector (with the male 3.5mm connector on the other end) of the second "short" high frequency cable to Network Analyzer Port 2

11) Calibration Kit, model number 85052D (male and female standards), is needed to perform the full 2-port calibration. Select the Cal function located on the analyzer front panel and perform the following steps:

a. Select the Correction Factor function and set to On mode

b. Select the Cal Kit Menu

c. Select the 3.5 mm, 85052 from the Select Cal Kit menu

d. Select the Cal Menu and choose the Full 2-Port Calibration under the Calibrate Menu

e. Select Reflection Menu

f. Perform the following three steps under the Forward Menu

i. Connect the male Open 3.5 mm standard (from Cal Kit) to the female 3.5mm end of the coaxial cable connected to Network Analyzer port 1 and select the Open button. Wait until you hear a

beep before you remove it (pull down menu will be underlined **OPEN**)

ii. Connect the male Short 3.5 mm standard (from Cal Kit) to the female 3.5mm end of the coaxial cable connected to Network Analyzer port 1 and select the Short button. Wait until you hear a beep before you remove it (pull down menu will be underlined **SHORT**)

iii. Connect the male load (Broadband) 3.5 mm standard (from Cal Kit) to the female 3.5mm end of the coaxial cable connected to Network Analyzer port 1 and select the load (broadband) button (pull down menu will be underlined **Broadband**). Select Done Loads. Wait until you hear a beep before you proceed with the rest of the calibration.

g. Perform the following three steps under the Reverse Menu

i. Connect the female Open 3.5 mm standard (from Cal Kit) to the male 3.5mm end of the coaxial cable connected to Network Analyzer port 2 and select the Open button. Wait until you hear a beep before you remove it (will be underlined **OPEN**)

ii. Connect the female Short 3.5 mm standard (from Cal Kit) to the male 3.5mm end of the coaxial cable connected to Network Analyzer port 2 and select the Short button. Wait until you hear a beep before you remove it (will be underlined **SHORT**)

iii. Connect the female load (Broadband) 3.5 mm standard (from Cal Kit) to the male 3.5mm end of the coaxial cable connected to Network Analyzer port 2 and select the load (broadband) button (will be underlined **Broadband**). Select Done Loads. Wait until you hear a beep before you proceed with the rest of the calibration.

h. Select the Standards Done function

i. Select the Isolation menu, and select the Omit Isolation soft key

j. Connect the two 3.5 mm (male and female ends of the cables) connectors together and select the Transmission menu and perform a Both Forward and Reverse Thru.

k. Wait until you hear the beep sound and select the *Done* 2-Port Calibration function and wait until the analyzer computes the S-Parameters coefficients.

l. Perform a "*double check*" procedure:

   i. Connect the two 3.5mm coaxial cable ends together.

   ii. Select Ch 3 from the Active Channel Menu and observe the display marker value (which is the insertion loss value). This number should be very close to zero (in the ~0.05 dB range)

   iii. Select Scale/Ref function

      1. Select Reference Value function and set it to 0dB

      2. Select the Marker → Reference function

   iv. Select Format menu

   v. Select Delay function

vi. Observe the marker value for the electrical delay. It should be a number in the format (xx.xx ps) in the range of 10.00 fs (very close to zero).

vii. Disconnect the two cables

To "calibrate out" the effects/contribution (from the open ended capacitor/fringing effects) of the board mount SMA connectors used on the circuit boards for testing, perform the following steps:

12) Connect the "Male 3.5mm" connector to the female coaxial connector end (cable connected to Network Analyzer Port 1). Select Ch 1, and monitor the active marker's value. The connector's "open-ended fringing effects" will add delay to the actual reading. From the Scale/Ref menu, select the Electrical Delay function and adjust the "Dial Knob" on the Network Analyzer front panel to get a "perfect" open circuit on the Smith Chart display (Ch 1).

13) Connect the "Female 3.5mm" connector to the male coaxial connector end (cable connected to Network Analyzer Port 2). Select Ch 2 and monitor the active marker's value. The connector's "open-ended fringing effects" will add delay to the actual reading. From the Format menu, select the Electrical Delay function and adjust the "Dial Knob" on the Network Analyzer front panel to get a "perfect" open circuit on the Smith Chart display (Ch 2).

To compensate for the connectors' insertion loss, solder a male and a female board mount connectors back-to-back (to obtain a male-female SMA adapter), connect the assembly to both ends of the Network Analyzer cables and perform the following step:

14) Select Ch 3 from the Active Channel Menu (S21)

15) Take note of the insertion loss number due to the hand-made SMA male-female adapter added to the cables. This number will be divided by 2 to obtain the insertion loss due to each individual connector. This number will be added to the measured DUT insertion loss to obtain the actual insertion loss.

16) Select the Save/Recall menu and select the Save State function to save the calibration parameters. Take note of the registry number (in this format Reg xx) for future recall for the cable harnesses screening procedure.

Note: To avoid measurements errors, the same high frequency coaxial cables and adapters used in the calibration procedure should be used during measurements. If any changes to the original setup are required, it is recommended that a new full 2-port calibration procedure be performed.

Please note that the 3.5 mm connectors used in the calibration kit and the high frequency coaxial cables are equivalent to the SMA connectors used on the circuit boards under test. The difference between the two types is that the 3.5 mm connector's core is made from air dielectric ($\epsilon r = 1$) and the SMA connector's core is made from Teflon dielectric (typically $\epsilon r = 2.2$). For this reason, the SMA connector introduces extra insertion loss than the 3.5 mm connector.

5. STEPPED-IMPEDANCE LOW-PASS FILTERS

We start our discussion with one of the circuits involved in the experimental work of this thesis: the Stepped-Impedance Low-Pass Filters. Firstly, we present the theoretical part of LPFs. Secondly, we discuss the design procedure stage. Thirdly, simulation and bench measurements and results are presented. And lastly, we conclude with discussions and conclusions between simulation and bench results.

5.1 Theory

Stepped-impedance filters, otherwise known as *hi-Z, low-Z filters*, are relatively simple, off-the-shelf implementation of low-pass filters for microstrip circuits. Consisting of alternating sections of high and low characteristic impedance lines, this form of filter is popular because of its simple design; although not as precise in performance as other approaches because of approximations involved, this design is nonetheless an excellent solution for applications where a sharp cutoff is not of prime importance. The approximate T-equivalent circuit for a length of line with $\beta\ell < \pi/2$ is illustrated in Figure 5.1(a) [38].

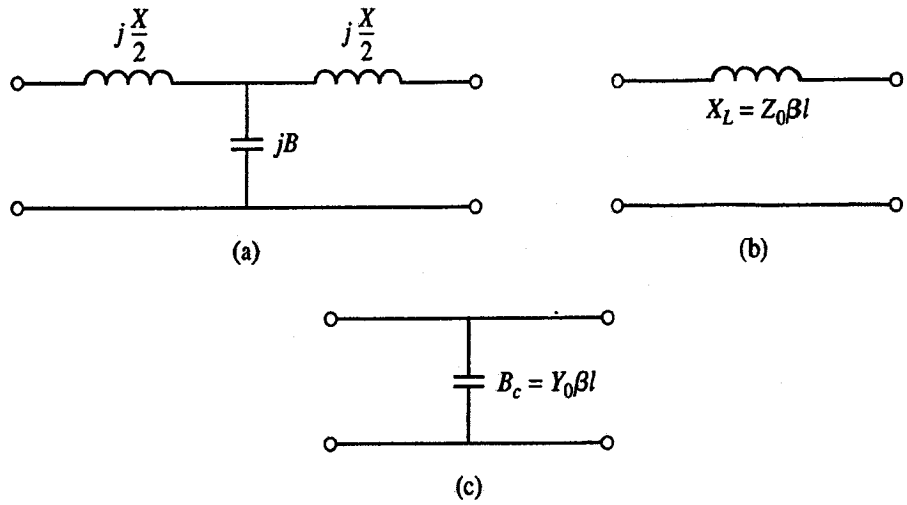

Figure 5.1: Approximate equivalent circuits for short sections of transmission lines. (a) T-equivalent circuit for a line with $\beta l < \pi/2$. (b) Equivalent circuit for a line with small βl and large Z_0. (c) Equivalent circuit for a line with small βl and small Z_0.

The component values are given by

$$\frac{X}{2} = Z_0 \tan\left(\frac{\beta\ell}{2}\right) \tag{5.1.1a}$$

$$B = \frac{1}{Z_0}\sin\beta\ell \ . \tag{5.1.1b}$$

From the generic line of Figure 5.1(a), a high-impedance section for the stepped-impedance design can be obtained by assuming a short line ($\beta l < \pi/4$) and a large characteristic impedance; applying these constraints on (5.1.1a) and (5.1.1b) yields

$$X \approx Z_0\beta\ell \tag{5.1.2a}$$

$$B \approx 0 . \tag{5.1.2b}$$

and results in Figure 5.1 (b) [39]. Similarly, a low-impedance section for the stepped-impedance design can be obtained by assuming a short line ($\beta l < \pi/4$) and a large characteristic impedance; applying these constraints on (5.1.1a) and (5.1.1b) yields

$$X \approx 0 \tag{5.1.3a}$$

$$B \approx Y_0 \beta \ell . \tag{5.1.3b}$$

and results in Figure 5.1(c) [40].

In short, "...the series inductors of a low-pass prototype can be replaced with high-impedance line sections ($Z_0 = Z_h$), and the shunt capacitors can be replaced with low-impedance line sections ($Z_0 = Z_l$)" [41]. The characteristic impedances Z_h and Z_l are set to the highest and lowest possible values, respectively, so as to maximize the ratio Z_h / Z_l; the actual electrical lengths are given by

$$\beta \ell = \frac{L R_0}{Z_h} \tag{5.1.4a}$$

$$\beta \ell = \frac{C Z_l}{R_0} . \tag{5.1.4b}$$

where (5.1.4a) applies to a high-impedance section, and (5.1.4b) applies to a low-impedance section. R_0 is the filter impedance, and L and C are the low-pass prototype normalized element values. The normalized values for maximally flat, 0.5 dB ripple, 3.0 dB ripple, and maximally flat time delay low-pass prototypes are listed in Tables 5.1, 5.2, 5.3, and 5.4 on the following pages, respectively (for further detail on these tables, refer to [42, 43]).

N	g_1	g_2	g_3	g_4	g_5	g_6	g_7	g_8	g_9	g_{10}	g_{11}
1	2.0000	1.0000									
2	1.4142	1.4142	1.0000								
3	1.0000	2.0000	1.0000	1.0000							
4	0.7654	1.8478	1.8478	0.7654	1.0000						
5	0.6180	1.6180	2.0000	1.6180	0.6180	1.0000					
6	0.5176	1.4142	1.9318	1.9318	1.4142	0.5176	1.0000				
7	0.4450	1.2470	1.8019	2.0000	1.8019	1.2470	0.4450	1.0000			
8	0.3902	1.1111	1.6629	1.9615	1.9615	1.6629	1.1111	0.3902	1.0000		
9	0.3473	1.0000	1.5321	1.8794	2.0000	1.8794	1.5321	1.0000	0.3473	1.0000	
10	0.3129	0.9080	1.4142	1.7820	1.9754	1.9754	1.7820	1.4142	0.9080	0.3129	1.0000

Table 5.1: Element Values for Maximally Flat Low-Pass Filter Prototypes (g0 =1, ωc=1, N=1 to 10).

N	g_1	g_2	g_3	g_4	g_5	g_6	g_7	g_8	g_9	g_{10}	g_{11}
1	0.6986	1.0000									
2	1.4029	0.7071	1.9841								
3	1.5963	1.0967	1.5963	1.0000							
4	1.6703	1.1926	2.3661	0.8419	1.9841						
5	1.7058	1.2296	2.5408	1.2296	1.7058	1.0000					
6	1.7254	1.2479	2.6064	1.3137	2.4758	0.8696	1.9841				
7	1.7372	1.2583	2.6381	1.3444	2.6381	1.2583	1.7372	1.000			
8	1.7451	1.2647	2.6564	1.3590	2.6964	1.3389	2.5093	0.8796	1.9841		
9	1.7504	1.2690	2.6678	1.3673	2.7239	1.3673	2.6678	1.2690	1.7504	1.0000	
10	1.7543	1.2721	2.6754	1.3725	2.7392	1.3806	2.7231	1.3485	2.5239	0.8842	1.9841

Table 5.2: Element Values for 0.5 dB Ripple Low-Pass Filter Prototypes (g0 =1, ωc=1, N=1 to 10).

N	g_1	g_2	g_3	g_4	g_5	g_6	g_7	g_8	g_9	g_{10}	g_{11}
1	1.9953	1.0000									
2	3.1013	0.5339	5.8095								
3	3.3487	0.7117	3.3487	1.0000							
4	3.4389	0.7483	4.3471	0.5920	5.8095						
5	3.4817	0.7618	4.5381	0.7618	3.4817	1.0000					
6	3.5045	0.7685	4.6061	0.7929	4.4641	0.6033	5.8095				
7	3.5182	0.7723	4.6386	0.8039	4.6386	0.7723	3.5182	1.0000			
8	3.5277	0.7745	4.6575	0.8089	4.6990	0.8018	4.4990	0.6073	5.8095		
9	3.5340	0.7760	4.6692	0.8118	4.7272	0.8118	4.6692	0.7760	3.5340	1.0000	
10	3.5384	0.7771	4.6768	0.8136	4.7425	0.8164	4.7260	0.8051	4.5142	0.6091	5.8095

Table 5.3: Element Values for 3.0 dB Ripple Low-Pass Filter Prototypes (g0 =1, ωc=1, N=1 to 10).

N	g_1	g_2	g_3	g_4	g_5	g_6	g_7	g_8	g_9	g_{10}	g_{11}
1	2.0000	1.0000									
2	1.5774	0.4226	1.0000								
3	1.2550	0.5528	0.1922	1.0000							
4	1.0598	0.5116	0.3181	0.1104	1.0000						
5	0.9303	0.4577	0.3312	0.2090	0.0718	1.0000					
6	0.8377	0.4116	0.3158	0.2364	0.1480	0.0505	1.0000				
7	0.7677	0.3744	0.2944	0.2378	0.1778	0.1104	0.0375	1.0000			
8	0.7125	0.3446	0.2735	0.2297	0.1867	0.1387	0.0855	0.0289	1.0000		
9	0.6678	0.3203	0.2547	0.2184	0.1859	0.1506	0.1111	0.0682	0.0230	1.0000	
10	0.6305	0.3002	0.2384	0.2066	0.1808	0.1539	0.1240	0.0911	0.0557	0.0187	1.0000

Table 5.4: Element Values for Maximally Flat Time Delay Low-Pass Filter Prototypes (g0 =1, ωc=1, N=1 to 10).

Along with the above tables, it is necessary to determine the filter order or size. This is usually dictated by the specifications of the insertion loss in the stopband of the filter.

Figure 5.2 [44] is used to determine the frequency at which specific amount of attenuation is required in the stopband for a specific filter order (for maximum N=10).

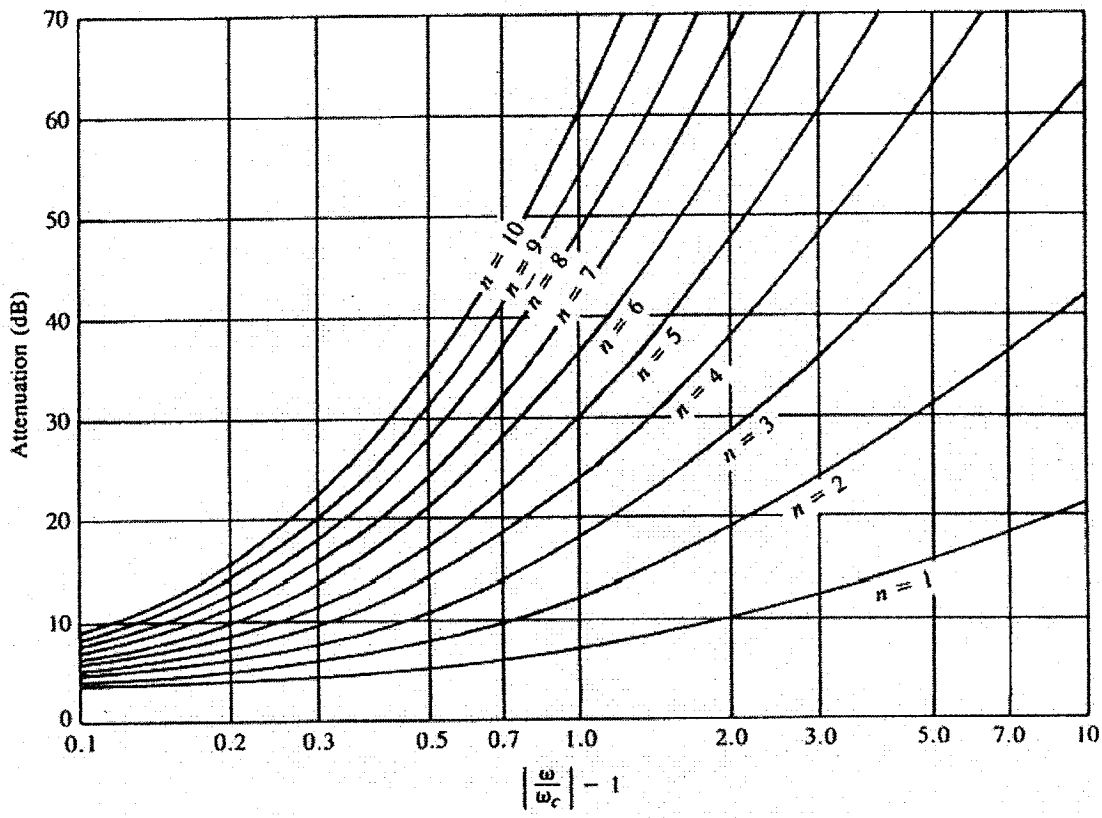

Figure 5.2: Attenuation versus normalized frequency for maximally flat filter prototypes.

5.2 Design

The design stage begins with determining, defining and understanding the requirements of the circuit under design. The design requirements for this LPF are summarized below:

Filter type: Maximally Flat Low Pass Filter,

Number of sections: N=5,

Cutoff Frequency (f_c) = 3GHz,

Attenuation: 30dB @ 6GHz,

The first step of the design procedure for the stepped-impedance LPF is to choose the appropriate values for both the low-impedance "Z_l" and high-impedance "Z_h" sections. Since the LPF will be printed on a 0.031" thick, 3.38 dielectric constant substrate, and for design constraints for minimum trace widths, we determined that "Z_h" to be 125Ω which yields a trace width of 0.01507", which is a reasonable trace width to be realized on this substrate material. Also, we chose 10Ω for "Z_l" which gives a trace width of 0.5095".

Next, using the 'n=5' curve and attenuation value of 30dB in Figure 5.2, we read off the value: $\left|\frac{\omega}{\omega_c}\right| - 1 = 1$.

From this equation and cutoff frequency (f_c) of 3GHz (and $\omega=2\pi f$), we calculate f to be 6GHz at which we get 30dB attenuation.

From Table 5.1 for a maximally flat LPF and using the filter order N=5, we read off element values (g_n) of:

$g_1 = 0.6180 = C1$,

$g_2 = 1.6180 = L2$,

$g_3 = 2.0 = C3$,

$g_4 = 1.6180 = L4$,

$g_5 = 0.6180 = C5$,

$g_6 = 1.0$.

The filter topology is a 'LC' ladder circuit that starts with a shunt capacitor 'C1' followed by a series inductor 'L2' as shown in Figure 5.3:

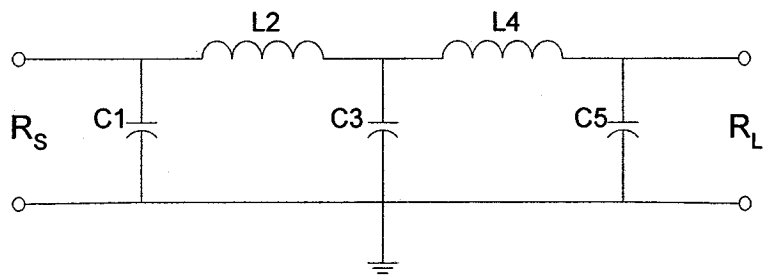

Figure 5.3: Low-pass maximally flat filter ladder circuit.

Next, using equations (5.1.4a) and (5.1.4b), which are $\beta\ell = \frac{LR_0}{Z_h}$ for the inductors and $\beta\ell = \frac{CZ_l}{R_0}$ for the capacitors, and the element values g_n's, we can determine the filter's transmission lines electrical lengths, βl's, to obtain the "printed" filter topology shown in Figure 5.4.

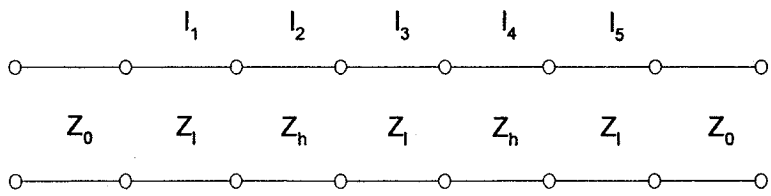

Figure 5.4: Stepped impedance implementation for the low-pass filter.

Next, the transmission lines lengths and widths are calculated as follows:

$$\beta l_1 = C1\frac{Z_l}{R_0} = 0.6180\frac{10}{50} = 7.08°@10\Omega \rightarrow w_1 = 0.5095", l_1 = 0.05488",$$

$$\beta l_2 = L2\frac{R_0}{Z_h} = 1.6180\frac{50}{125} = 37.082°@125\Omega \rightarrow w_2 = 0.01507", l_2 = 0.3104",$$

$$\beta l_3 = C3\frac{Z_l}{R_0} = 2.0\frac{10}{50} = 22.918°@10\Omega \rightarrow w_3 = 0.5095", l_3 = 0.17764",$$

$$\beta l_4 = L4\frac{R_0}{Z_h} = 1.6180\frac{50}{125} = 37.082°@125\Omega \rightarrow w_4 = 0.01507", l_4 = 0.3104",$$

$$\beta l_5 = C5\frac{Z_l}{R_0} = 0.6180\frac{10}{50} = 7.08°@10\Omega \rightarrow w_5 = 0.5095", l_5 = 0.05488".$$

The above values are used for the transmission lines widths and lengths in the Serenade simulator and to create the "Serenade" printed stepped-impedance low-pass filter, which will be presented and discussed next.

5.3 Simulations

Presented next in this chapter are the simulation results of the Stepped-Impedance LPF from both simulators, PUFF and Serenade.

5.3.1 PUFF Simulation Results:

The widths (w_n) and lengths (l_n) values of the low-impedance "Z_l" and high-impedance "Z_h" sections obtained in section 5.2 are used to obtain the "*ideal*" transmission lines (*tline*) dimensions (shown below) in PUFF to get the circuit and response shown in Figure 5.5:

$L_a = 0.0437$", $W_a = 0.558$",

$L_b = 0.2618$", $W_b = 0.0098$",

$L_c = 0.1413$", $W_c = 0.5586$".

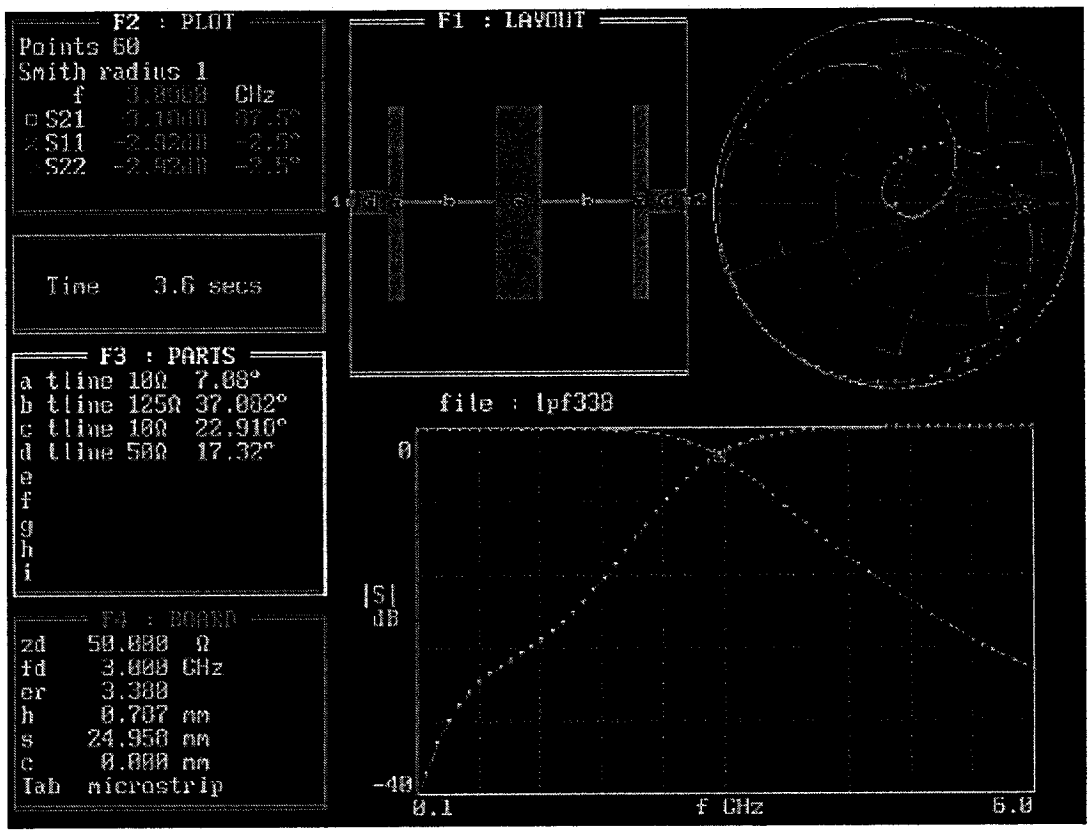

Figure 5.5: PUFF's "*Ideal*" transmission line (*tline*) model for LPF.

The marker in the above display is placed at 3.0GHz (the design frequency, f_c). As can be seen, the insertion loss of the LPF (S21) is -3.10dB and the input and output return loss (S11) and (S22) are both at -2.92dB. Moreover, it can be seen from the above graph that the attenuation (S21) at 6GHz is approximately 26dB, which is very close to the design specification (30dB).

Also in PUFF, using the "*advanced*" transmission line model (*tline!*) to account for losses in the transmission lines and to account for dependency of both the effective dielectric constant and impedance on frequency, we get:

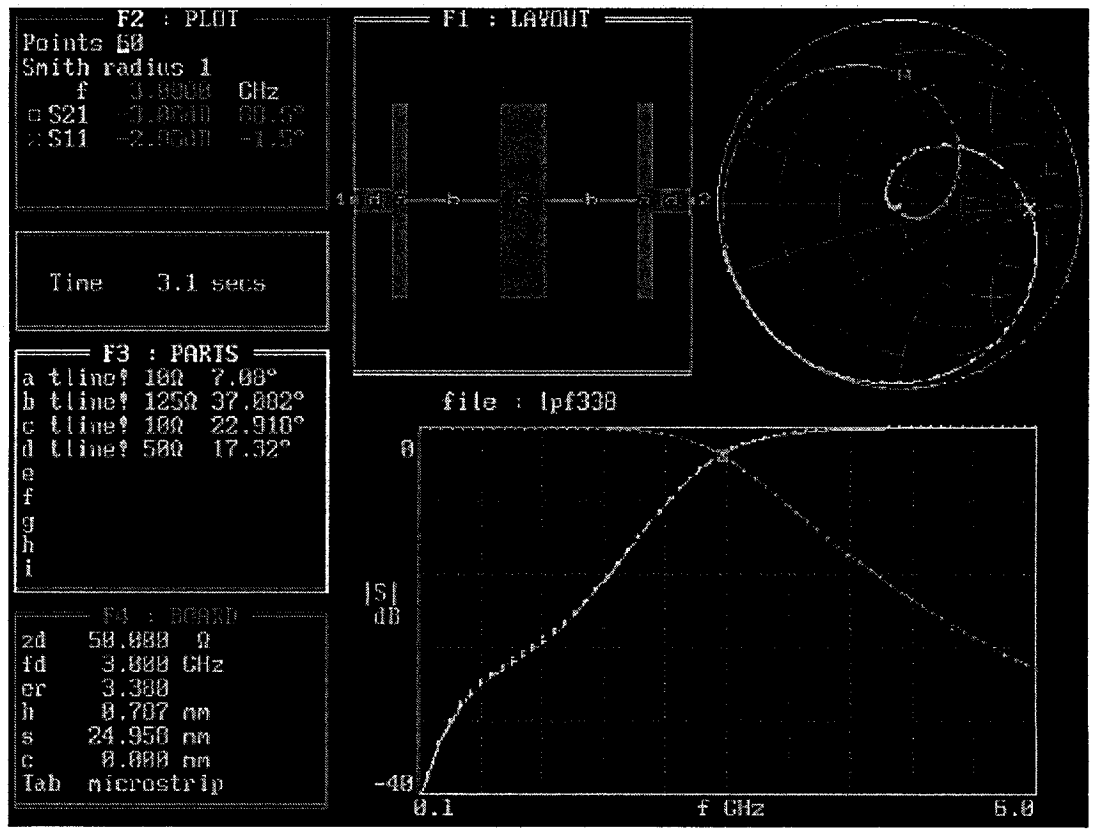

Figure 5.6: PUFF's "*advanced*" transmission line (*tline!*) model for LPF.

The marker in the above graph is also placed at 3.0GHz. As can be seen, the insertion loss of the LPF (S21) is -3.06dB and the input and output return loss (S11) and (S22) are both at -2.96dB. Also, it can be seen from the above graph that the insertion loss (S21) at 6GHz is approximately 26dB, which is very close to the design specification (30dB).

Please note that the results in both cases ("*ideal*" and "*advanced*") are very similar to each other for both input return loss (S11) and insertion loss (S21) as illustrated in Figure 5.7 and Figure5.8 respectively.

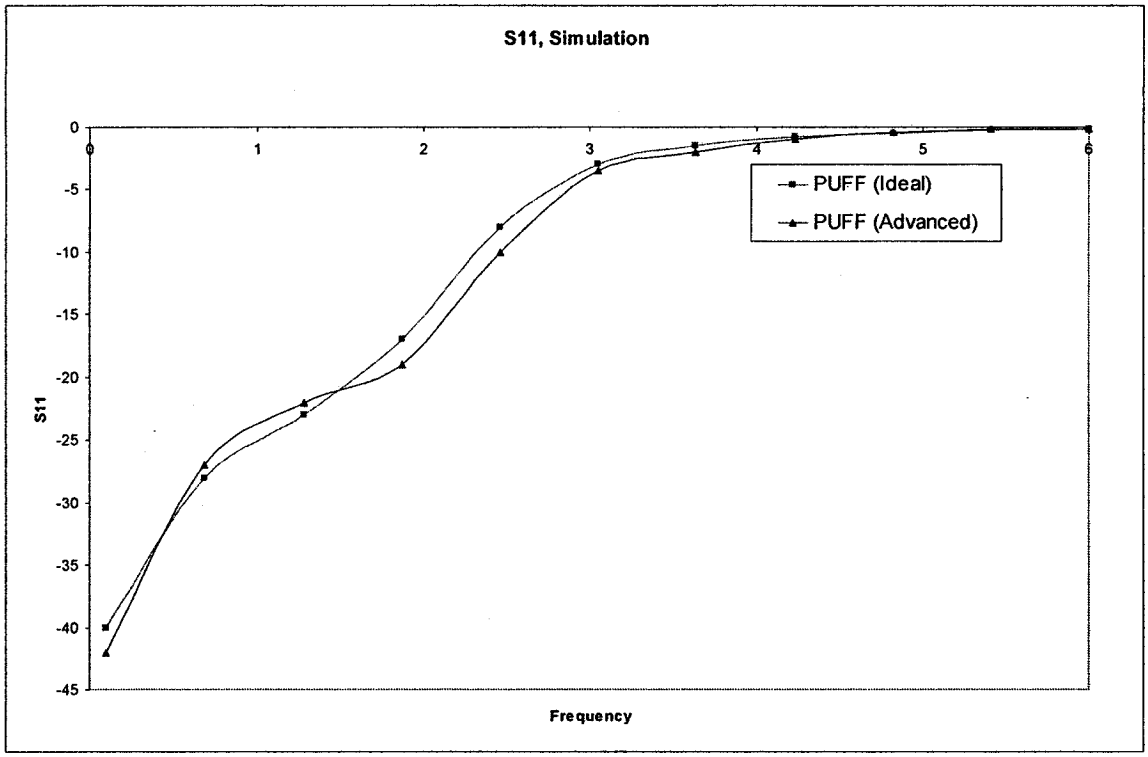

Figure 5.7: PUFF's (S11) comparison between "*Ideal*" and "*Advanced*" LPF models.

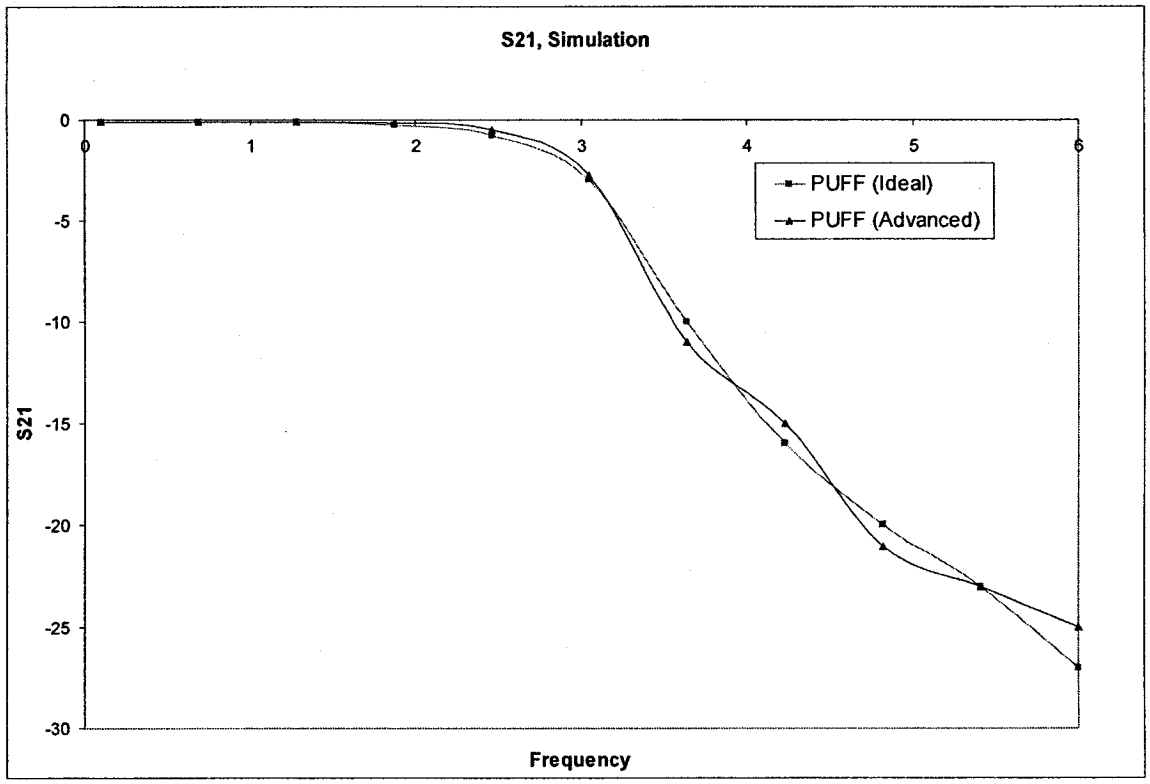

Figure 5.8: PUFF's (S21) comparison between "*Ideal*" and "*Advanced*" LPF models.

It is clear from Fig. 5.7 and Fig. 5.8 that both the "*ideal*" and the "*advanced*" models are extremely close to each other, both S11 and S21. For this reason, only the circuit obtained using the "*advanced*" LPF model will be analyzed on the bench. The analysis and comparisons will be discussed in Section 5.5.

5.3.2 Serenade Simulation Results:

Using the same design parameters and the LPFs' line lengths and widths obtained from the design equations in section 5.2, we obtain from Serenade the input and output return loss (S11) and (S22) (Figure 5.9):

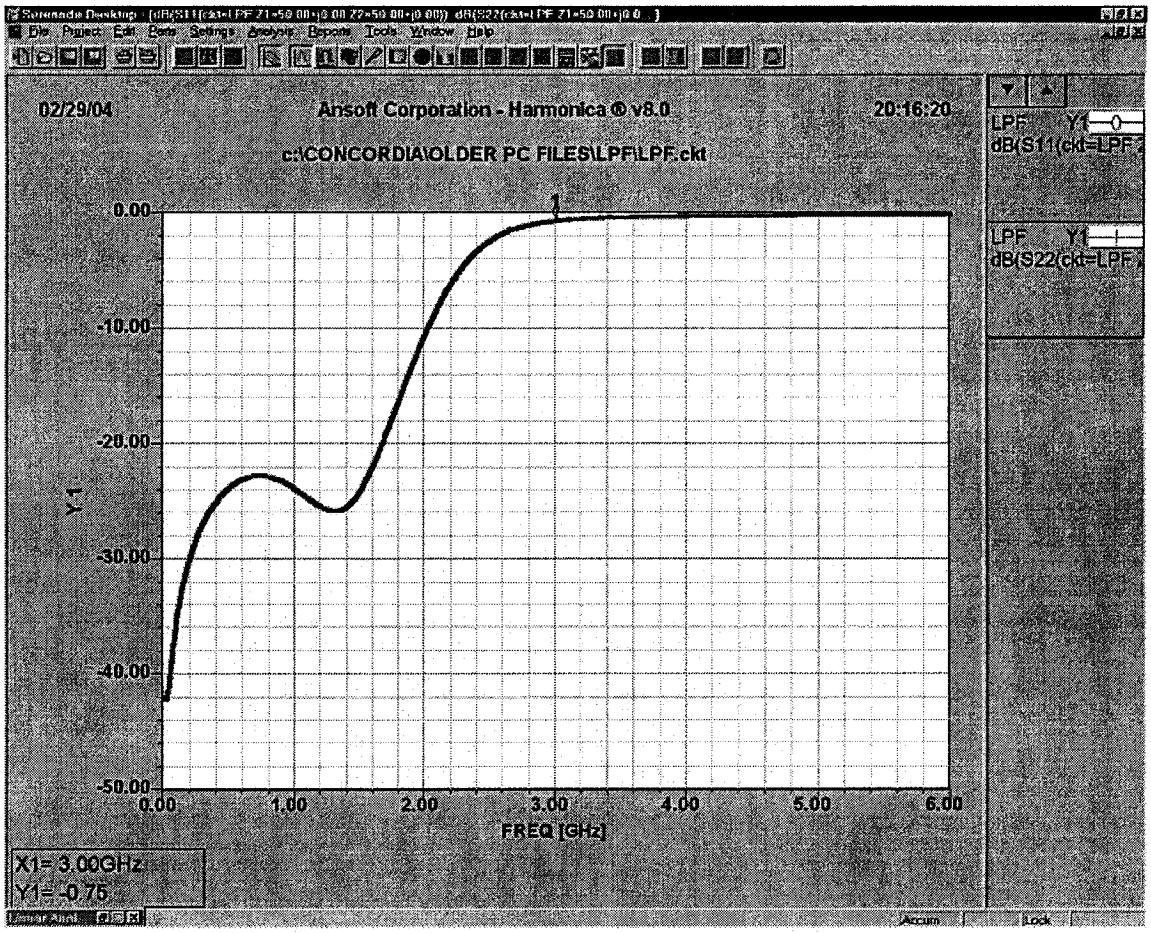

Figure 5.9: Serenade's Input and Output Return Loss (S11, S22) for LPF.

and the LPF's Insertion loss (S21) (Figure 5.10):

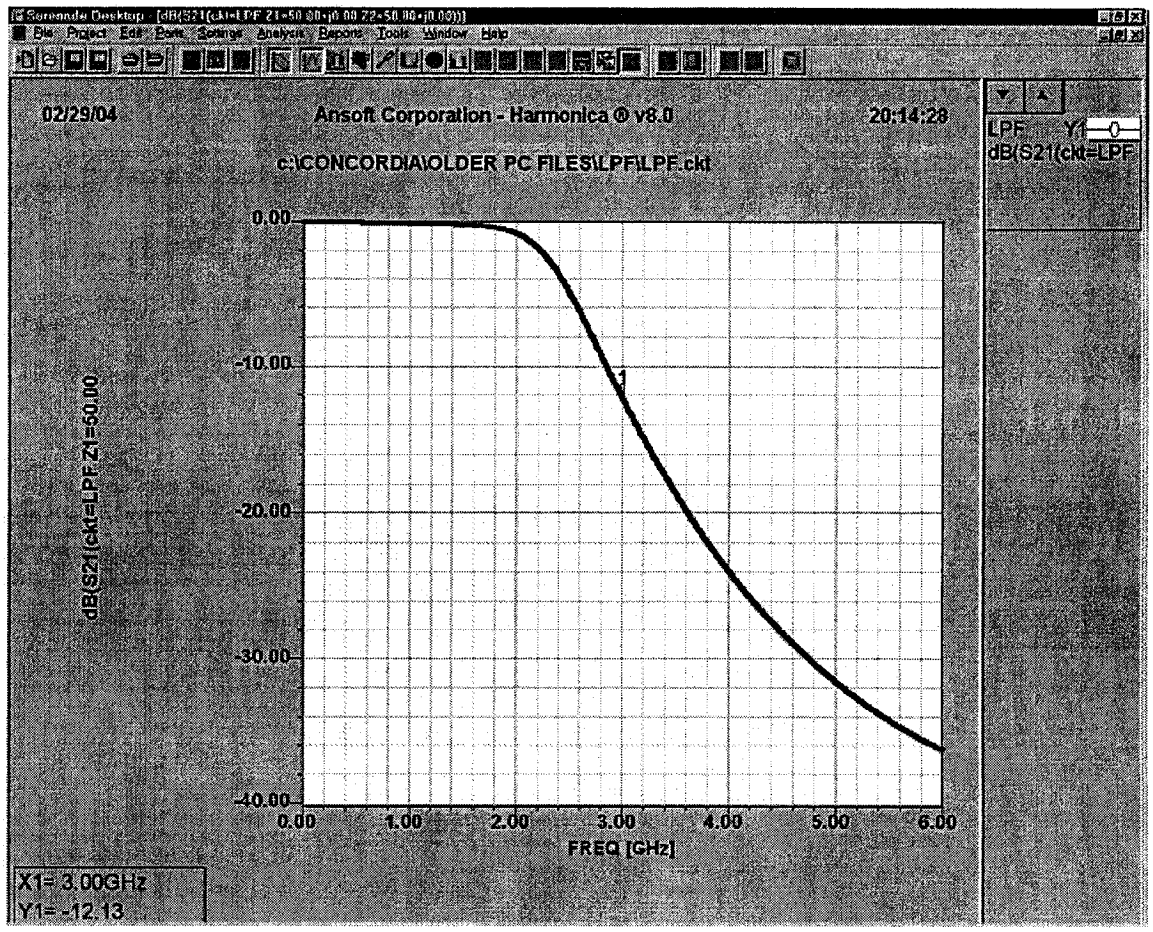

Figure 5.10: Serenade's Frequency Response (S21) for LPF.

The marker in the above display is placed at 3.0GHz. As can be seen, the insertion loss (S21) at 3.0GHz of the LPF is -12.13dB and input and output return loss (S11) and (S22) is -0.75dB. It can also be seen from the above graph that the attenuation (S21) at 6GHz is approximately 36dB, which meets the design specification (30dB).

5.4 Measurements

Using network analyzer 8720ES to measure the circuits on the bench, presented next are both circuits from PUFF and Serenade designs. Figure 5.11 is a picture of the LPF.

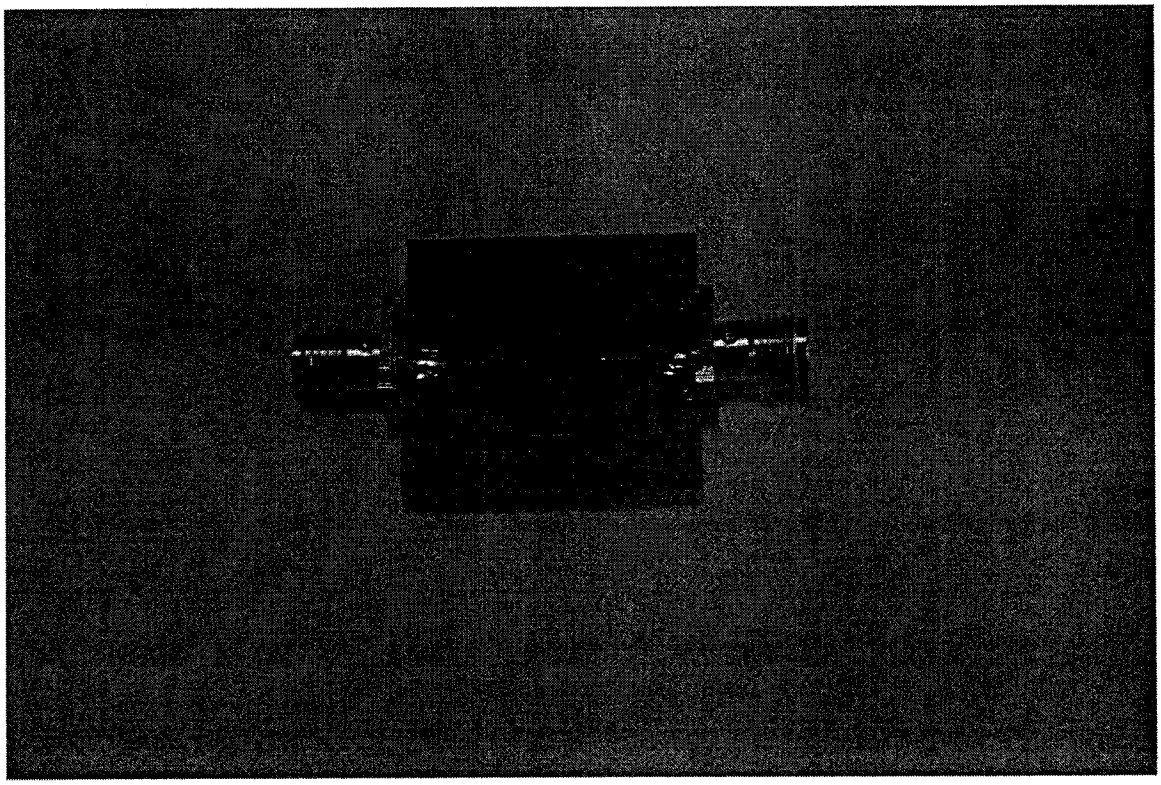

Figure 5.11: Picture of the LPF.

5.4.1 PUFF Circuit:

The network analyzer snap shot in Fig. 5.12 below is for the LPF generated from PUFF:

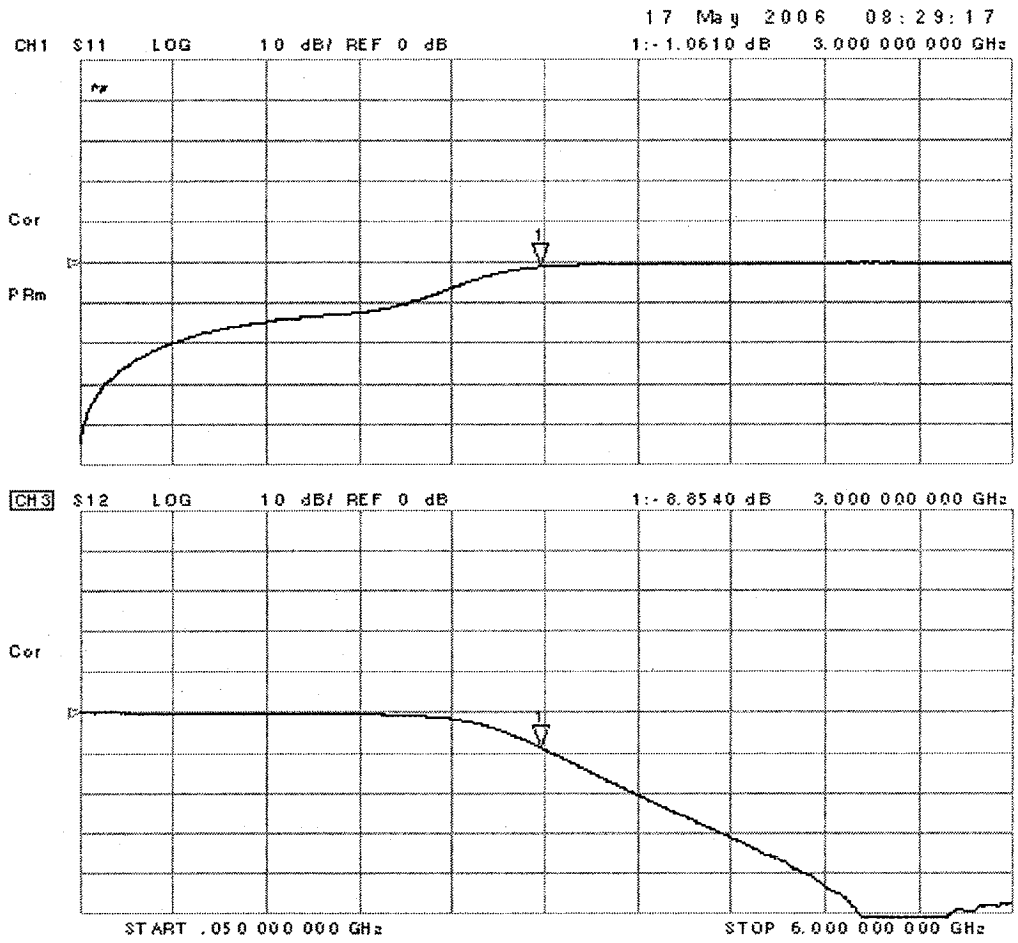

Figure 5.12: PUFF's bench measurements (S11, S21) for LPF.

The marker in the above display is placed at 3.0GHz. As can be seen, the insertion loss of the LPF (S21) is -8.854dB and the input and output return loss (S11) and (S22) are both at -1.061dB. Also, it can be seen from the above graph that the attenuation (S21) at 6GHz is lower than -40dB, which meets the design specification (30dB).

Please note that the insertion loss and phase delay introduced to the measurements from the SMA connectors will be accounted for in the discussion in Section 5.5.

5.4.2 Serenade Circuit:

The network analyzer snap shot below is for the LPF generated from Serenade:

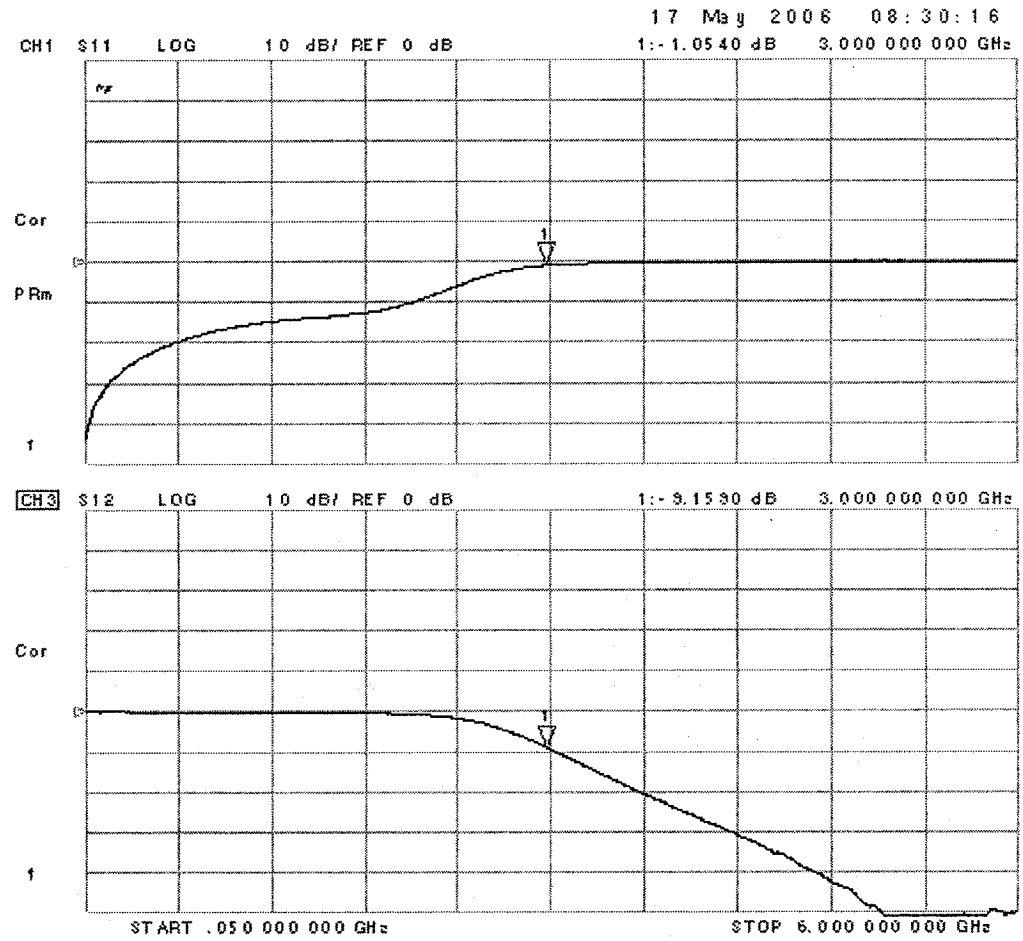

Figure 5.13: Serenade's bench measurements (S11, S21) for LPF.

The marker in the above display is placed at 3.0GHz. As can be seen, the insertion loss of the LPF (S21) is -9.159dB and the input and output return loss (S11) and (S22) are

both at -1.054dB. Also, it can be seen from Figure 5.13 that the attenuation (S21) at 6GHz is approximately 50dB, which meets the design specification (30dB).

Please note that the insertion loss and phase delay introduced to the measurements from the SMA connectors will be accounted for in the discussion in Section 5.5.

5.5 Discussion

The purpose of this section is to discuss and compare the simulation results obtained from PUFF ("*advanced*" model) and Serenade to their corresponding printed circuit board bench results. The graphs presented in this section are obtained from the simulation results and bench measurements for the LPF circuits presented in Sections 5.3 and 5.4. Presented firstly are the return loss (S11, S22) plots, simulation and bench, shown in Figure 5.13, and the frequency response (insertion loss, S21) plots, simulation and bench, shown in Figure 5.14, obtained from PUFF.

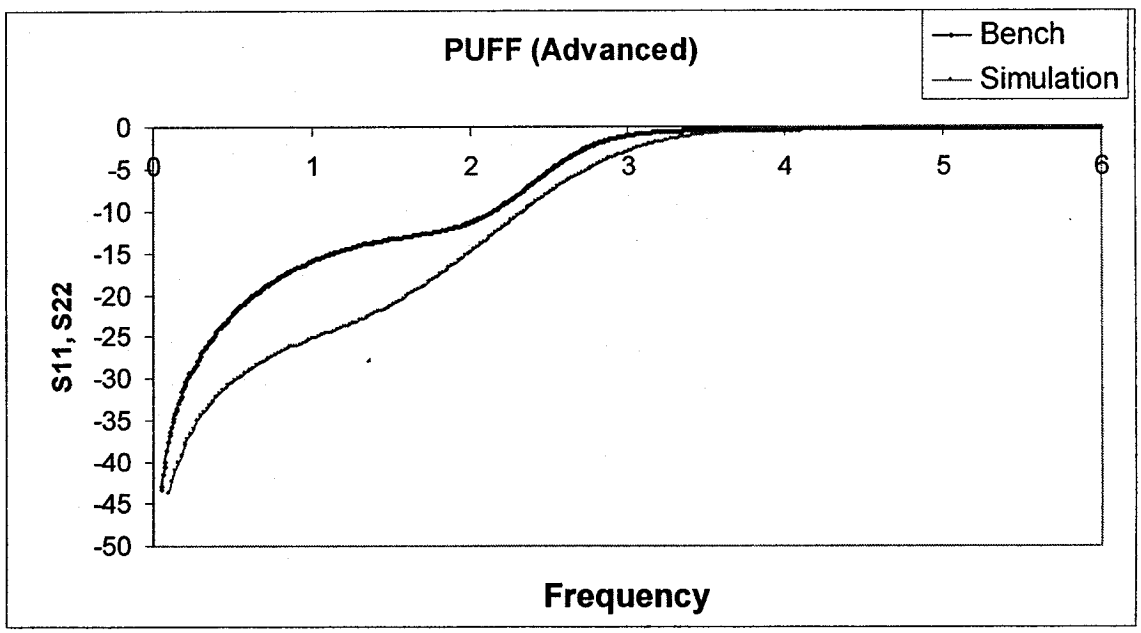

Figure 5.14: PUFF's LPF Input Return Loss simulation vs. bench results.

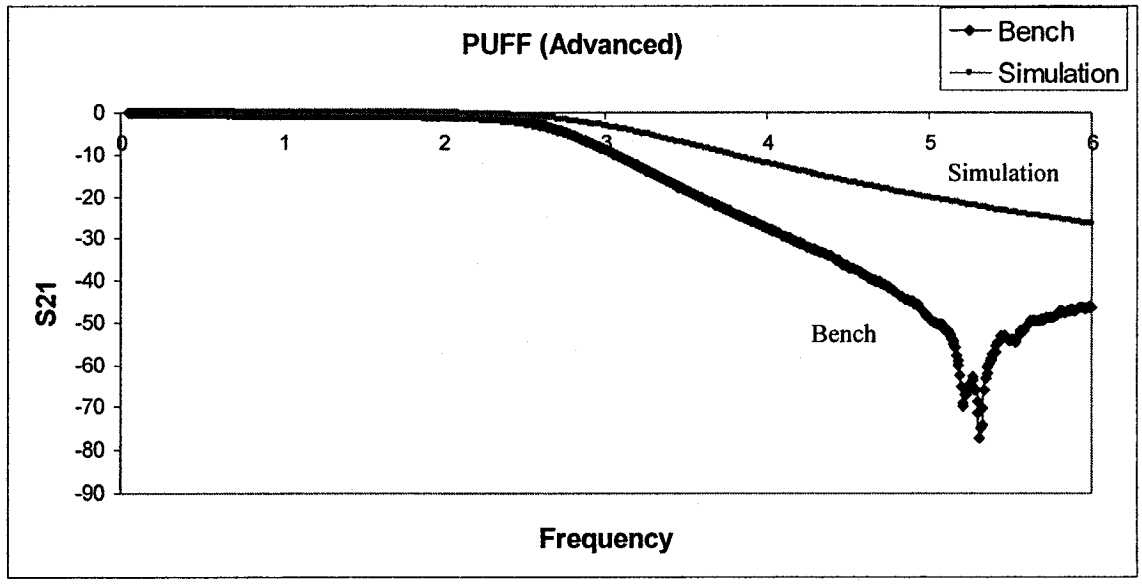

Figure 5.15: PUFF's LPF Frequency Response simulation vs. bench results.

Comparing the LPF's simulation results obtained from PUFF to their corresponding bench results, it can be obviously seen that the plots do not match! There is a slight difference in return loss, S11 (-1.276dB measured on bench @ 3.0GHz vs. -2.96dB for simulation @ 3.0GHz) and a significant difference in the frequency response, S21 (-8.84dB measured on bench @ 3.0GHz vs. –3.06dB for simulation @ 3.0GHz). The design parameters values obtained in section 5.2 for the low-impedance "Z_l" and high-impedance "Z_h" sections were used in PUFF. The transmission lines impedance and electrical length are the only two parameters required in PUFF for the different impedance sections of the LPF. Observing the frequency response plot in Figure 5.15, it can be obviously seen that the simulation shows the proper -3dB response at 3GHz, but the measured results does not.

Presented secondly are the return loss (S11) plots, simulation and bench, shown in Figure 5.16, and the frequency response (insertion loss, S21) plots, simulation and bench, shown

in Figure 5.17, obtained from Serenade. The same transmission lines physical dimensions obtained in Section 5.2, that were used in PUFF were used in Serenade. Comparing the Serenade simulation results to its bench measurement results, we can see a smaller difference (than PUFF's results) in insertion loss, S21 (-9.04dB measured on bench @ 3.0GHz vs. –12dB for simulation @ 3.0GHz). The difference in return loss (S11) is also smaller than that obtained from PUFF (-1.13dB measured on bench @ 3.0GHz vs. –0.75dB for simulation @ 3.0GHz). It is clearly seen from the plots in Figure 5.16 and Figure 5.17 that the difference between the simulation results and bench measurements is smaller than that obtained from PUFF. The frequency response plots are closer and more comparable to each other than the case in PUFF.

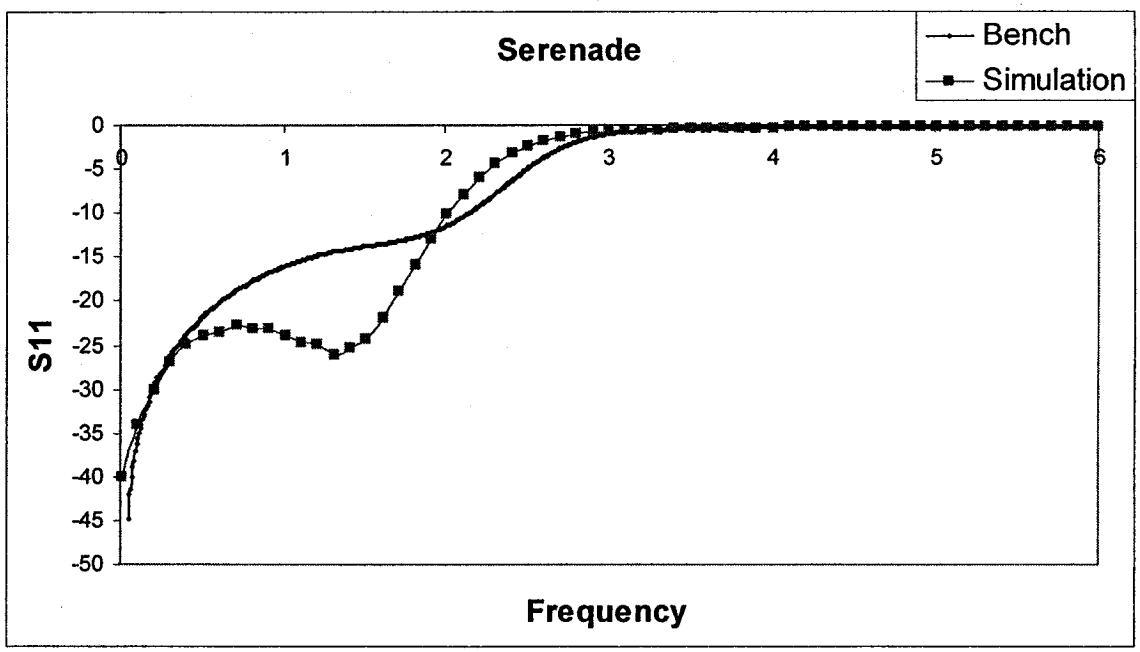

Figure 5.16: Serenade's LPF Input Return Loss simulation vs. bench results.

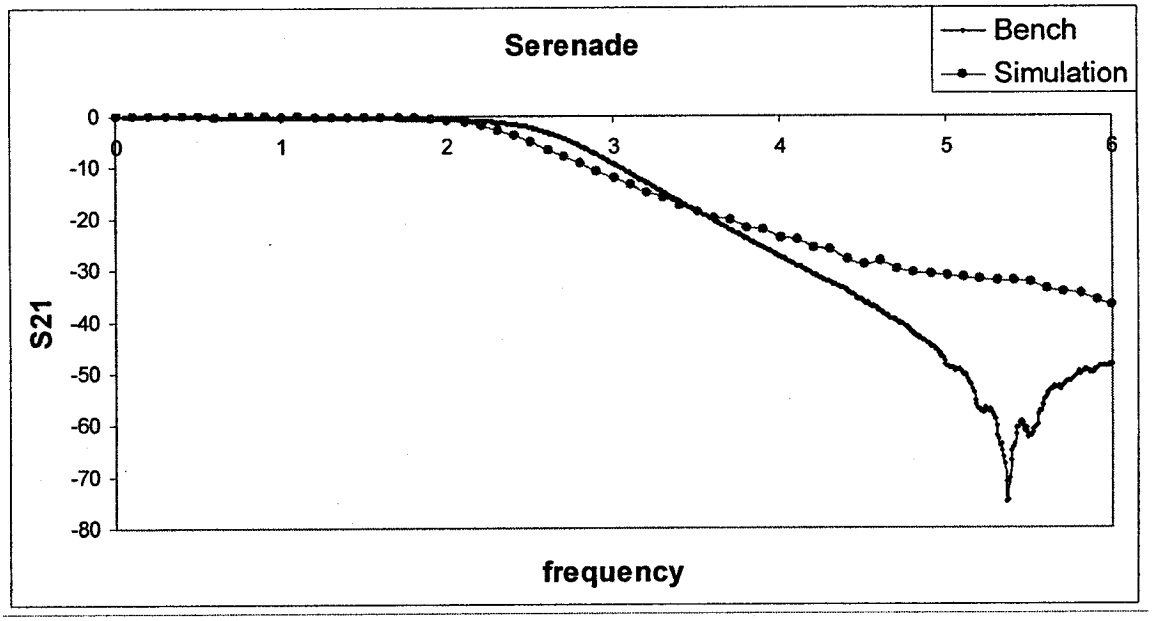

Figure 5.17: Serenade's LPF Frequency Response simulation vs. bench results.

The insertion loss of the two SMA connectors adds to the total insertion loss of the filter. This extra loss, which was measured separately on the same Network Analyzer amounts to 0.15dB for each connector (total of 0.30dB). This extra loss should be subtracted from the total insertion loss values measured on the bench to obtain the filter's loss. The electrical delay added by the two connectors is not a concern for this thesis discussion.

In conclusion, unlike PUFF, Serenade simulation depicted a reasonably comparable frequency response and insertion loss to the bench measurement results. However, the difference between the PUFF simulation and its corresponding bench measurements was very significant.

6. COUPLED MICROSTRIP LINES AND BAND-PASS FILTERS

6.1 Theory

Coupled microstrip lines consist of two edge-coupled microstrip lines in close proximity of one another as shown in Figure 6.1 [45].

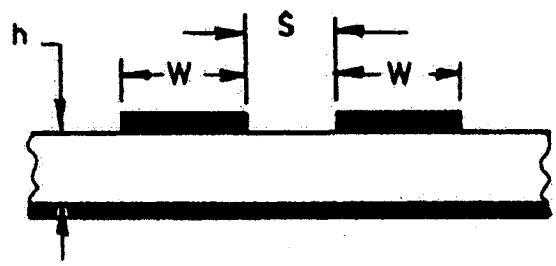

Figure 6.1: Coupled microstrip line.

The quantity S is the spacing between the microstrip lines, and W and h are the usual quantities of line width and dielectric thickness, respectively. For most applications, W is identical for both lines, and this assumption is made herein.

Like single microstrip lines, coupled microstrip lines exhibit hybrid TE-TM behavior, but the quasi-TEM model may be applied as successfully as in the single-line case. Unlike single microstrip lines, however, coupled lines exhibit even- and odd-mode excitations, with correspondingly different field patterns for each as illustrated in Figure 6.2 [46].

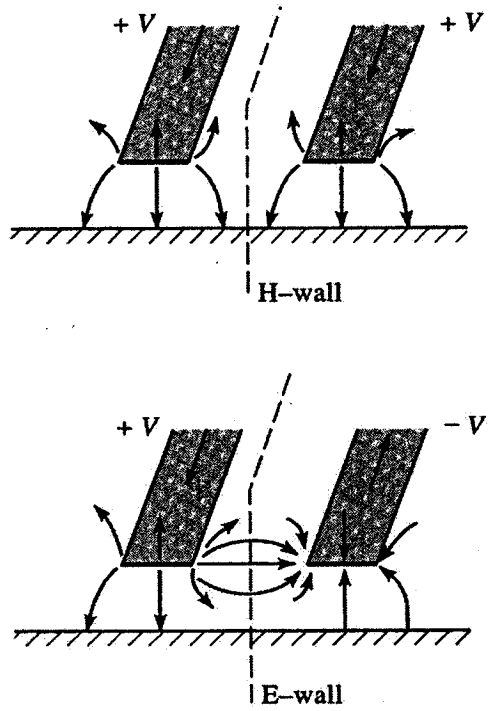

Figure 6.2: Even- (top) and odd- mode (bottom) excitations of a coupled microstrip line.

6.1.1 Even-Mode and Odd-Mode Characteristic Impedances

The proportion of field lines confined within the substrate to field lines extending beyond the substrate is clearly mode-dependent; thus the phase velocity differs between the two modes [47]. As a result, it can be seen from equation (2.1.1d) that each mode has its own characteristic impedance: Z_{0e} for the even case and Z_{0o} for the odd case.

To obtain the expressions for Z_{0e} and Z_{0o}, the following equation is used in conjunction with (2.1.1d):

$$\varepsilon_{eff} = \frac{C}{C_1}. \qquad (6.2.1a)$$

where C is the per-strip capacitance in the presence of the substrate, and C_1 is the per-strip capacitance in the absence of the substrate (air-spaced). For even- and odd-mode excitations, (3.2.1a) becomes

$$\varepsilon_{effe} = \frac{C_e}{C_{1e}} \tag{6.2.1b}$$

$$\varepsilon_{effo} = \frac{C_o}{C_{1o}} \tag{6.2.1c}$$

where the subscripts denote even- and odd-mode excitations, respectively. Substituting (6.2.1b) and (6.2.1c) into (2.1.1d) finally yields

$$Z_{0e} = \frac{1}{cC_{1e}\sqrt{\varepsilon_{effe}}} \tag{6.2.2a}$$

$$Z_{0o} = \frac{1}{cC_{1o}\sqrt{\varepsilon_{effo}}} \tag{6.2.2b}$$

or, alternatively,

$$Z_{0e} = \frac{1}{c\sqrt{C_e C_{1e}}} \tag{6.2.2c}$$

$$Z_{0o} = \frac{1}{c\sqrt{C_o C_{1o}}}. \tag{6.2.2d}$$

via substitution of (6.2.1) into (6.2.2a) and (6.2.2b) (analytical methods for determining C_e, C_o, C_{1e}, and C_{1o} will be discussed in Section 6.1.3).

Lastly, given the coupling factor, C', in dB, the characteristic impedances can be approximated as

$$Z_{0e} \approx Z_0\sqrt{\frac{1+10^{C'/20}}{1-10^{C'/20}}} \tag{6.2.3a}$$

$$Z_{0o} \approx Z_0 \sqrt{\frac{1-10^{C'/20}}{1+10^{C'/20}}} \tag{6.2.3b}$$

where

$$C' = 20\log\left|\frac{Z_{0e}-Z_{0o}}{Z_{0e}+Z_{0o}}\right|. \tag{6.2.3c}$$

6.1.2 Matching to External Lines

A coupled microstrip line can be matched to an external line of characteristic impedance Z_0 with the aid of

$$Z_0^2 \approx Z_{0e}Z_{0o}. \tag{6.2.4a}$$

which reduces to $Z_{in}=Z_0$.

This approximation is acceptable in instances where the coupling is 10dB or less; an exact expression for matching is given by

$$Z_0^2 = Z_{0e}Z_{0o}\frac{Z_{0e}\sin\theta_e + Z_{0o}\sin\theta_o}{Z_{0e}\sin\theta_o + Z_{0o}\sin\theta_e}. \tag{6.2.4b}$$

It should be noted that equations (6.2.4) might also be used as a quick check of the characteristic impedances provided by equations (6.2.2) and (6.2.3).

6.1.3 Analytical Determination of Even- and Odd-Mode Capacitances

The per-strip capacitance $C_{e,o}$ can be decomposed into several capacitances, as illustrated in Figure 6.3 [48].

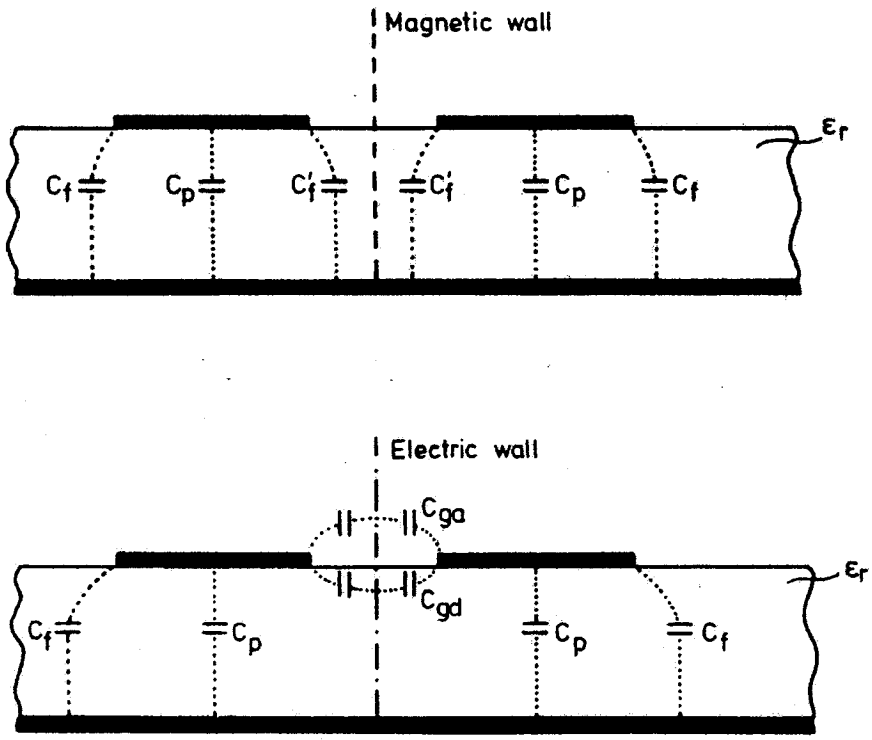

Figure 6.3: Separation of per-strip capacitances: even-mode (top) and odd-mode (bottom).

As can be seen, the total per-strip capacitances can be expressed as

$$C_e = C_p + C_f + C_{f'} \tag{6.2.5a}$$

and

$$C_o = C_p + C_f + C_{ga} + C_{gd} \tag{6.2.5b}$$

where

i. C_p is the parallel-plate capacitance, given by

$$C_p = \varepsilon_0 \varepsilon_r \frac{w}{h} \tag{6.2.5c}$$

ii. C_f is the fringing capacitance, given by

$$C_f = \frac{1}{2}\left(\frac{\sqrt{\varepsilon_{eff}}}{cZ_0} - C_p\right) \tag{6.2.5d}$$

iii. $C_{f'}$ is the fringing capacitance as affected by the presence of the other strip, given by

$$C_{f'} = \frac{C_f}{1+(Ah/s)\tanh(8s/h)}\sqrt{\frac{\varepsilon_r}{\varepsilon_{eff}}} \tag{6.2.5e}$$

$$A = \exp\{-0.1\exp(2.33 - 2.53w/h)\} \tag{6.2.5f}$$

iv. C_{ga} is the odd-mode fringing capacitance in the air across the coupling gap, given by

$$C_{ga} = \varepsilon_0 \frac{K(k')}{K(k)} \tag{6.2.5g}$$

$$k = \frac{s/h}{s/h + 2w/h} \tag{6.2.5h}$$

$$k' = \sqrt{1-k^2} \tag{6.2.5i}$$

$$\frac{K(k')}{K(k)} = \frac{1}{\pi}\ln\left(2\frac{1+\sqrt{k'}}{1-\sqrt{k'}}\right), \quad 0 \le k^2 \le 0.5 \tag{6.2.5j}$$

$$\frac{K(k')}{K(k)} = \frac{\pi}{\ln\left\{2\left(1+\sqrt{k}\right)/\left(1-\sqrt{k}\right)\right\}}, \quad 0.5 \le k^2 \le 1 \tag{6.2.5k}$$

v. C_{gd} is the odd-mode fringing capacitance in the dielectric across the coupling gap, given by

$$C_{gd} = \frac{\varepsilon_0 \varepsilon_r}{\pi} \ln\left\{\coth\left(\frac{\pi}{4}\frac{s}{h}\right)\right\} + 0.65C_f\left(\frac{0.02}{s/h}\sqrt{\varepsilon_r} + 1 - \varepsilon_r^{-2}\right). \qquad (6.2.5i)$$

It should be stressed that all the capacitances in expressions (6.2.5) are the values for a *"single"* microstrip of the coupled line. Also, Z_0 in (6.2.5d) and ε_{eff} in (6.2.5d), (6.2.5e) are the single-strip values discussed in Chapter 2, and k in (6.2.5g-k) is restricted to [0,1] because the associated functions are elliptic. Elliptic functions are mathematical functions used to yield the squarest possible amplitude fitter response with a given number of circuit elements. The elliptic function has a Chebychev response in both passband and the stopband. The elliptic function filter is doubly periodic and has a poorer phase response and transient response than any of the classical transfer functions. Lastly, $C_{1e,o}$ is the per-strip capacitance in the absence of the substrate (air-spaced). $C_{1e,o}$ can be readily obtained from equations (6.2.5) by noting that, in the absence of dielectric, ε_r=1 and $C_{gd} = C_{ga}$ (i.e., the expression for C_{gd} is (6.2.5g)); thus

$$C_{1e} = C_p + C_f + C_f. \qquad (6.2.6a)$$

and

$$C_{1o} = C_p + C_f + 2C_{ga}. \qquad (6.2.6b)$$

6.2 Design

6.2.1 Dimensional Design

Design of the shape ratio, *w/h*, and the spacing ratio, *s/h*, is accomplished through the use of either Bryant and Weiss curves or Akhtarzad synthesis curves (albeit the second approach is generally not as accurate as the first) [49].

With the first method, the characteristic impedances are determined using equations (6.2.2) or (6.2.3); the impedances are then used to read the ratios off a set of Bryant and Weiss curves, a graph relating a strip's dimensional quantities to the even- and odd-mode impedances [50]. Different relative substrate permittivities (ε_r) have different curves; Figure 6.4 [51] depicts two plots, one for a line with no substrate (air-spaced, ε_r=1) and another for a line with a substrate of ε_r=9.

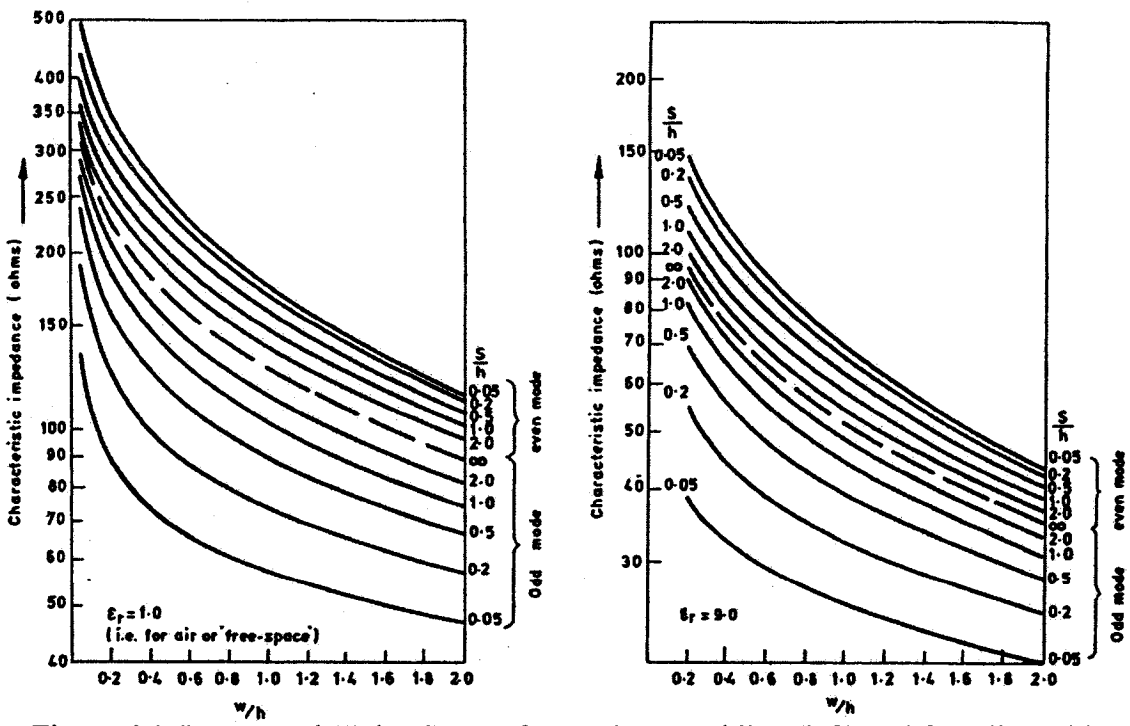

Figure 6.4: Bryant and Weiss Curves for an air-spaced line (left) and for a line with a substrate having ε_r=9 (right).

With the second method, equivalent *single* microstrip line shape ratios $(w/h)_{se,so}$ are first determined for each mode [52]. This is accomplished by converting the even- and odd-mode impedances to their single microstrip equivalent via the following:

$$Z_{0se} = \frac{Z_{0e}}{2} \tag{6.2.7a}$$

$$Z_{0so} = \frac{Z_{0o}}{2}. \tag{6.2.7b}$$

where (6.2.7a) corresponds to $(w/h)_{se}$ and (6.2.7b) corresponds to $(w/h)_{so}$. Using the results of equations (6.2.7) and the single-line design methods presented in Section 2.1, the equivalent single-line ratios are determined, and the coupled line shape and spacing ratios are read off a set of Akhtarzad curves; Figure 6.5 [53] below depicts a family of such curves.

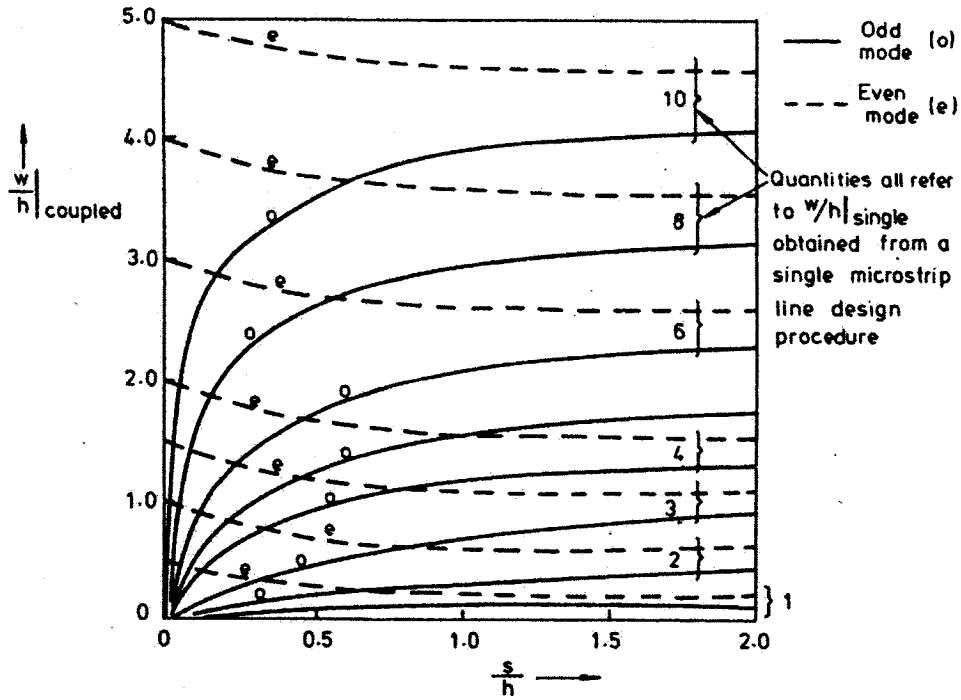

Figure 6.5: Akhtarzad curves.

The Akhtarzad method can be made more accurate- although intensively more laborious- by solving the following expressions in place of using the graph:

$$\left(\frac{w}{h}\right)_{se} = \frac{2}{\pi}\cosh^{-1}\left(\frac{2d-g+1}{g+1}\right) \tag{6.2.8a}$$

$$\left(\frac{w}{h}\right)_{so} = \frac{2}{\pi}\cosh^{-1}\left(\frac{2d-g-1}{g-1}\right)+\frac{4}{\pi(1+\varepsilon_r/2)}\cosh^{-1}\left(1+2\frac{w/h}{s/h}\right),\ \varepsilon_r \le 6 \tag{6.2.8b}$$

$$\left(\frac{w}{h}\right)_{so} = \frac{2}{\pi}\cosh^{-1}\left(\frac{2d-g-1}{g-1}\right)+\frac{1}{\pi}\cosh^{-1}\left(1+2\frac{w/h}{s/h}\right),\ \varepsilon_r \ge 6 \tag{6.2.8c}$$

where

$$g = \cosh\left(\frac{\pi s}{2h}\right) \tag{6.2.8d}$$

$$d = \cosh\left(\pi\frac{w}{h}+\frac{\pi s}{2h}\right). \tag{6.2.8d}$$

It should be noted that (6.2.8a) must be solved simultaneously with (6.2.8b) or (6.2.8c). To facilitate the task somewhat, there exists a median between the Akhtarzad curves and the above equations; specifically, the second terms in (6.2.8b) and (6.2.8c) can be disregarded, yielding the following formula for the spacing ratio:

$$\frac{s}{h} = \frac{2}{\pi}\cosh^{-1}\left[\frac{\cosh\{(\pi/2)(w/h)_{se}\}+\cosh\{(\pi/2)(w/h)_{so}\}-2}{\cosh\{(\pi/2)(w/h)_{so}\}-\cosh\{(\pi/2)(w/h)_{se}\}}\right]. \tag{6.2.9}$$

6.2.2 Band Pass Filter Design

The equivalent circuit of a coupled line section is depicted Figure 6.6 [54].

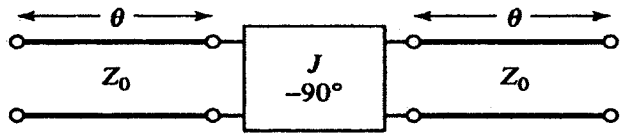

Figure 6.6: Equivalent circuit of a coupled line section.

The "rectangular element" in Figure 6.6 is an impedance inverter, which is useful in bandpass and bandstop filters with relatively narrow bandwidths. An impedance inverter is a device or circuit that has input impedance inversely proportional to the load impedance. More specifically, the normalized input impedance is equal to the normalized load admittance. These inverters can be used to transform series-connected elements to shunt-connected elements, or shunt-connected elements to series connected elements. This J inverter can be realized using a quarter-wave transformer of the appropriate characteristic impedance. A bandpass N^{th} order filter can be designed by cascading such sections as shown in Figure 6.7 [55].

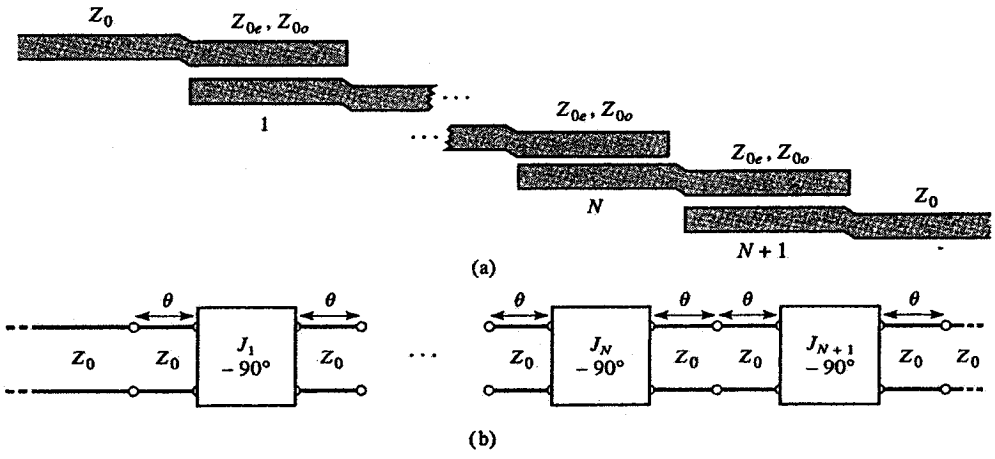

Figure 6.7: Design of a band pass filter by cascading coupled line sections: (a) Cascaded coupled line sections. (b) Equivalent circuit of (a).

The design process is relatively simple. Following the design procedure in Pozar [56], all the required parameters can be determined from the following set of expressions:

$$Z_0 J_1 = \sqrt{\frac{\pi\Delta}{2g_1}} \tag{6.2.10a}$$

$$Z_0 J_n = \frac{\pi\Delta}{2\sqrt{g_{n-1}g_n}},\ n = 2,3,...,N \tag{6.2.10b}$$

$$Z_0 J_{N+1} = \sqrt{\frac{\pi\Delta}{2g_N g_{N+1}}} \tag{6.2.10c}$$

$$Z_{0e} = Z_0\left[1 + J_n Z_0 + (J_n Z_0)^2\right],\ n = 1,2,...,N+1 \tag{6.2.10d}$$

$$Z_{0o} = Z_0\left[1 - J_n Z_0 + (J_n Z_0)^2\right],\ n = 1,2,...,N+1. \tag{6.2.10e}$$

where Z_0 is the characteristic impedance of the external line to which the filter is connected; Δ is fractional bandwidth of the filter; and the g_n quantities are the low-pass prototype values presented in Section 6.1. The design procedure proceeds by first determining the external impedance-admittance inverter constant products, $Z_0 J_n$, via (6.2.10a) to (6.2.10c), and then obtaining the even- and odd-mode characteristic impedances of each coupled line section via (6.2.10d) and (6.2.10e).

Now, for this specific BPF example discussed in this thesis, a 90° coupled line BPF example provided in the PUFF documentation was used as a reference and was scaled down to the desired frequency and dielectric material. Listed below are the parameters for the BPF from the PUFF documentation:

f_c = 5.0GHz,

ε_r = 10.2,

Thickness = 1.27mm,

Coupled lines lengths = 90° @ 5GHz,

Coupled lines impedance = 66Ω for the 2 external coupled lines resonators,

Coupled lines impedance = 55Ω for the internal resonator.

Since the BPF example discussed in this thesis is designed at 3.0GHz, the coupled lines lengths have to be scaled down accordingly. Also, since the dielectric material is 0.787mm thick and $\varepsilon_r = 3.38$, the widths of the lines have also to be changed accordingly.

In summary, the design requirements for the BPF are:

Center Frequency (f_c) = 3GHz,

Number of sections: N=3,

Frequency Bandwidth = 250MHz,

The physical dimensions of the resonators used in Serenade are:

External resonators: $W_b = 1.603$mm, $L_b = 15.0$mm, S_b=0.15mm,

Internal resonator: $W_a = 1.852$mm, $L_a = 14.80$mm, $S_a = 0.9$mm.

The design parameters used in PUFF are:

External resonators: $Z_{be} = 66\Omega$, $L_b = 89°$,

Internal resonator: $Z_{ae} = 55\Omega$, La = 90°.

The physical dimensions obtained from the PUFF layout are:

External resonators: $W_b = 1.603$mm, $L_b = 15.356$mm, $S_b = 0.137$mm,

Internal resonator: $W_a = 1.852$mm, $L_a = 15.27$mm, $S_a = 0.929$mm.

6.3 Simulations

Presented next are the simulation results of the coupled-microstrip lines BPF from both simulators, PUFF and Serenade.

6.3.1 PUFF Simulation Results:

Presented below in Figure 6.8 is the PUFF simulation graph of the coupled-microstrip lines BPF using the "*ideal*" edge coupled transmission lines element model (*clines*):

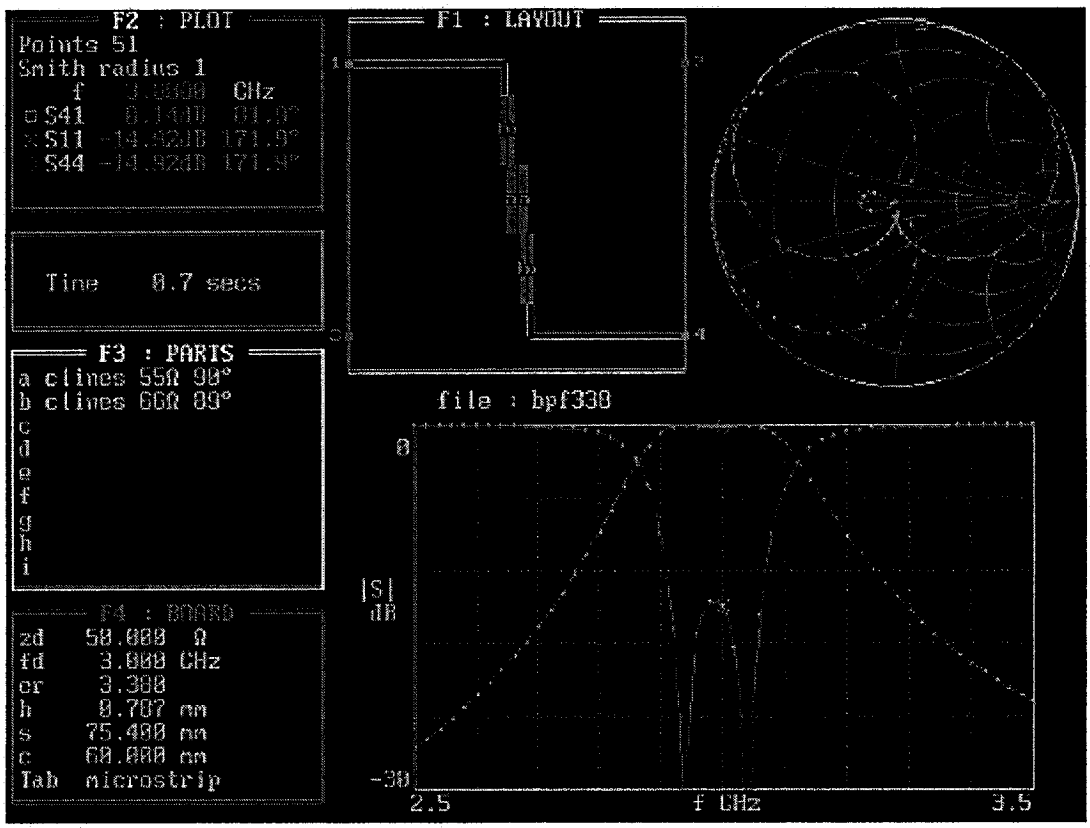

Figure. 6.8: PUFF's "*Ideal*" Coupled microstrip line (*cline*) model for BPF.

Please note that the marker is set at 3.0GHz. S41 is the insertion loss at -0.14dB and S11 and S22 are the input and output return loss at -14.92dB. the 3-dB bandwidth is 250MHz.

Also, presented next in Figure 6.9, is the PUFF simulation graph of the coupled-microstrip lines BPF using the "*advanced*" edge coupled transmission lines element model (*clines!*) to account for losses in the transmission lines and dependency of impedance and effective dielectric constant on frequency, we get:

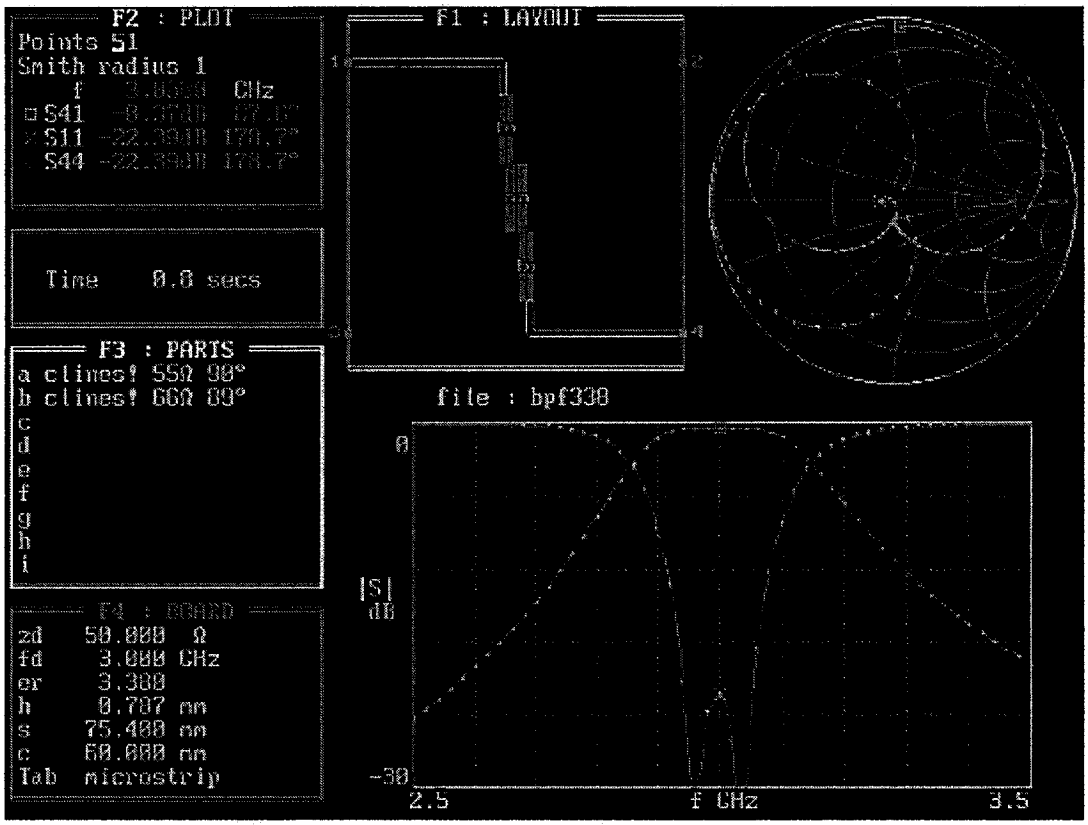

Figure 6.9: PUFF's "*Advanced*" Coupled microstrip line (*cline!*) model for BPF.

Please note that the marker is set at 3.0GHz. S41 is the insertion loss at -0.37dB and S11 and S22 are the input and output return loss at –22.39dB. The 3-dB bandwidth is 300MHz.

It should be noted that the insertion loss (S21) is larger in the "*advanced*" transmission line model (as expected) than the "*ideal*" model case, since there is virtually no loss in the "*ideal*" transmission line (-0.14dB vs. -0.37dB respectively). The frequency response is slightly narrower in the "*ideal*" model as can be seen in Figure 6.10. The return loss (S11and S22) is larger in the "*advanced*" transmission line model but have similar shapes as can be seen in Figure 6.11.

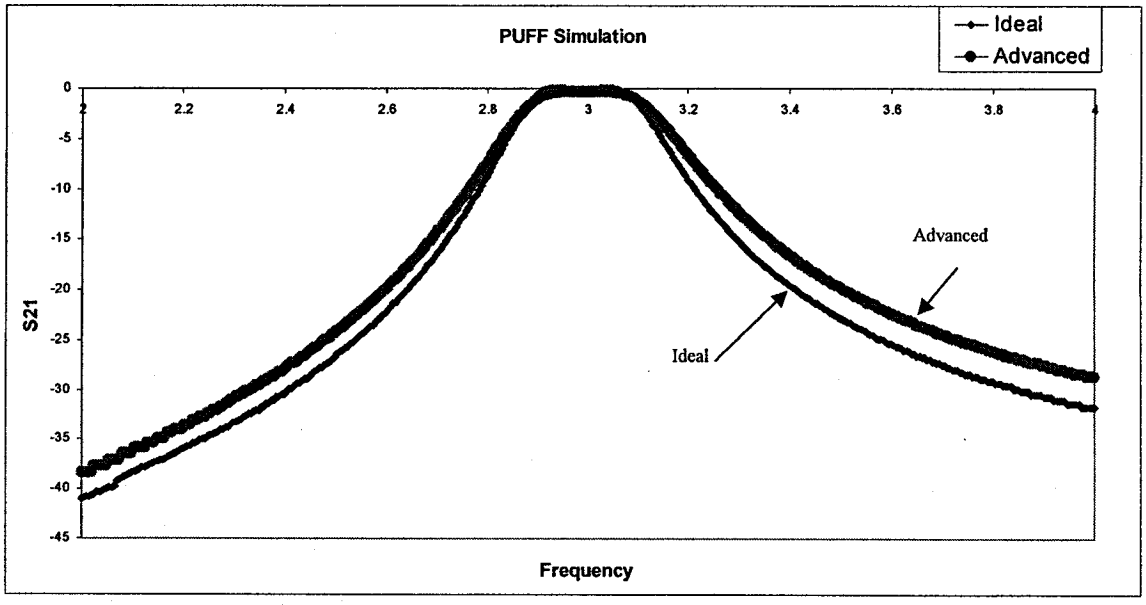

Figure 6.10: PUFF's (S21) comparison between "*Ideal*" and "*Advanced*" BPF models.

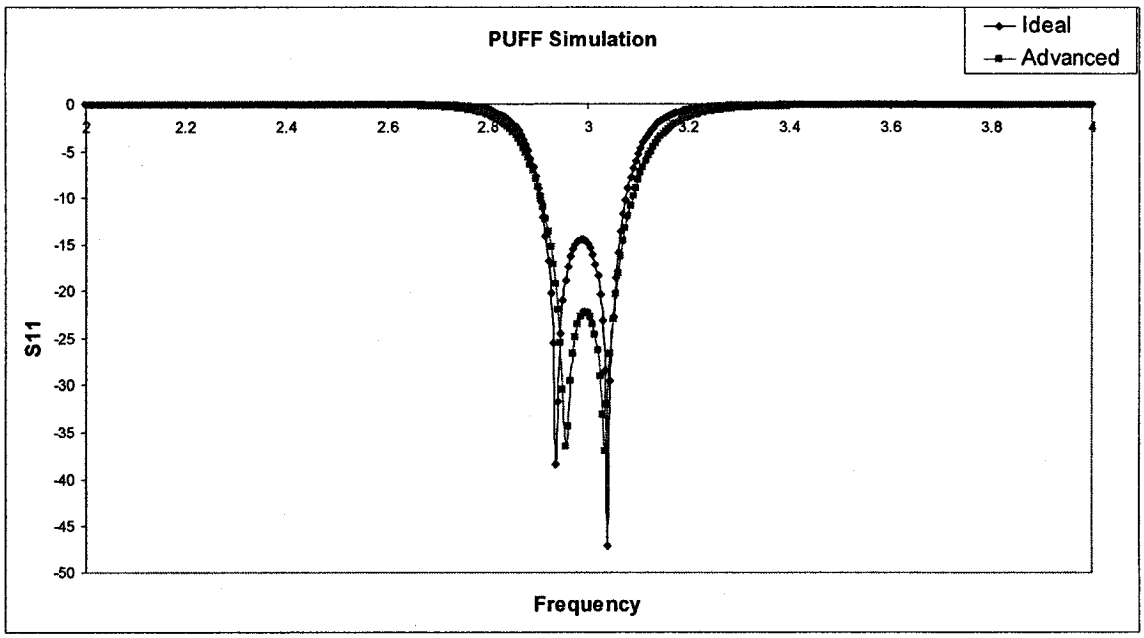

Figure 6.11: PUFF's (S11) comparison between "*Ideal*" and "*Advanced*" BPF models.

It is clear from Figure 6.10 and Figure 6.11 that both the "*ideal*" and the "*advanced*" models are close to each other, both S11 and S21. For this reason, only the "*advanced*" LPF model will be analyzed on the bench. The analysis and comparisons will be discussed in Section 6.5.

6.3.2 Serenade Simulation Results:

Presented next are the Serenade simulation graphs of the coupled-microstrip lines BPF using the same transmission lines physical dimensions for width and length used in PUFF simulation: BPF's frequency response, (S21):

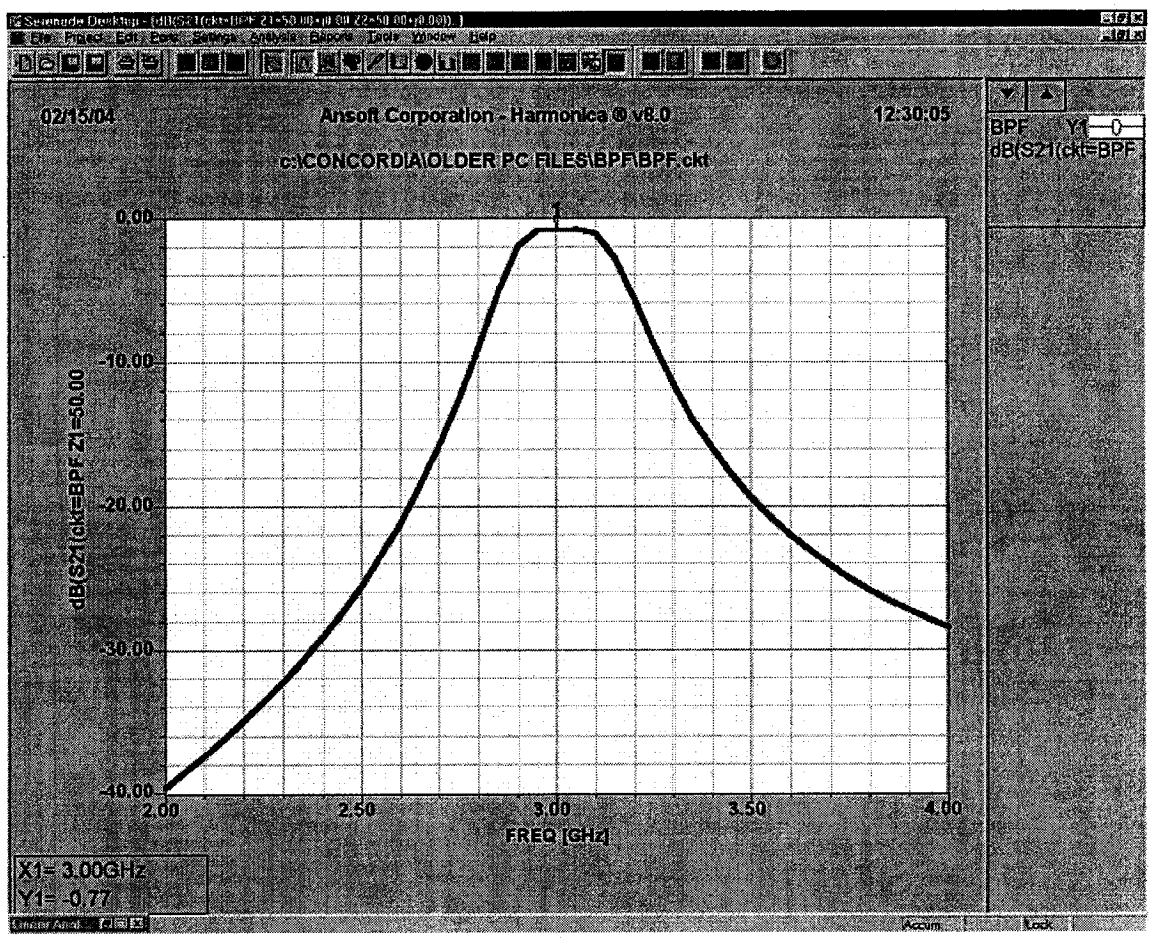

Figure 6.12: Serenade's Frequency Response (S21) for BPF.

BPF's input and output return loss, (S11) and (S22):

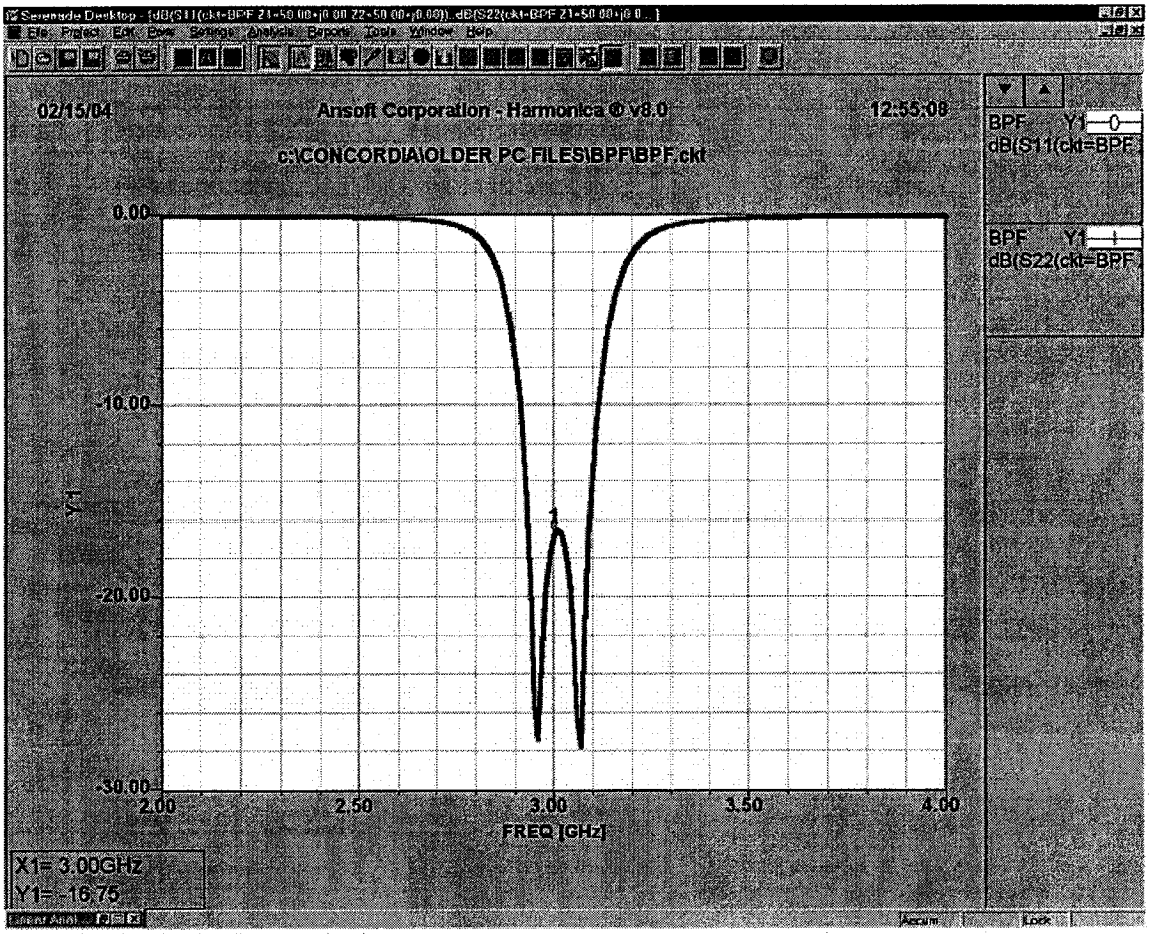

Figure 6.13: Serenade's Input and Output Return Loss (S11, S22) for BPF.

Please note that the marker is set at 3.0GHz, S21 is the insertion loss at -0.77dB, and (S11) and (S22) are the input and output return loss at -16.75dB.

6.4 Measurements

Using the network analyzer 8720ES to measure the circuits on the bench, presented next are both circuits from PUFF and Serenade designs. Figure 6.14 is a picture of the BPF to be measured on the bench.

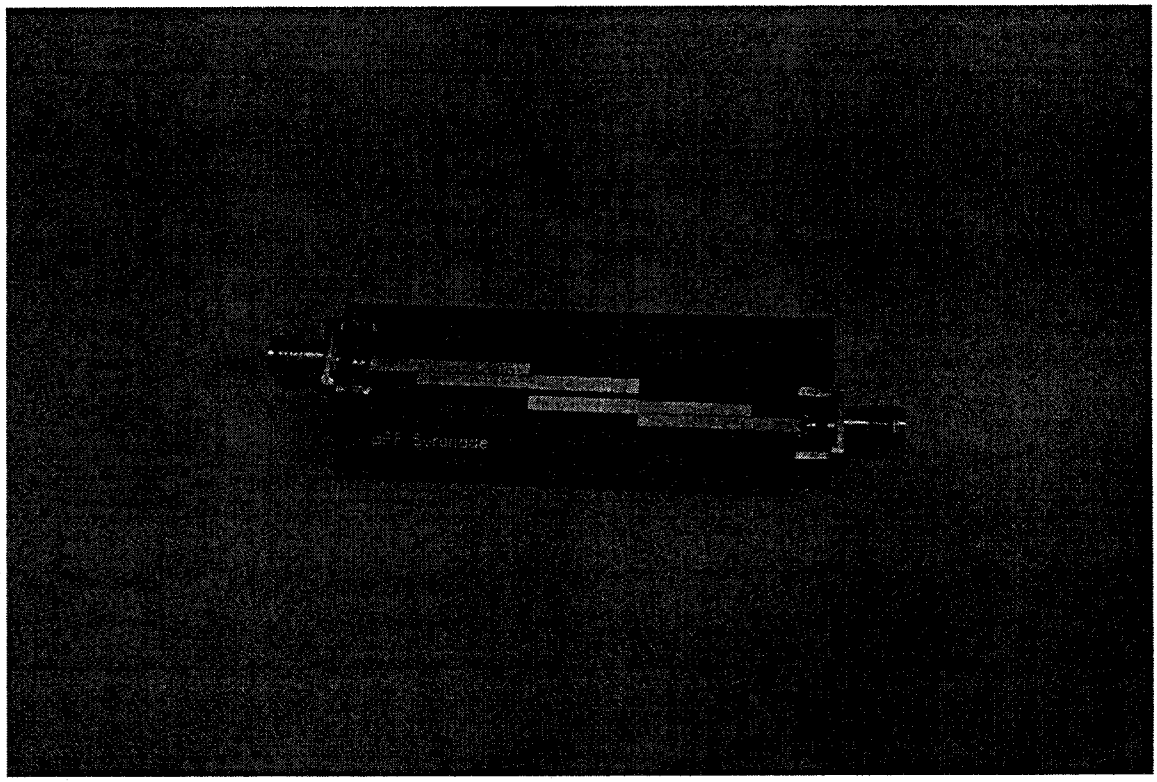

Figure 6.14: Picture of the BPF.

6.4.1 PUFF Circuit:

The network analyzer screen shot below is for the BPF generated from PUFF ("*advanced*" model):

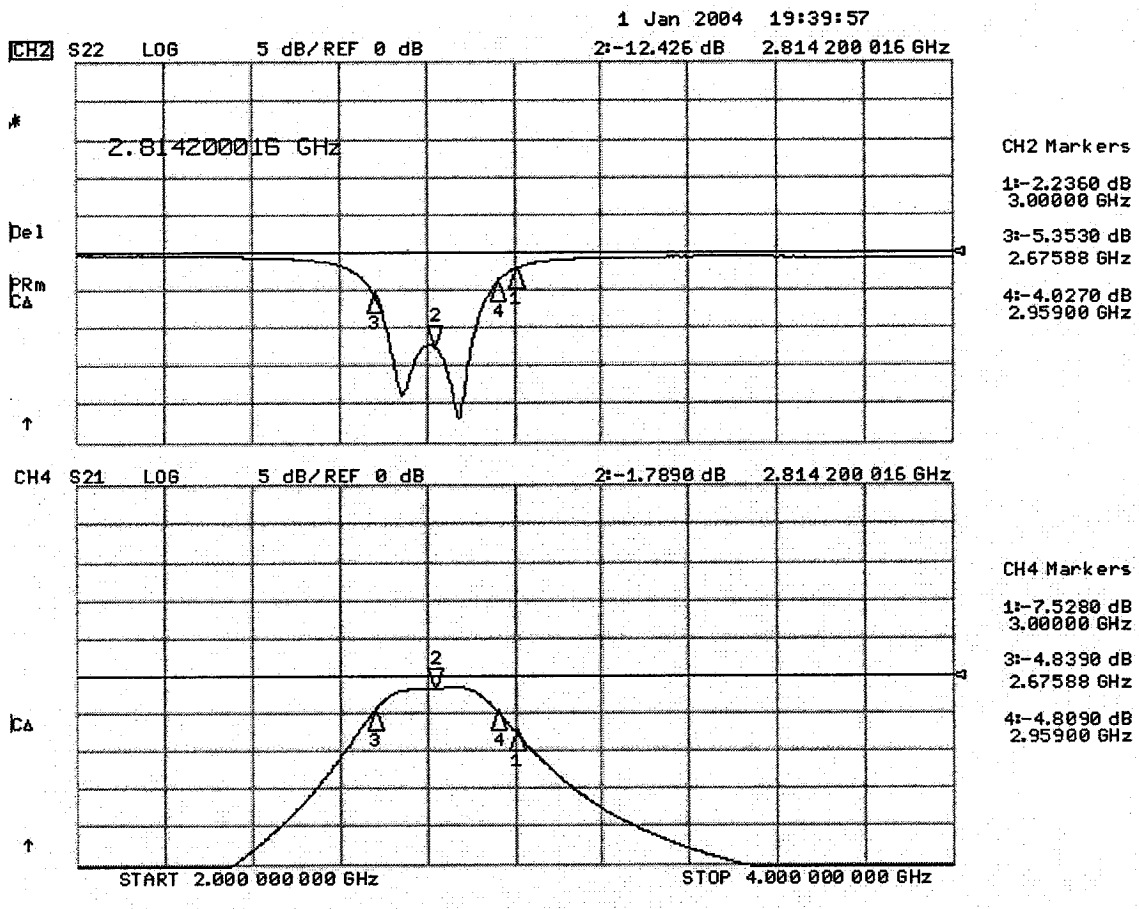

Figure 6.15: PUFF's bench measurements (S11, S21) for BPF.

Marker 1 is placed at 3.0GHz. Please note the frequency shift in the frequency response in the above display. This phenomenon will be discussed in Chapter 6.5. Marker 2 in the above displays is placed at 2.8142GHz (the "*new center frequency*"). As can be seen, the insertion loss of the BPF (S21) is -2.236dB and the input and output return loss (S11) and (S22) are both at -7.528dB.

6.4.2 Serenade Circuit:

The network analyzer snap shot below is for the BPF generated from Serenade:

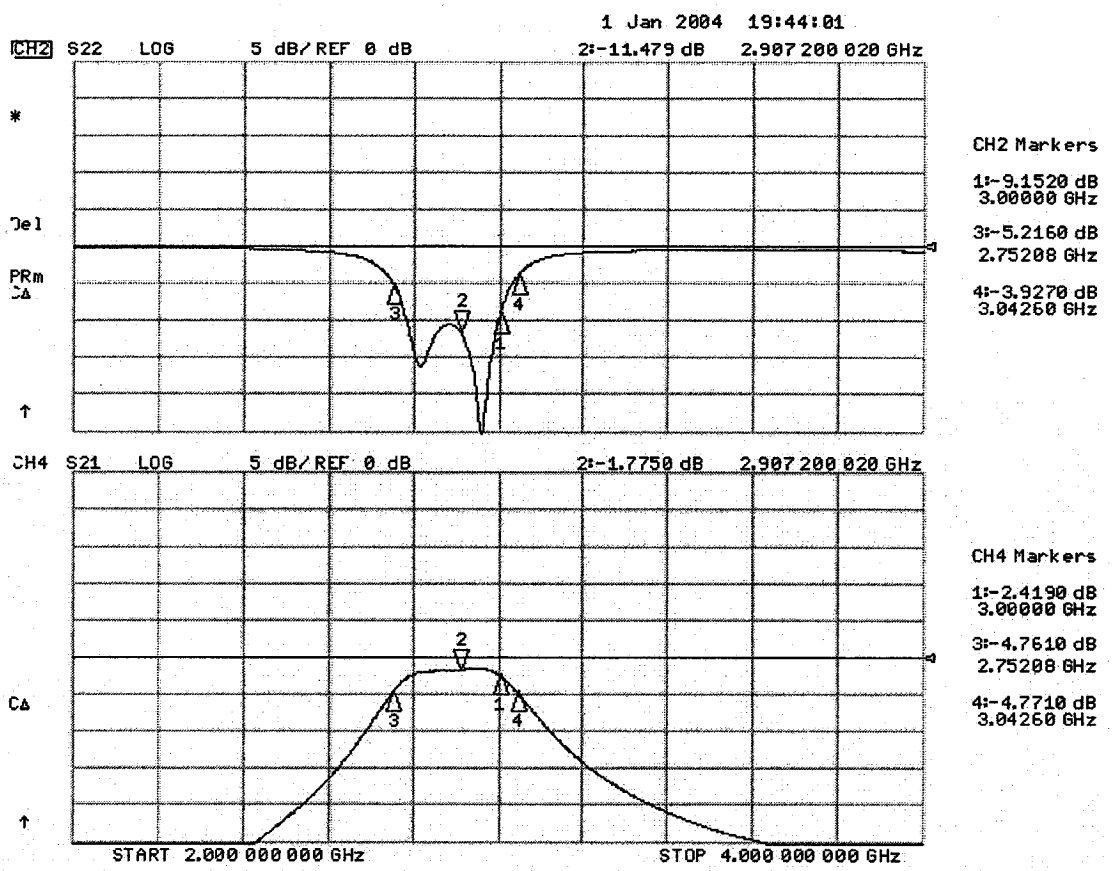

Figure 6.16: Serenade's bench measurements (S11, S21) for BPF.

Similar to the circuit from PUFF, a frequency shift in the frequency response is noticed in the above display. This will also be discussed in Section 6.5. Marker 2 in the above display is placed at 2.9072GHz (the "*new center frequency*"). As can be seen, the insertion loss of the BPF (S21) is –1.775dB and the input and output return loss (S11) and (S22) are both at -11.479dB.

6.5 Discussion

The purpose of this section is to discuss and compare the simulation results obtained from PUFF and Serenade to their corresponding printed circuit boards bench results. The

graphs presented in this section are obtained from the simulation results and bench measurements for the BPF circuits presented in sections 6.3 and 6.4 respectively.

Presented firstly are the return loss (S11) plots, simulation and bench, shown in Figure 6.17, and the frequency response (insertion loss, S21) plots, simulation and bench, shown in Figure 6.18, obtained from PUFF.

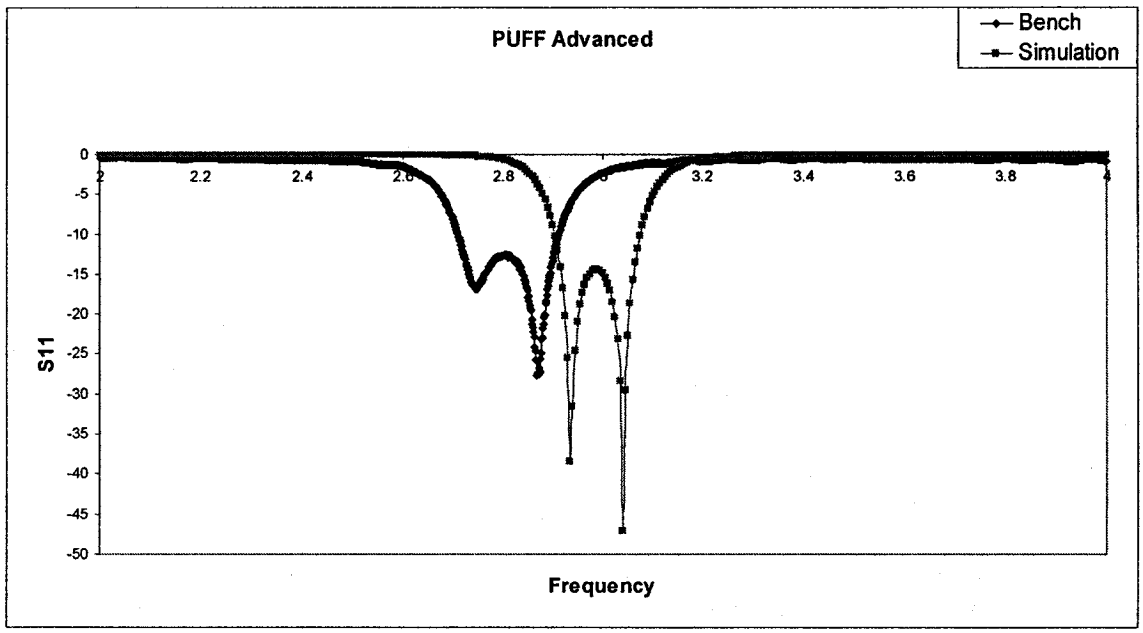

Figure 6.17: PUFF's BPF Input Return Loss simulation vs. bench results.

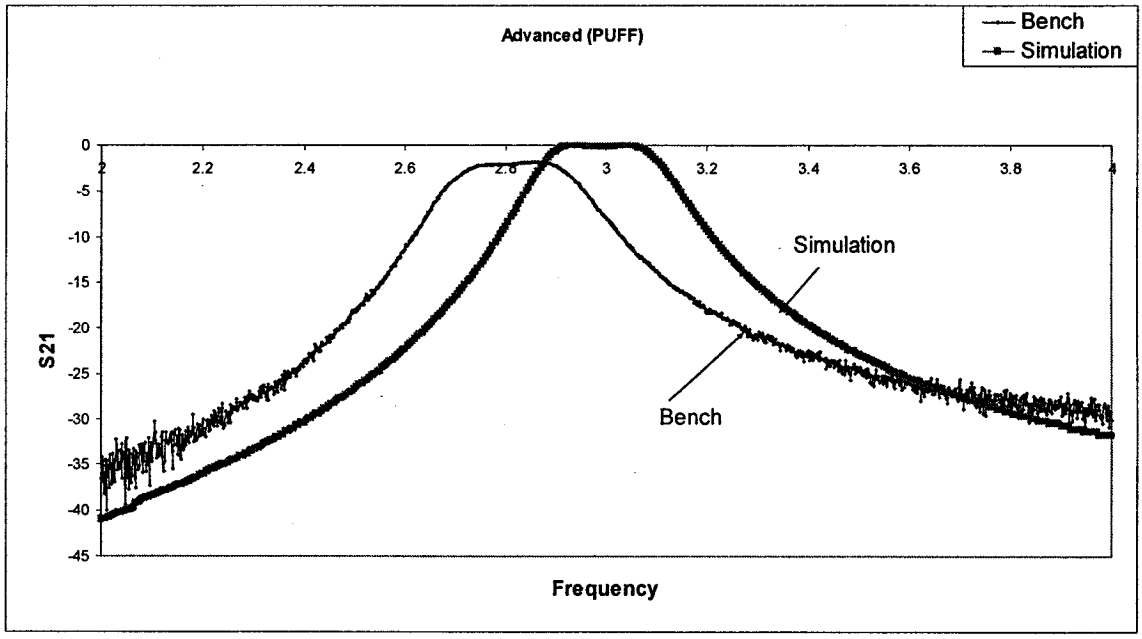

Figure 6.18: PUFF's BPF Frequency Response simulation vs. bench results.

Comparing the BPF's simulation results to their corresponding bench results presented in Figure 6.17 and Figure 6.18, a frequency shift in both frequency response (S21) and return loss (S11) can be obviously seen. This frequency shift, from 3.0GHz (which is the design center frequency, f_c) to the "*new*" center frequency of 2.8142GHz (Δf_c of 185MHz), is a result of the way the coupled transmission lines are modeled in PUFF. Similar to the LPF results obtained in Chapter 5, the BPF bench results behavior correspond to a circuit designed for f_c = 2.8142GHz. This lower frequency BPF corresponds to a simulated circuit with electrically longer coupled lines resonators. A difference of 1mm in extra length for each coupler section yields in a BPF centered at 2.8142GHz. Similar to the single open-ended transmission lines, PUFF does not account for open-ended effects in coupled lines either. Also, it can be seen in the above graph that the measured frequency response is wider than the simulated response which is an indication of a higher coupling between the transmission lines. Assuming no frequency

shift, as can be seen from the results shown above, the difference in insertion loss, S21 (-1.79dB measured on bench @ 2.8142GHz vs. –0.37dB @ 3.0GHz for simulation). The difference in return loss however is not very significant (-12.43dB measured on bench @ 2.8142GHz vs. –22.39dB @ 3.0GHz for simulation).

Presented secondly are the return loss (S11) plots, simulation and bench, shown in Figure 6.19, and the frequency response (insertion loss, S21) plots, simulation and bench, shown in Figure 6.20, obtained from Serenade. The same transmission lines physical dimensions obtained in Section 6.2, that were used in PUFF were used in Serenade.

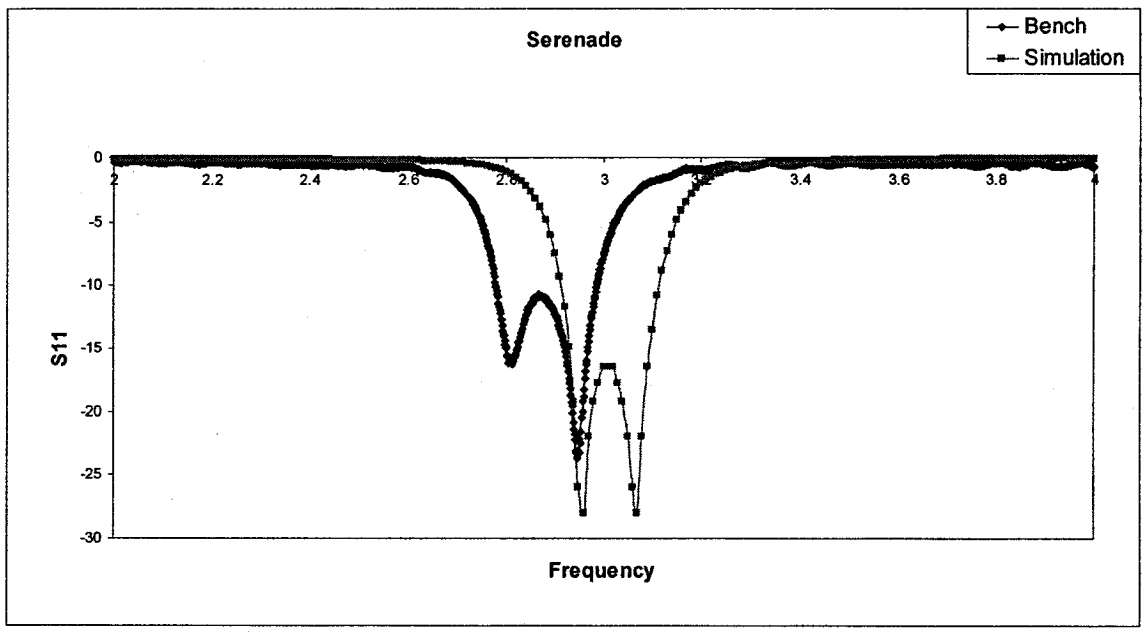

Figure 6.19: Serenade's BPF Input Return Loss simulation vs. bench results.

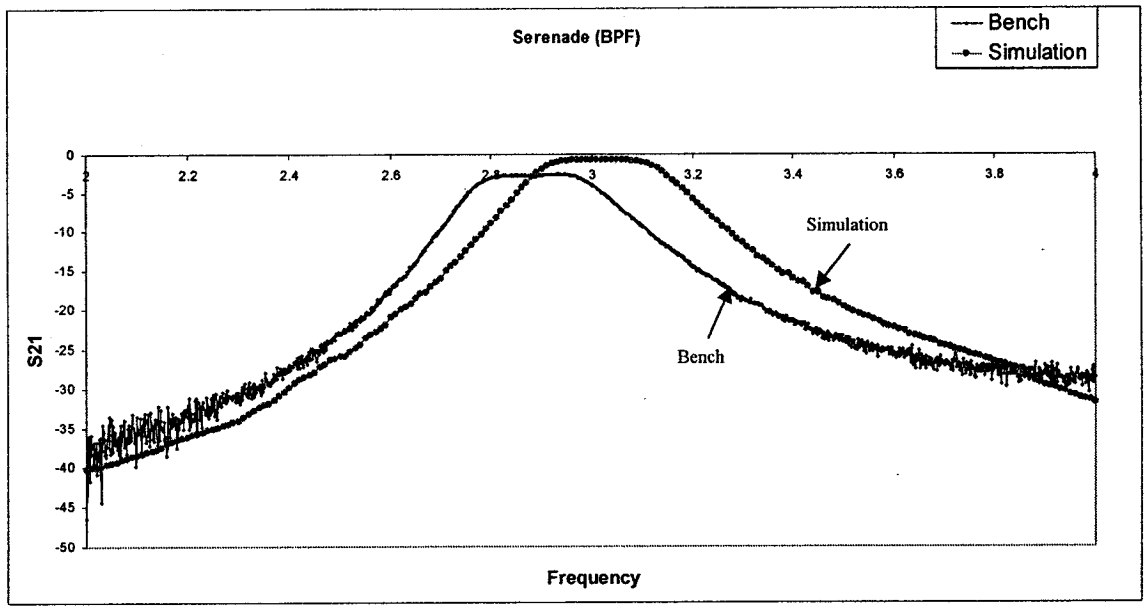

Figure 6.20: Serenade's BPF Frequency Response simulation vs. bench results.

Also, comparing Serenade's simulation results with its corresponding bench results, similar to PUFF's behavior, the frequency shift in both frequency response and return loss can be noticed. This frequency shift from 3.0GHz (which is the design center frequency, f_c) to 2.9072GHz (Δf_c of 92.8MHz), which is a smaller shift than the frequency shift experienced with PUFF. Since the frequency shift is smaller in Serenade than PUFF, this implies that the fringing fields are partially accounted for in Serenade. The measured frequency response is slightly wider than its simulation response, but it is smaller than that obtained by PUFF. Also, assuming no frequency shift, we can see a smaller difference in insertion loss, S21 (-1.775dB @ 2.9072GHz for measured on bench vs. –0.77dB @ 3.0GHz for simulation). The difference in return loss (S11) and (S22) is also smaller than that obtained from PUFF (-11.479dB @ 2.9072GHz for measured on bench vs. –16.75dB @3.0GHz for simulation).

The insertion loss of the two SMA connectors adds to the total insertion loss of the filter. This extra loss, which was measured separately on the same Network Analyzer amounts to 0.15dB for each connector (total of 0.30dB). This extra loss should be subtracted from the total insertion loss values measured on the bench to obtain the filter's loss. The electrical delay added by the two connectors is not a concern for this thesis discussion.

In conclusion, the frequency shift depicted by Serenade was closer to the center frequency by 100MHz than obtained by PUFF. Also, the insertion loss depicted by Serenade simulation was also closer to the real measurement than PUFF depicted. These are indications that the coupled transmission lines are modeled more accurately in Serenade than in PUFF.

7. THE 3-DB 90° HYBRID

7.1 Theory

The 3dB 90° hybrids (also known as quadrature hybrids or branch-line couplers) are 3dB directional couplers that have 90° phase difference between the "through" (port2) and "coupled" (port3) arms as shown in Figure 7.1 [57].

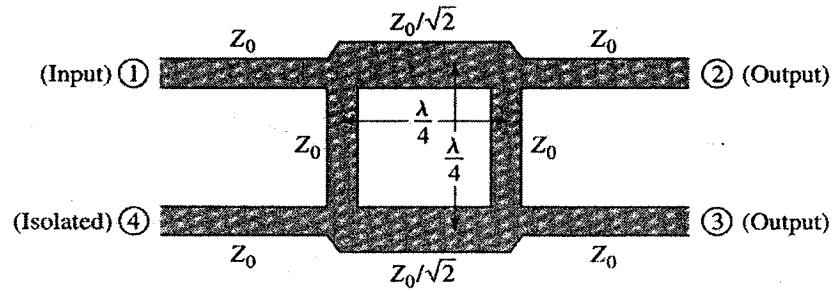

Figure 7.1: Quadrature hybrid.

As can be seen in Figure 7.1, power from the input port is distributed equally to the "through" and "coupled" arms, with a phase difference of 90° between the two output ports; further, owing to the geometry's symmetry, any one of the ports can be used as the input port.

The equivalent circuit of the hybrid coupler and the decomposition of the equivalent circuit into even-mode and odd-mode excitations are shown in Figure 7.2 [58] and Figure 7.3 [59] respectively.

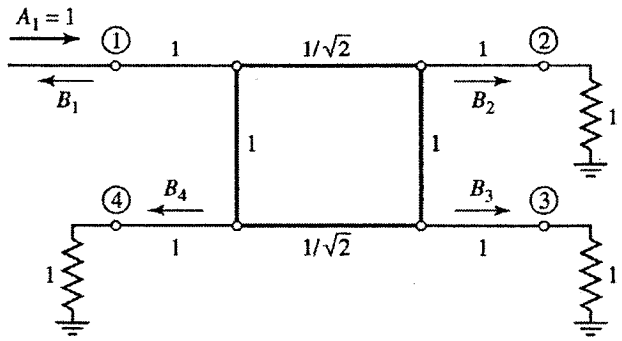

Figure 7.2: Equivalent circuit of 3dB 90° hybrid.

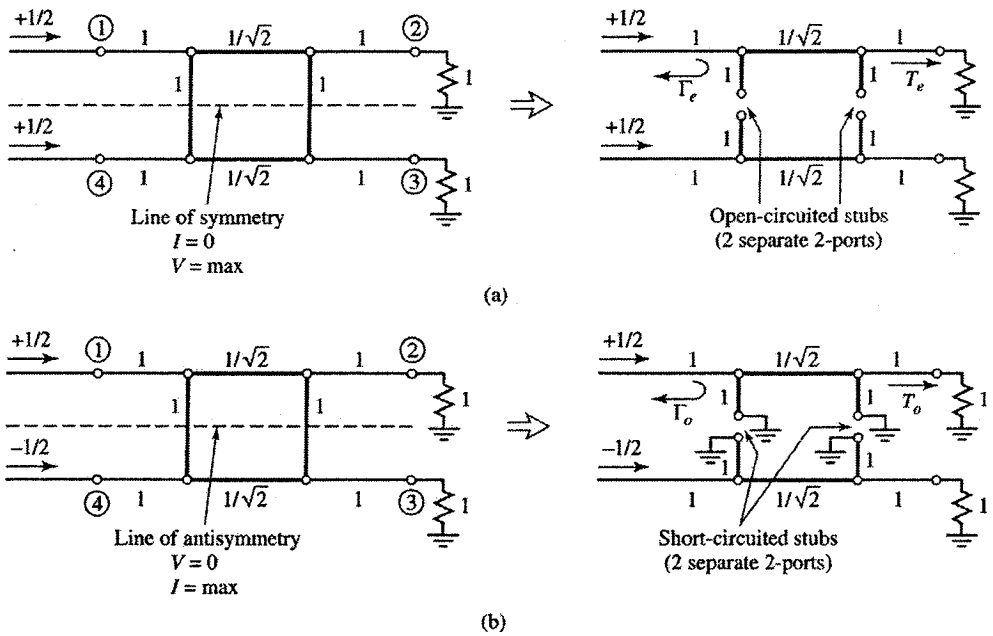

Figure 7.3: Even- and odd-mode excitations of equivalent circuit. (a) Even mode. (b) Odd mode.

The wave amplitudes are given by

$$B_1 = \frac{1}{2}\Gamma_e + \frac{1}{2}\Gamma_o \tag{7.3.1a}$$

$$B_2 = \frac{1}{2}T_e + \frac{1}{2}T_o \tag{7.3.1b}$$

$$B_3 = \frac{1}{2}T_e - \frac{1}{2}T_o \tag{7.3.1c}$$

$$B_4 = \frac{1}{2}\Gamma_e - \frac{1}{2}\Gamma_o . \tag{7.3.1d}$$

where $\Gamma_{e,o}$ and $T_{e,o}$ are even-mode and odd-mode reflection and transmission coefficients. Using (7.3.1), it can be shown that the scattering matrix for the branch-line coupler is of the form

$$[S] = \frac{-1}{\sqrt{2}}\begin{bmatrix} 0 & j & 1 & 0 \\ j & 0 & 0 & 1 \\ 1 & 0 & 0 & j \\ 0 & 1 & j & 0 \end{bmatrix}. \tag{7.3.2}$$

Design of the branch-line impedances is trivial; given an external line of characteristic impedance Z_0, it can be seen from Figure 7.2 that the branch-line impedances are given by $Z_0/\sqrt{2}$.

Lastly, it should be noted that the quarter-wavelength requirement of the 3dB 90° hybrid limits the bandwidth of single stage couplers to 10-20%. Greater bandwidths can be attained by cascading sections.

7.2 Design

The important parameters required to design the 3dB 90° hybrid are the trace widths of the "*series*" and "*shunt*" arms which are $Z_0/\sqrt{2}$ (35.35Ω) and Z_0 (50Ω) respectively, and their electrical length which is 90° (quarter-wave long, $\lambda_c/4$) at the desired center frequency, f_c. Once the nominal lines impedances and lengths are established as independent elements, depending on the substrate material (εr) and thickness (h), the transmission lines are connected together (as shown in Figure7.1) to obtain the complete circuit. These connections form discontinuities (impedance mismatch) at the 4 junctions, which may add parasitic elements, typically capacitive. Therefore, the final circuit may require tuning (trace widths and lengths) to optimize its performance. Tuning the transmission lines widths results in optimizing for even power split (3-dB) in the two output ports. It also improves isolation between ports (1) & (4) and ports (2) & (3), and also return loss (matching) at all 4 ports. Optimizing phase delay relationship between relative ports can be achieved by tuning the transmission lines lengths.

To allow for 4 SMA connectors to be soldered to the PCB for bench measurements, short 50Ω lines will be added to all 4 ports. These transmission lines and SMA connectors will introduce extra phase delay and insertion loss to the circuit which will be discussed and compensated for during the simulation and bench measurements.

The design parameters used in PUFF are:

Series arm: $Z_f = 50\Omega$, $L_f = 90°$,

Shunt arm: $Z_e = 50\Omega$, $L_e = 90°$.

The physical dimensions obtained from PUFF are:

Series arm: $W_f = 3.022$mm, $L_f = 14.894$mm,

Shunt arm: $W_e = 1.824$mm, $L_e = 15.197$mm.

The physical dimensions used in Serenade are:

Series arm: $W_f = 3.0$mm, $L_f = 14.9$mm,

Shunt arm: $W_e = 1.825$mm, $L_e = 14.7$mm.

7.3 Simulations

Presented next in this section are the simulation results of the 3-dB 90° hybrid from both simulators, PUFF and Serenade.

7.3.1 PUFF Simulation Results:

Using the design equations and procedure presented in Section 7.2 for the 3-dB 90° hybrid design example, presented below is the graph obtained from PUFF using the "*ideal*" transmission line model:

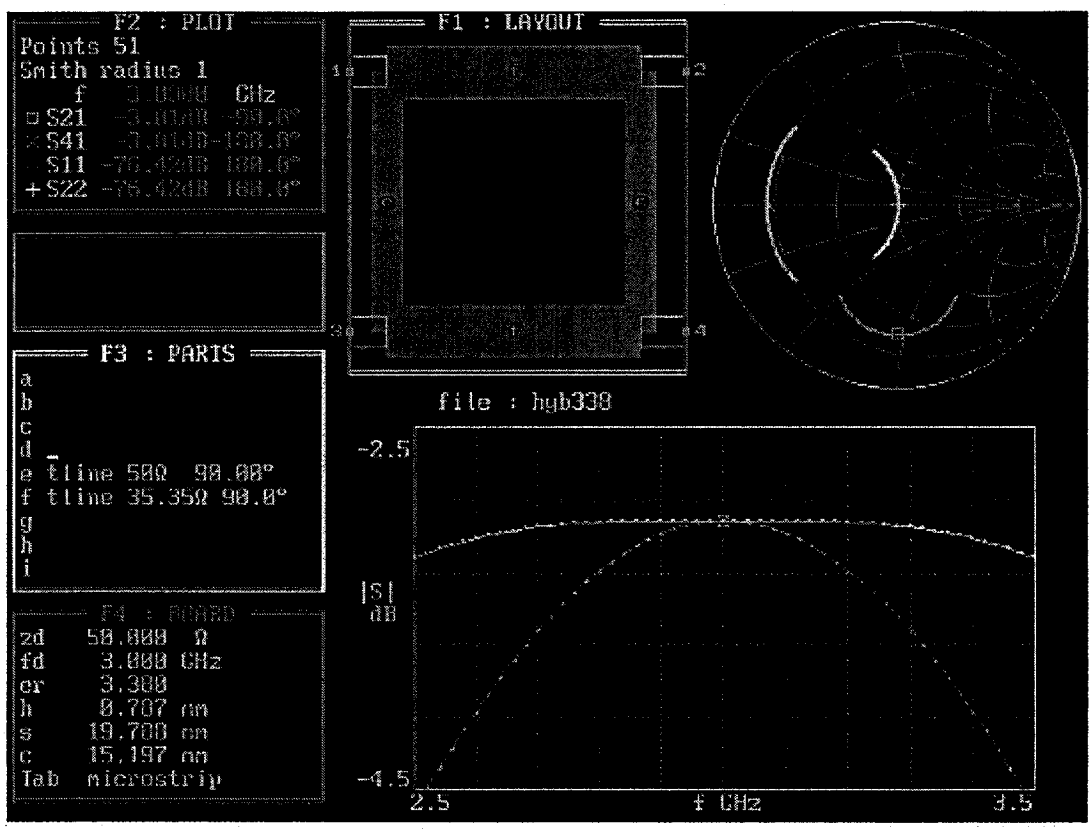

Figure 7.4: Frequency Response in "through" and "coupled" ports (S21 & S41) using "*Ideal*" transmission line (*tline*) model for the 3-dB 90° hybrid in PUFF.

From the results in the above graph, it can be seen that the insertion loss in the "through" and "coupled" arms (S21) and (S41) is –3.01dB. The return loss at all 4 ports is –76.42dB.

Also presented below is the graph obtained from PUFF using the "*advanced*" transmission line model:

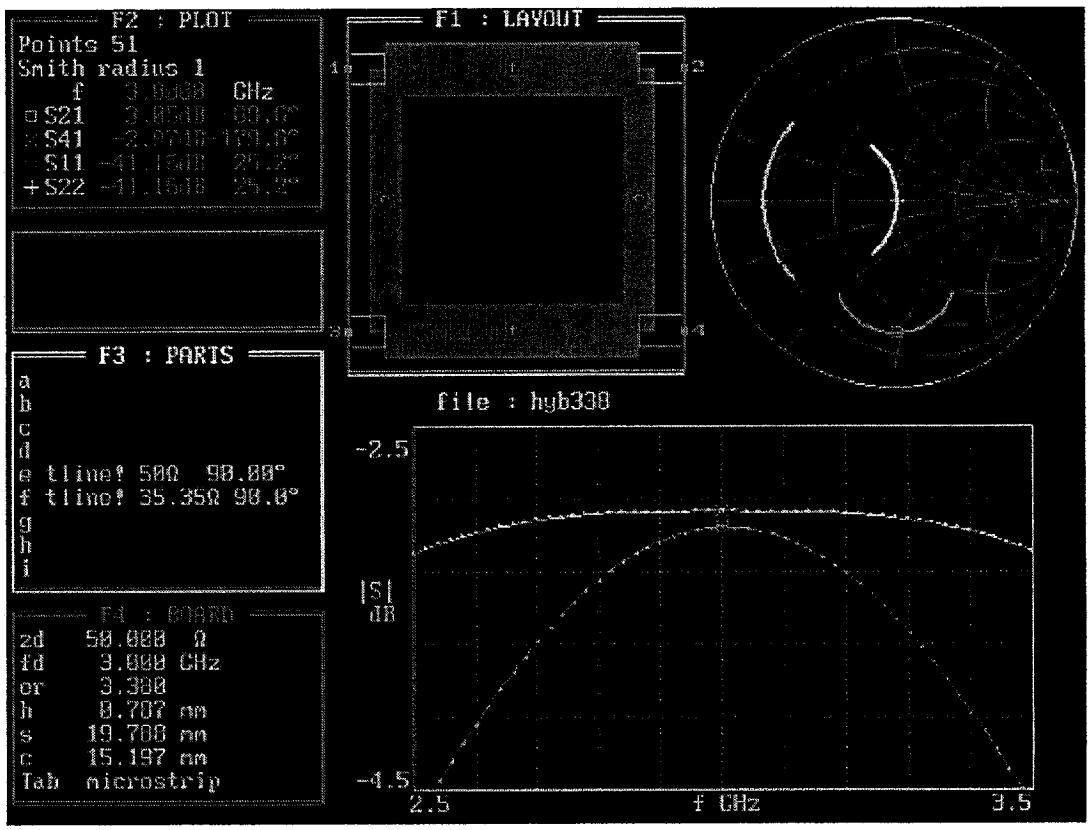

Figure 7.5: Frequency Response in "through" and "coupled" ports (S21 & S41) using "*advanced*" transmission line (*tline!*) model for the 3-dB 90° hybrid in PUFF.

From the results in the above graph, it can be seen that the insertion loss in the "through" and "coupled" arms (S21) and (S41) are –3.05dB and –2.97dB respectively. The return loss at all 4 ports is –41.16dB.

It should be noted that the frequency response results in both cases, "*ideal*" and "*advanced*", are extremely similar to each other for both arms (S21) & (S41) as shown in Figure 7.6 and Figure7.7 respectively.

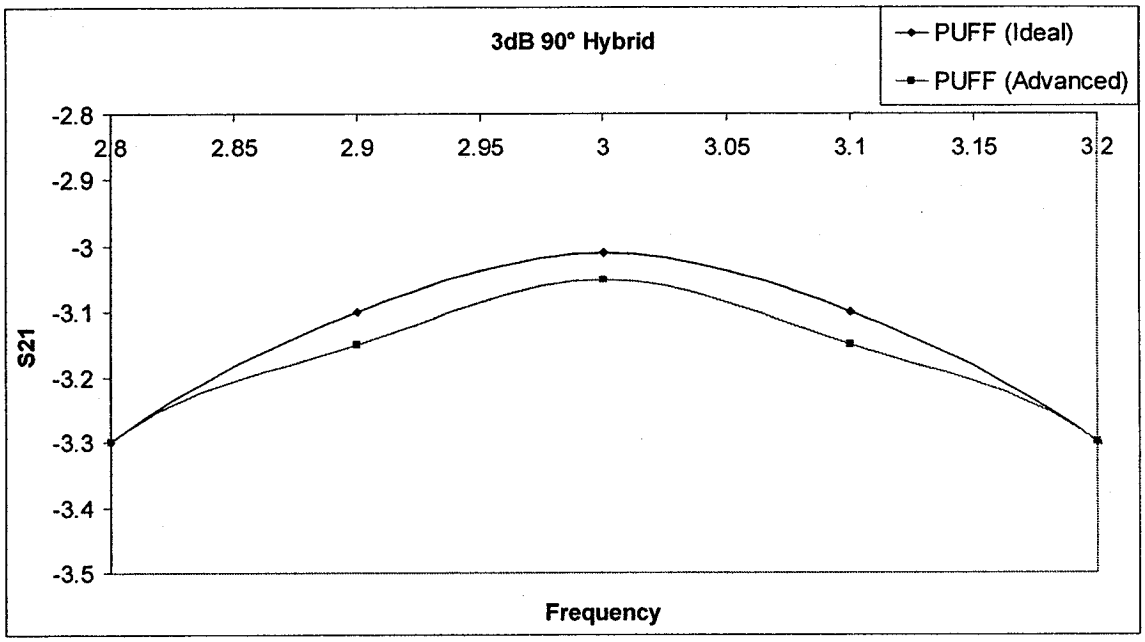

Figure 7.6: PUFF's (S21) comparison between "*ideal*" and "*advanced*" models for the 3-dB 90° hybrid. S21 in dB vs. frequency in GHz.

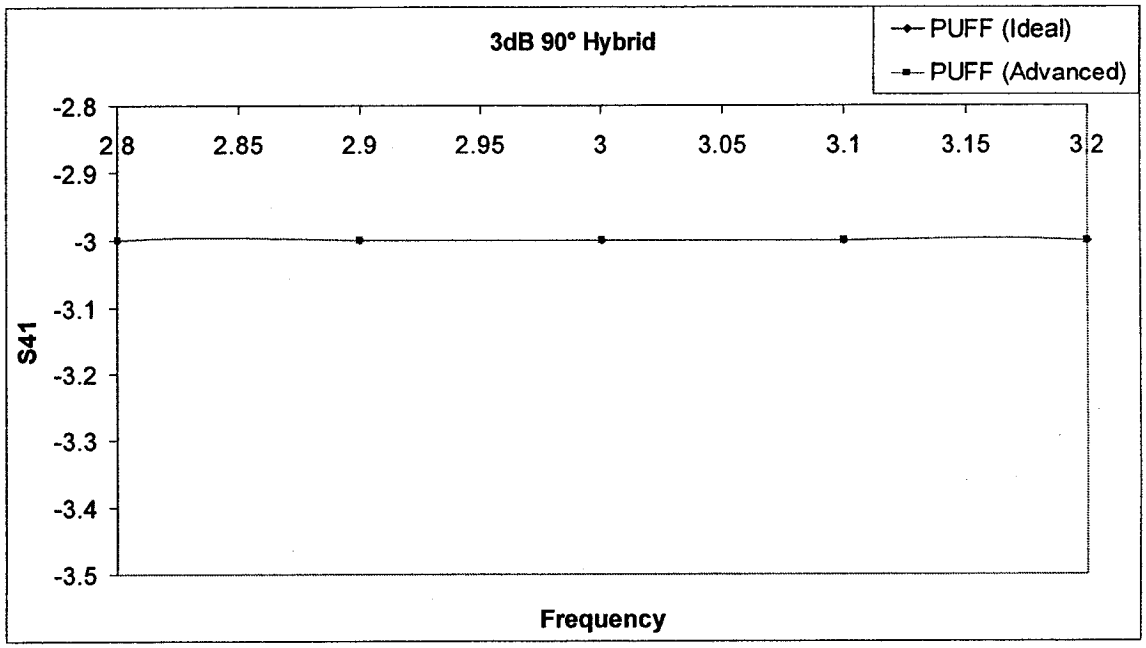

Figure 7.7: PUFF (S41) comparison between "*ideal*" and "*advanced*" models for the 3-dB 90° hybrid. S11 in dB vs. frequency in GHz.

It is clear from Figure 7.6 and Figure 7.7 that the frequency response of the "through" and "coupled" (S21 and S41) arms of both the "*ideal*" and "*advanced*" models are significantly close to each other. For this reason, only the "*advanced*" transmission line model will be analyzed on the bench. The analysis and comparison will be discussed in Section 7.5.

7.3.2 Serenade Simulation Results:

Using the design equations and procedure presented in Section 7.2 for the 3-dB 90° hybrid design example, presented below are the graphs obtained from Serenade:

Return loss at all 4 ports (S11, S22, S33 and S44):

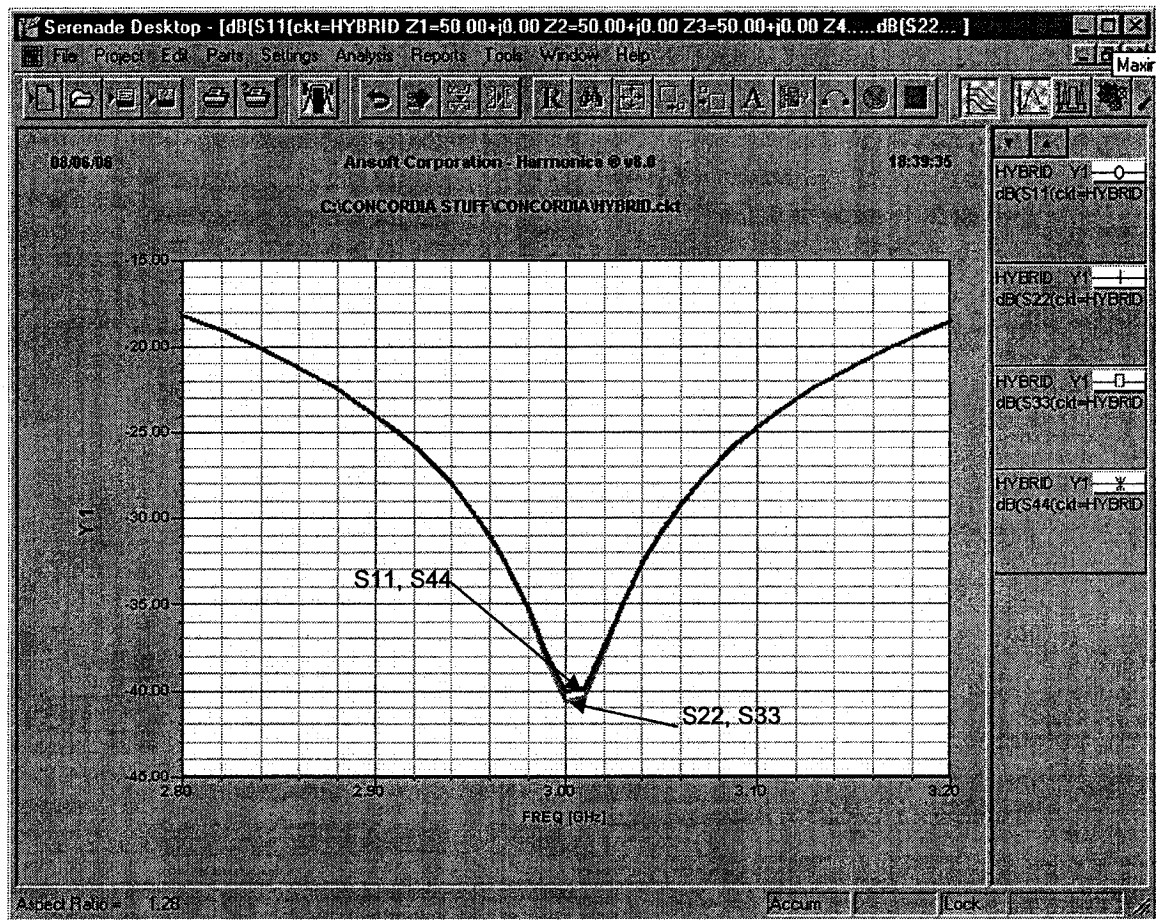

Figure 7.8: Serenade's Return Loss (S11, S22, S33 & S44) for the 3-dB 90° hybrid.

As can be seen in the above graph, the return loss at all 4 ports is –40dB at 3GHz.

Insertion loss in the "through" and "coupled" arms (S21 and S31):

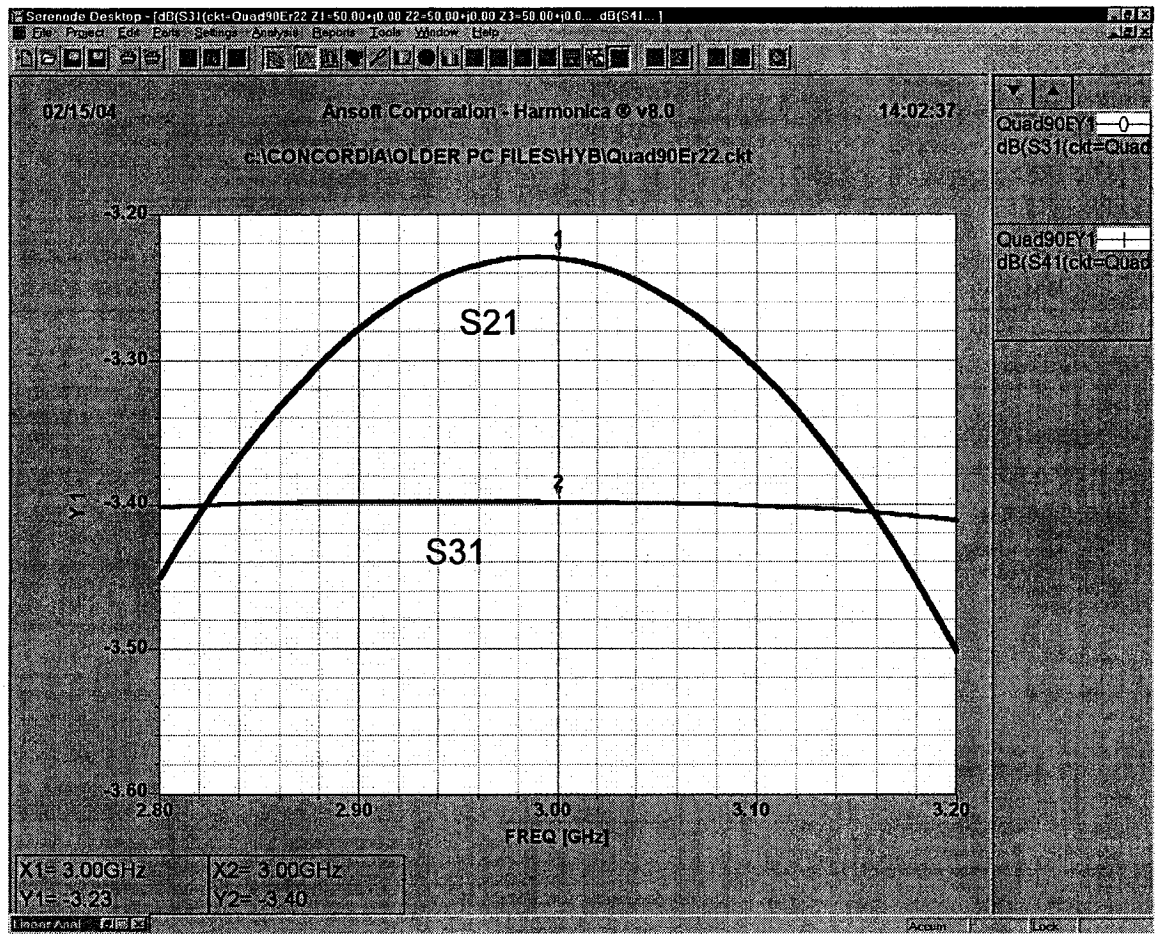

Figure 7.9: Serenade's Frequency Response in "through" and "coupled" ports (S21 & S31) for the 3-dB 90° hybrid. Curve 1 is S21 and curve 2 is S31.

As can be seen in the above graph, insertion loss in both output arms (S21 and S31) is -3.23dB and -3.4dB respectively at 3GHz.

Isolation between ports 1 and 4 (S41):

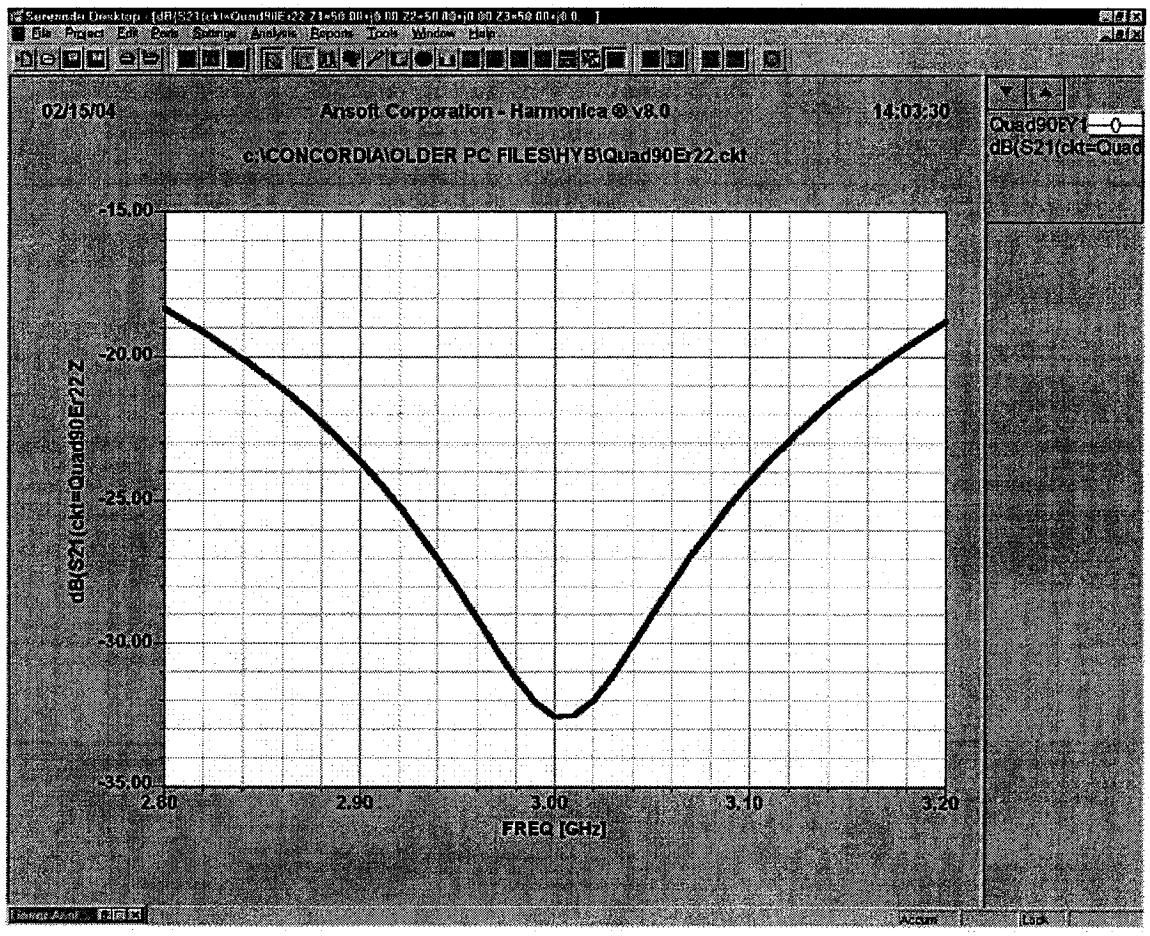

Figure 7.10: Serenade's Isolation (S41) for the 3-dB 90° hybrid.

As can be seen in the above graph, the isolation between ports 1 and 4 (S41) is –32.5dB at 3GHz. In theory, no power should be coupled to port 4.

In all of these results it is important to note that the return loss and isolation are strongly dependent on frequency whereas the coupling and through signals are not.

Phase delay in the "through" arm, Ang(S21):

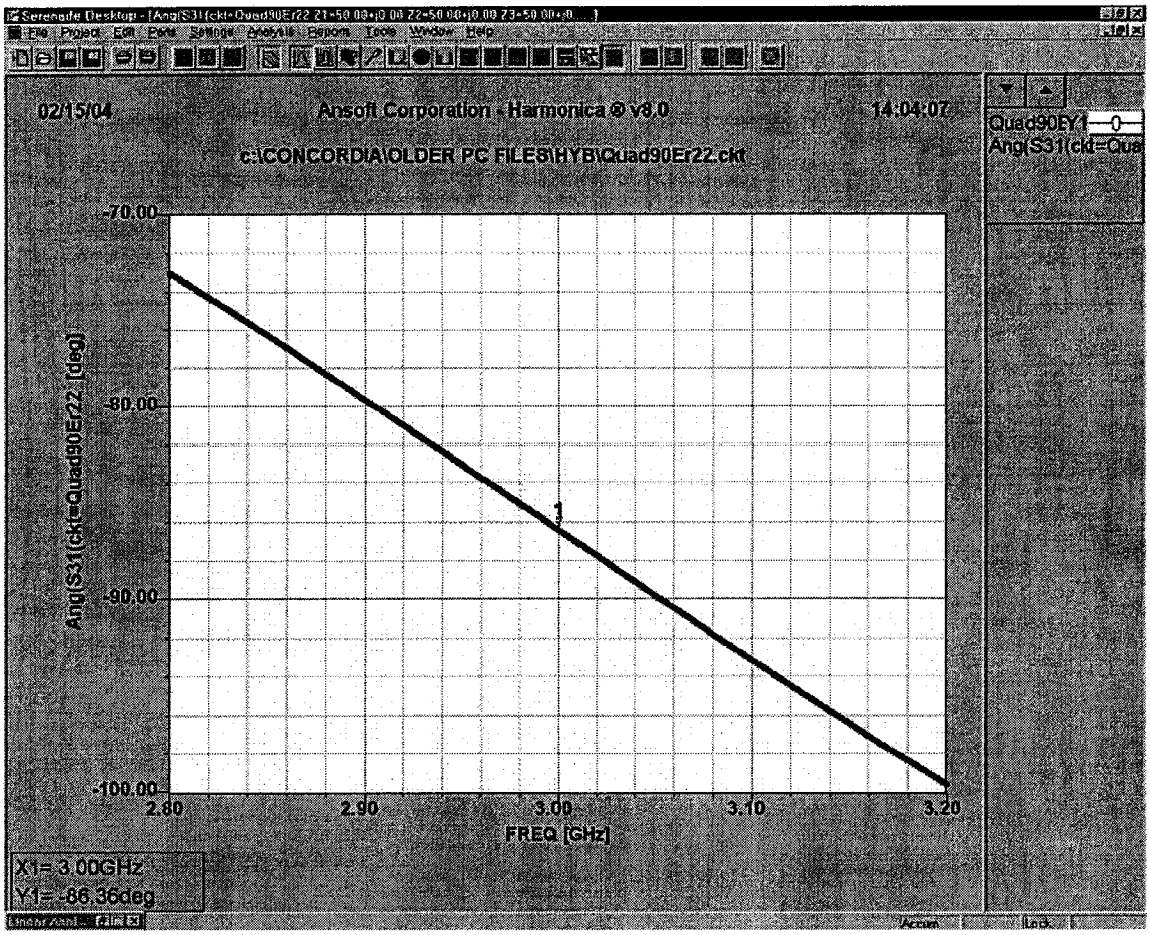

Figure 7.11: Serenade's Phase Delay in the "through" arm (Ang(S21)) for the 3-dB 90° hybrid.

As can be seen in the above graph, phase delay in the "through" arm Ang(S21) is –86.36° at 3GHz.

Phase delay in the "coupled" arm, Ang(S31):

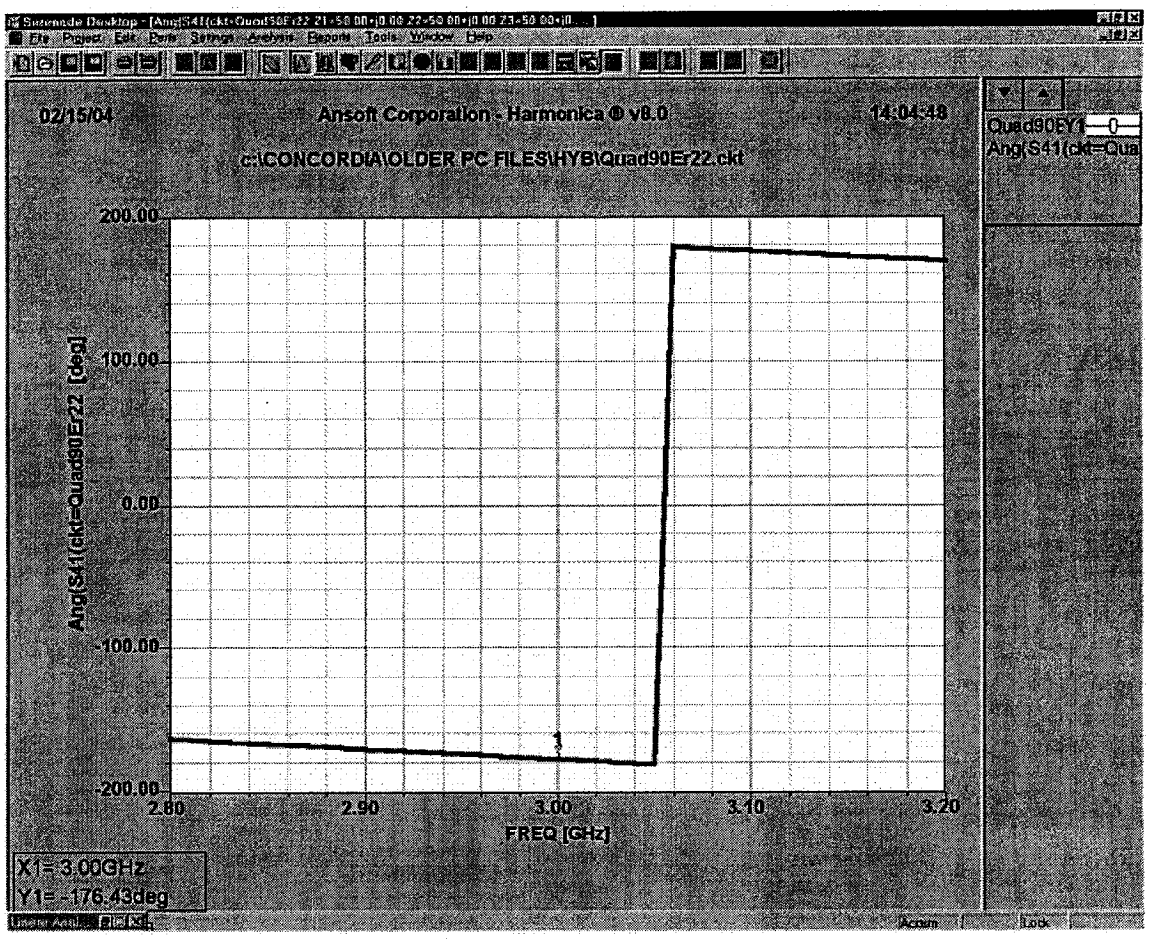

Figure 7.12: Serenade's Phase Delay in the "coupled" Port (Ang(S31)) for the 3-dB 90° hybrid.

As can be seen in the above graph, phase delay in the "coupled" port 3 (Ang(S31)) is – 176.43° at 3GHz.

From these results, it is seen that the through and coupled signals are 90° apart, as expected.

Phase delay in the Isolation port, Ang(S41):

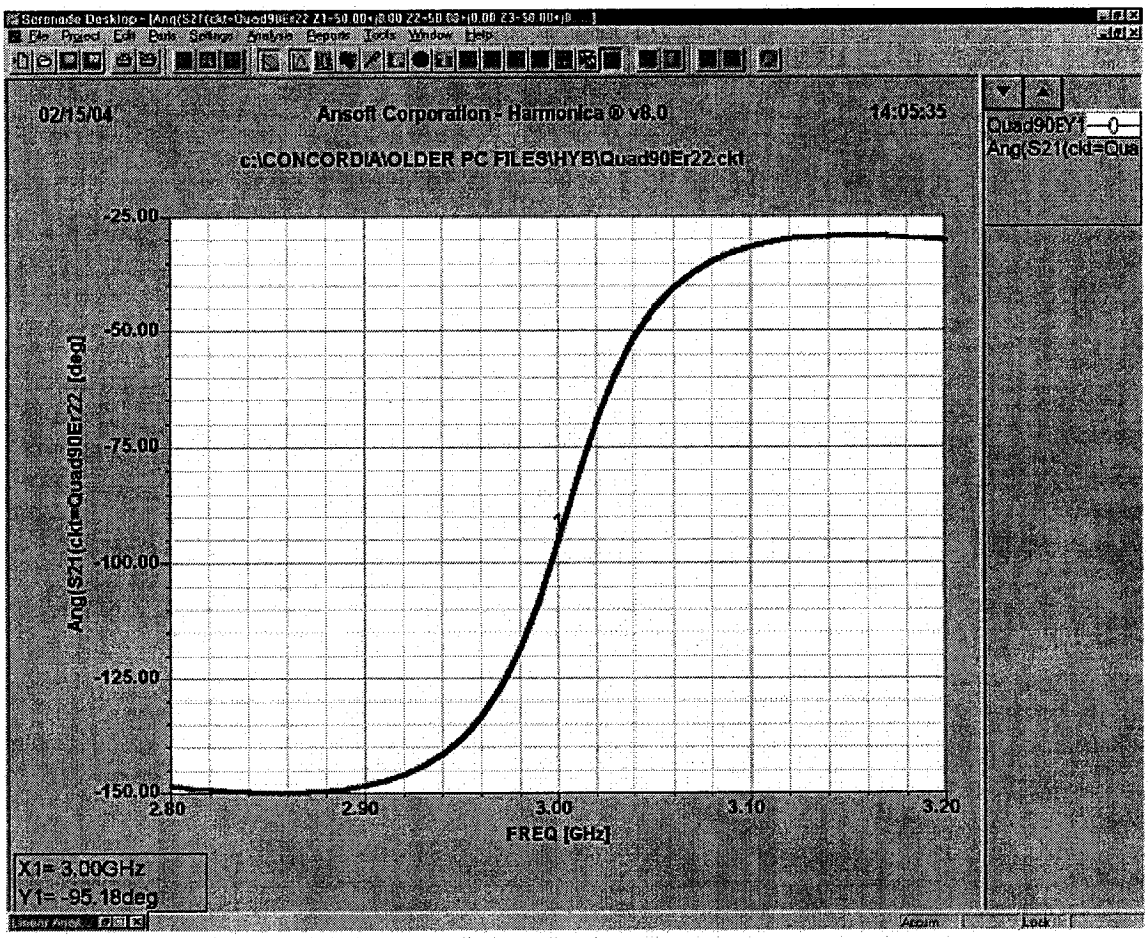

Figure 7.13: Serenade's Phase Delay in "Isolated" port (Ang(S41)) for the 3-dB 90° hybrid.

As can be seen in the above graph, the phase delay in the "isolated" port, Ang(S41) is – 95.18° at 3GHz. The expected value for the phase delay in the isolated port is 90°.

The bench results for both PUFF ("*advanced*" model) and Serenade circuits will be presented in the following section.

7.4 Measurements

Using Agilent's Network Analyzer 8720ES to measure the circuits on the bench, presented next are results of both circuits from PUFF and Serenade designs. Figure 7.14 is a picture of the hybrid to be measured on the bench.

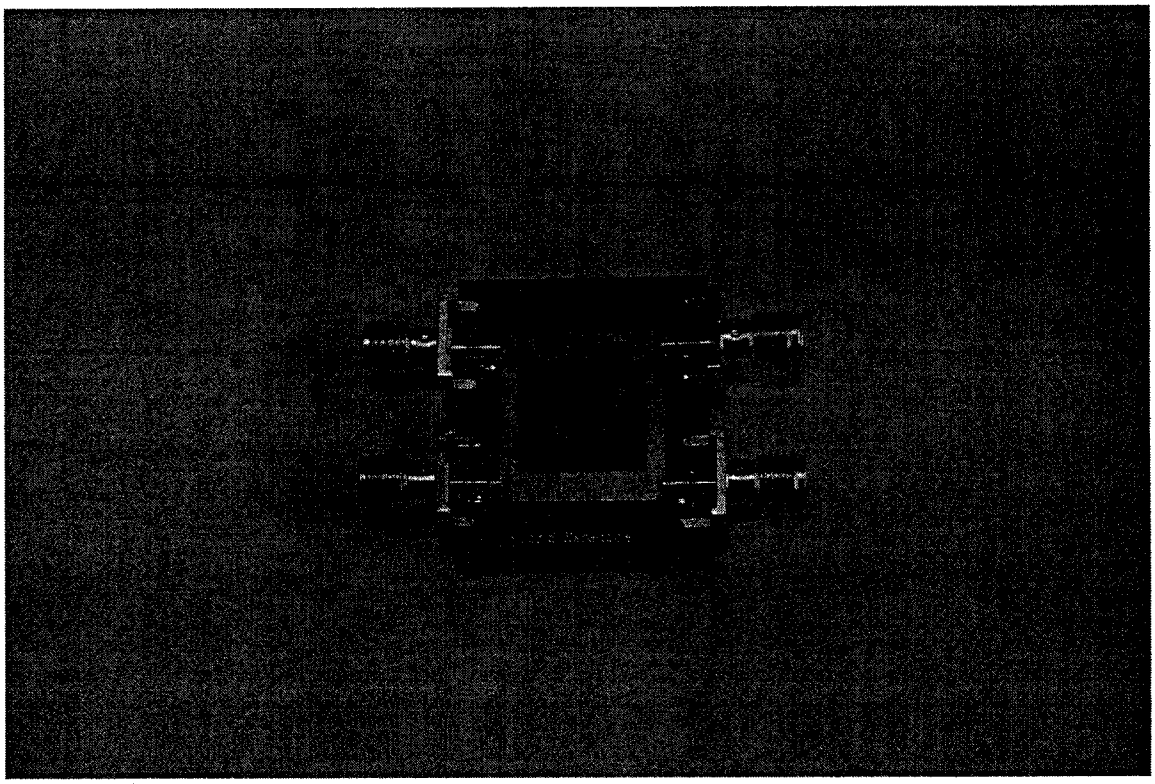

Figure 7.14: Picture of the 3dB 90° Hybrid.

7.4.1 PUFF Circuit:

Presented firstly is the network analyzer screen shot of the return loss (S22) at "port 2" of the 3-dB hybrid and the insertion loss (S21) in the 90° "through" arm:

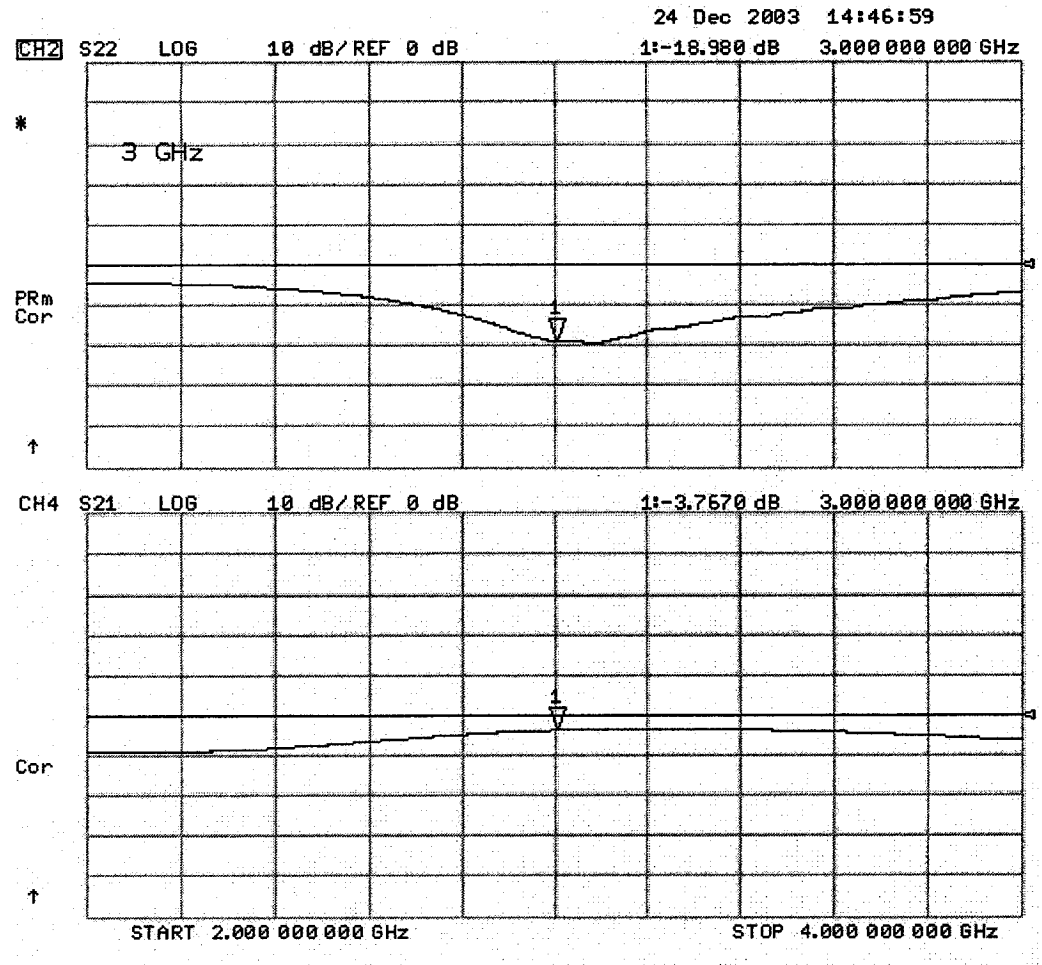

Figure 7.15: PUFF's bench measurements Return Loss & Frequency Response in the "through" arm (S22 & S21) for the 3-dB 90° hybrid.

As can be seen in the above graph, the return loss at port 1 (S11) and port 2 (S22) is equal to –18.98dB at 3GHz. The insertion loss in port 2 (S21) is equal to –3.767dB at 3GHz. Presented next is the network analyzer screen shot of the return loss (S33) at port 3 of the hybrid and the insertion loss (S31) in the 180° "coupled" arm:

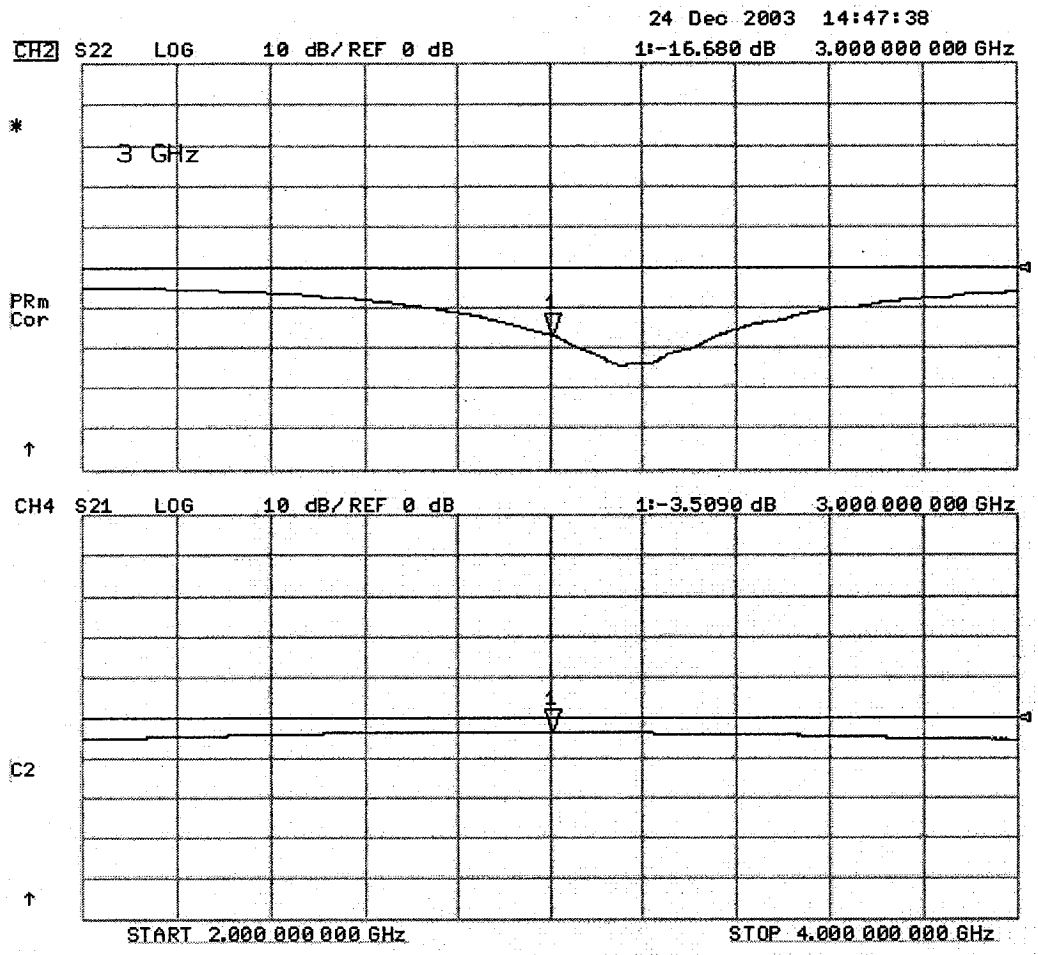

Figure 7.16: PUFF's bench measurements Return Loss & Frequency Response in the "coupled" port (S33 & S31) for the 3-dB 90° hybrid.

As can be seen in the above graph, the return loss at port 3 (S33) is equal to –16.68dB at 3GHz. The insertion loss at 3 GHz in port3 (S31) is equal to –3.509dB.

Presented next is a snap shot of the isolation (S41) in port 4:

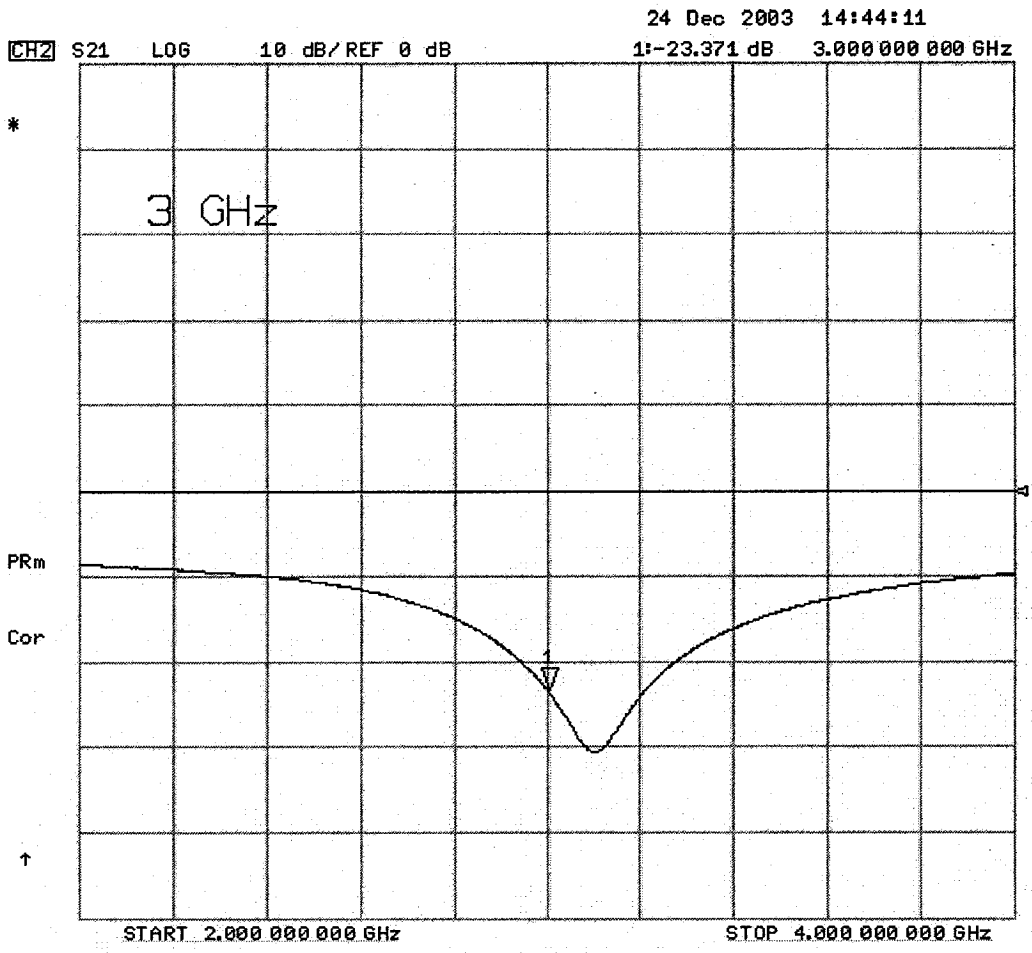

Figure 7.17: PUFF's bench measurements Isolation (S41) for the 3-dB 90° hybrid.

As can be seen in the above graph, the isolation between ports 1 and 4 (S41) is equal to – 23.371dB at 3GHz.

Presented next are the phase delay plots in ports 2, 3 and 4:

Ang (S21):

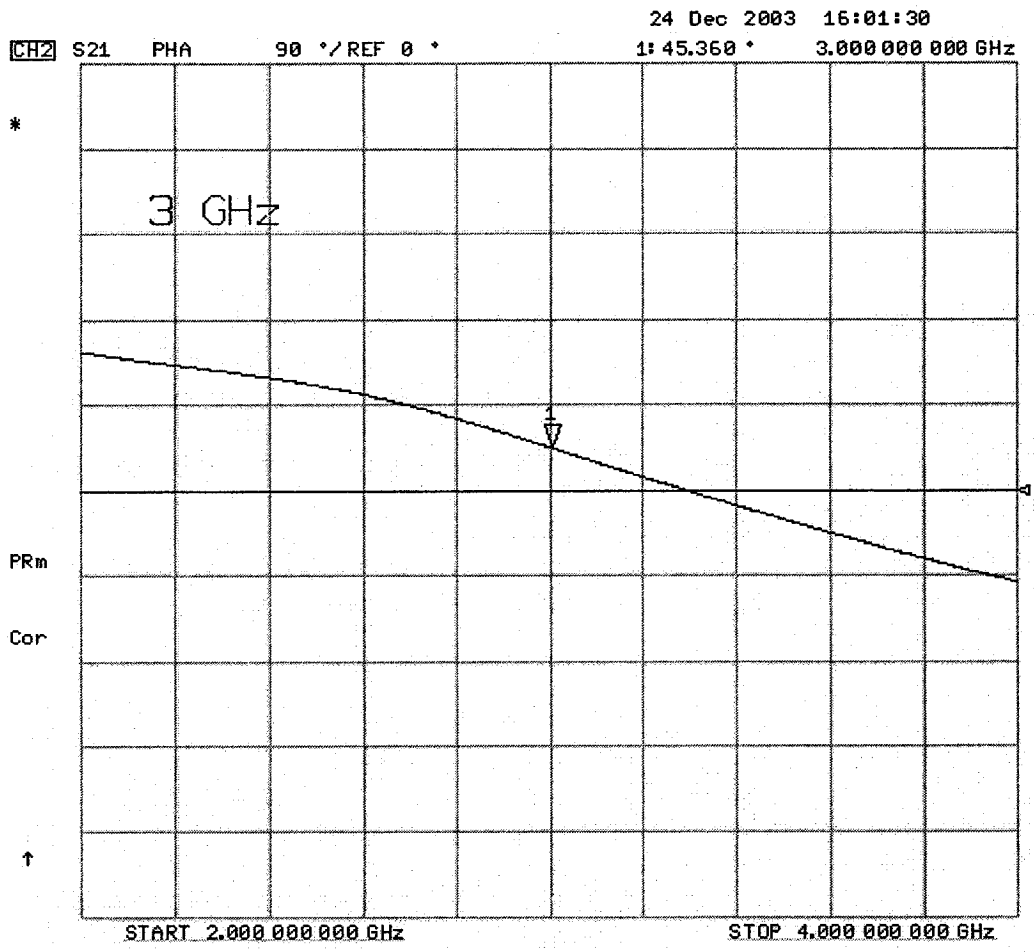

Figure 7.18: PUFF's bench measurements Phase Delay in "through" port (Ang(S21)) for the 3-dB 90° hybrid.

As can be seen in the above graph, the phase delay in the "through" port, Ang(S21), is equal to 45.36° at 3GHz.

Ang (S31):

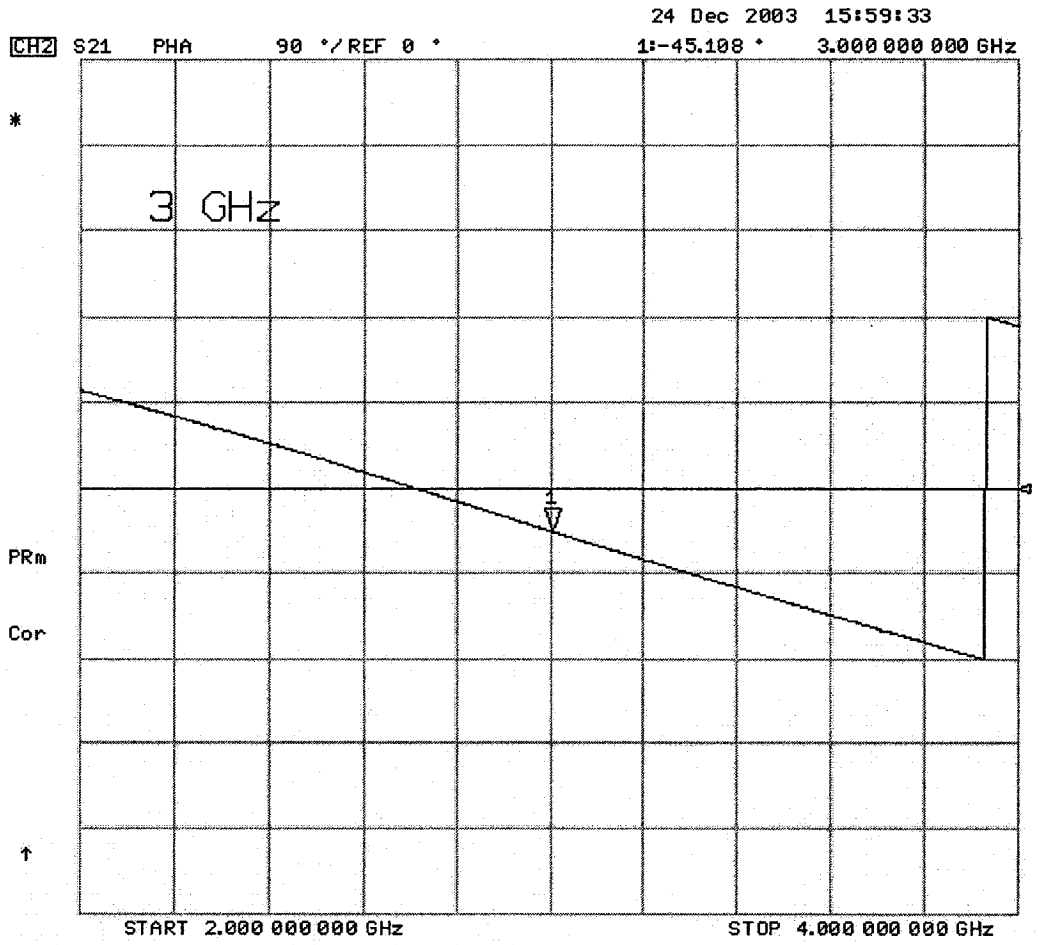

Figure 7.19: PUFF's bench measurements Phase delay in the "coupled" port (Ang(S31)) for the 3-dB 90° hybrid.

As can be seen in the above graph, the phase delay the "coupled" port, Ang(S31), is equal to -45.108° at 3GHz. The through and coupled ports are 90° apart.

Ang (S41):

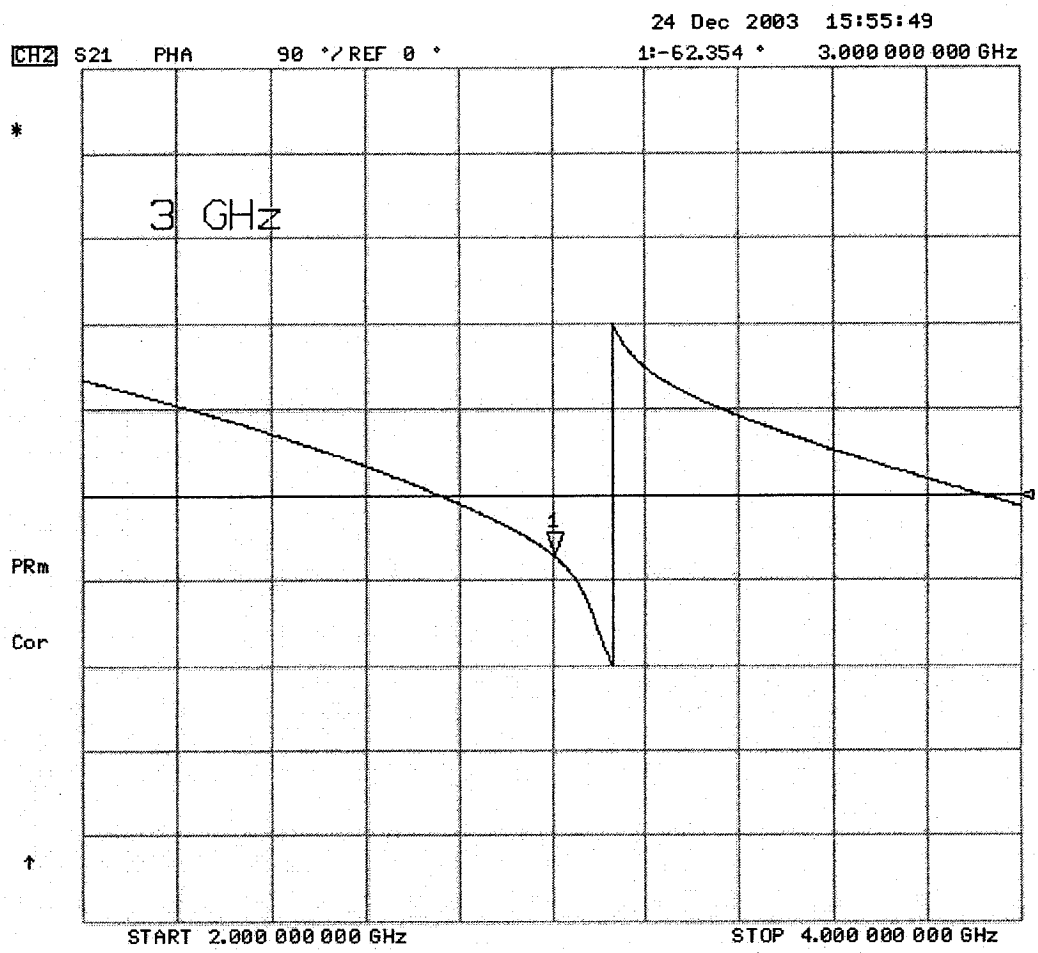

Figure 7.20: PUFF's bench measurements Phase delay in "Isolated" port (Ang(S41)) for the 3-dB 90° hybrid.

As can be seen in the above graph, the phase delay between ports 1 and 4, Ang(S41), is equal to -62.354° at 3GHz.

Please note that the extra insertion loss and phase delay introduced to the circuit from the SMA connectors soldered to the circuit boards and the 50Ω transmission lines have not been accounted for yet. They will be considered in the discussion section.

7.4.2 Serenade Circuit:

Presented firstly is a snap shot of the return loss (S22) at "port 2" of the 3-dB Hybrid and the insertion loss (S21) in the 90° through arm:

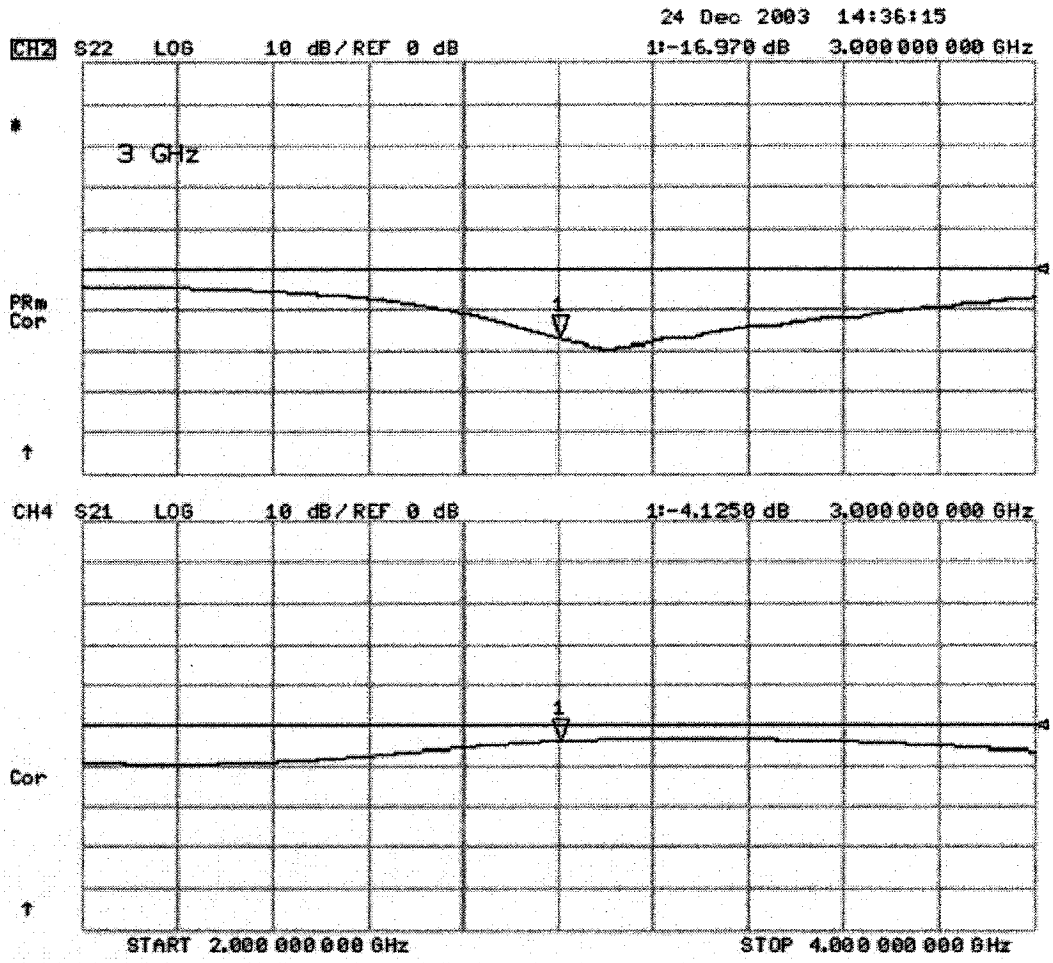

Figure 7.21: Serenade's bench measurements Return Loss & Frequency Response in "through" port (S22 & S21) for the 3-dB 90° hybrid.

As can be seen from the above graph, return loss at ports 1 and 2 (S11 & S22) is equal to –16.97dB at 3GHz. The insertion loss in port 2 (S21) is equal to –4.125dB at 3GHz.

Presented next is a snap shot of the return loss (S33) at "port 3" and the insertion loss (S31) in the 180° "through" arm:

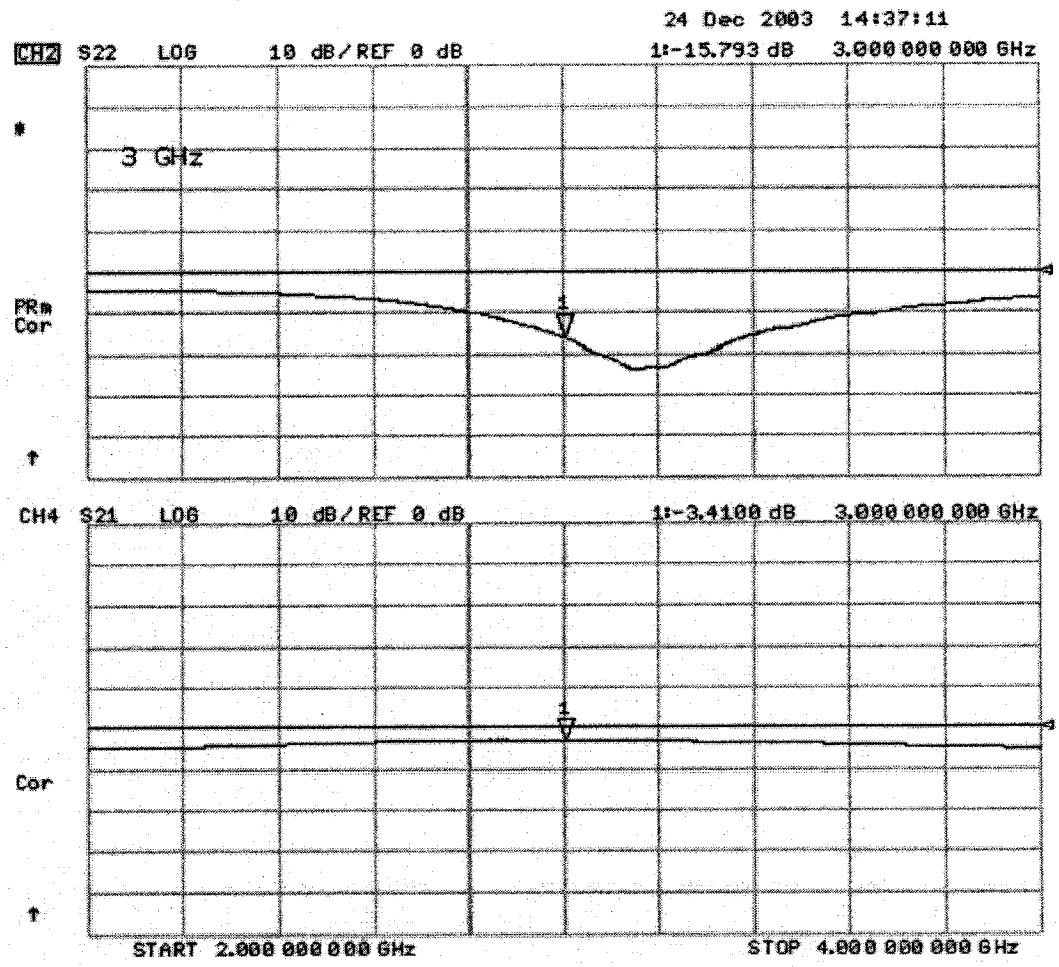

Figure 7.22: Serenade's bench measurements Return Loss & Frequency Response in the "coupled" port (S33 & S31) for the 3-dB 90° hybrid.

As can be seen from the above graph, the return loss at port 3 (S33) is equal to –15.793dB at 3GHz. The insertion loss in port 3 (S31) is equal to –3.41dB at 3GHz.

Presented next is a snap shot of the isolation (S41) in port 4:

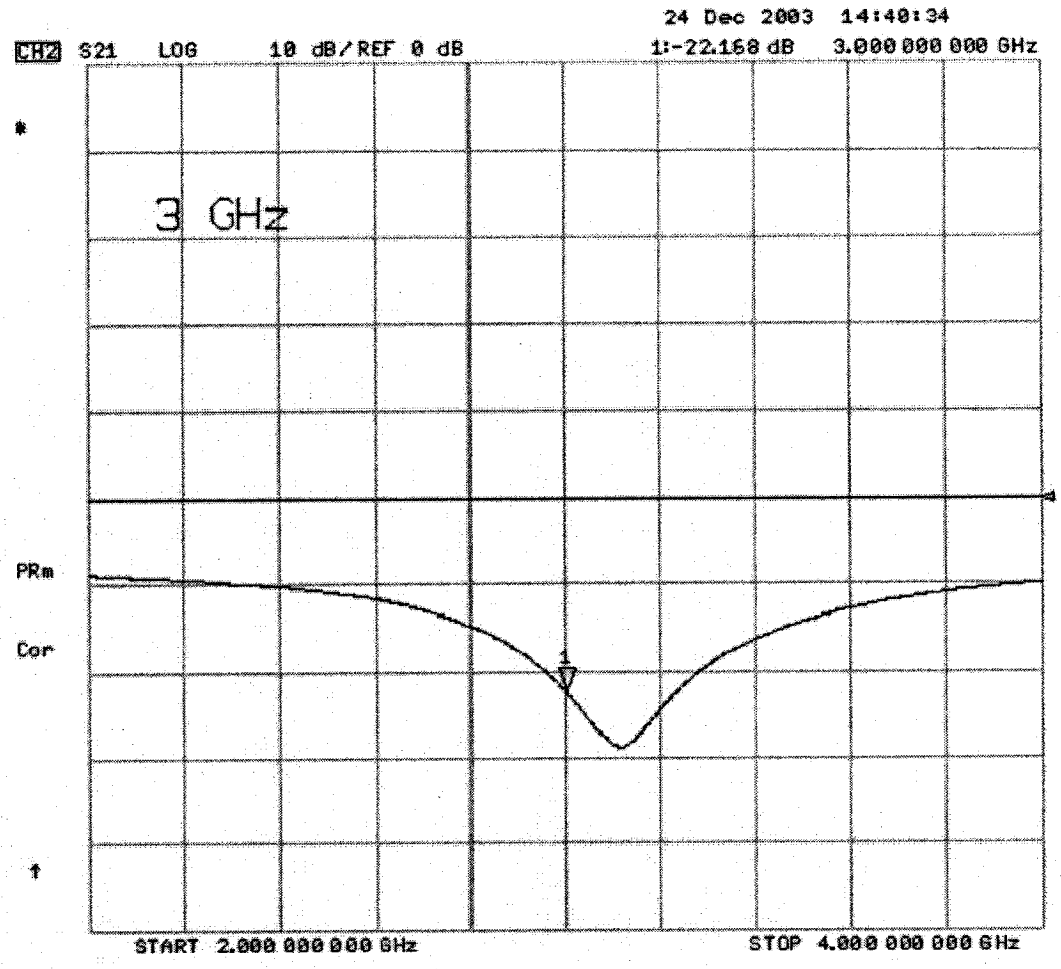

Figure 7.23: Serenade's bench measurements Isolation (S41) for the 3-dB 90° hybrid.

As can be seen in the above graph, isolation between ports 1 and 4 (S41) is equal to – 22.168dB at 3GHz.

Presented next are the phase delay graphs in ports 2, 3 and 4:

Ang (S21):

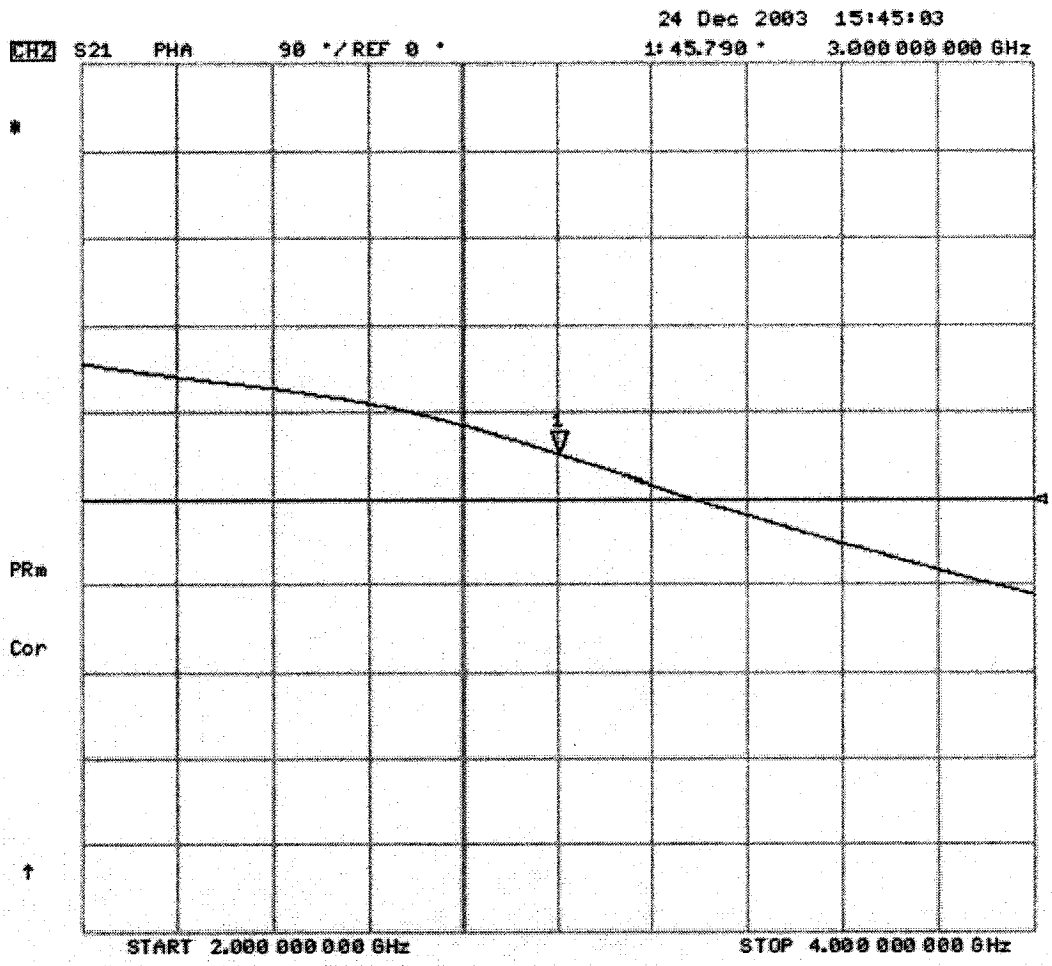

Figrue 7.24: Serenade's bench measurements Phase Delay in the "through" port (Ang(S21)) for the 3-dB 90° hybrid.

As can be seen from the above graph, the phase delay between ports 1 and 2, Ang(S21), is equal to 45.79° at 3GHz.

Ang (S31):

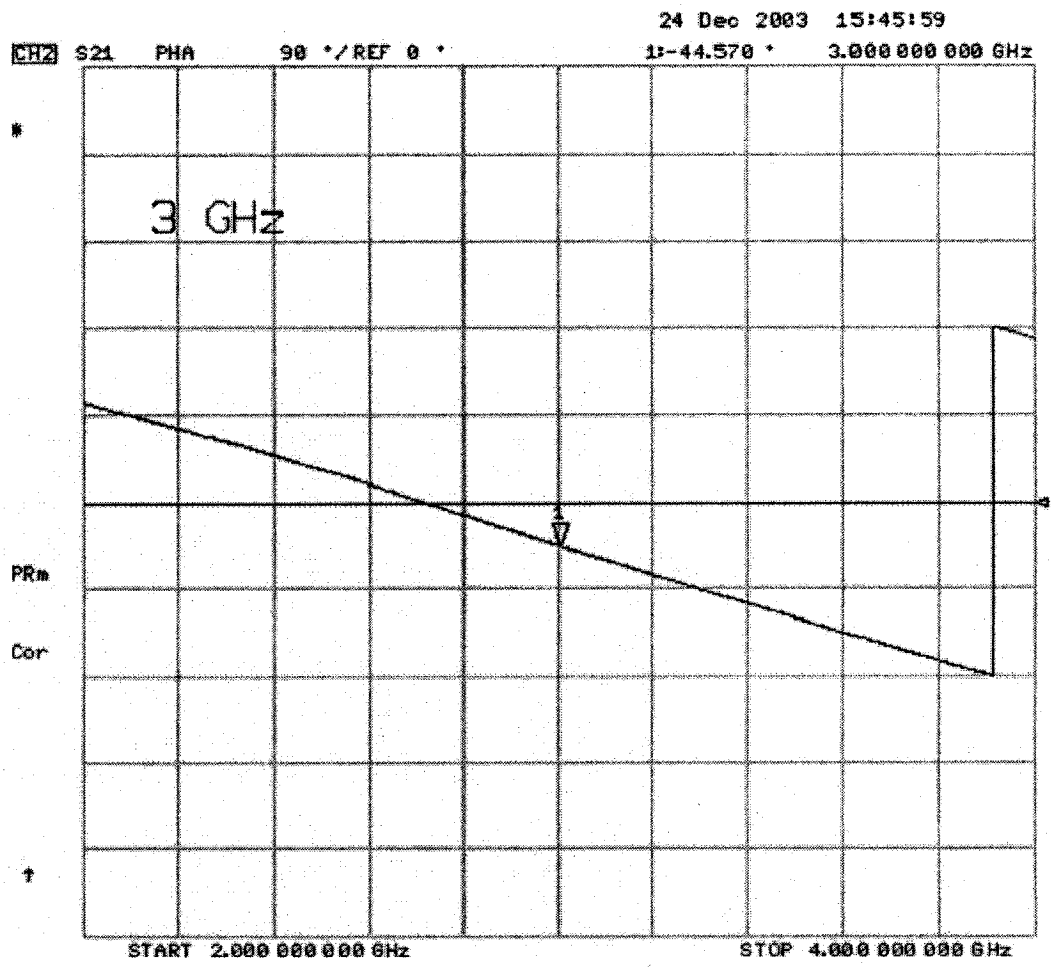

Figure 7.25: Serenade's bench measurements Phase Delay in the "coupled" port (Ang(S31)) for the 3-dB 90° hybrid.

As can be seen in the above graph, the phase delay between ports 1 and 3, Ang(S31), is equal to -44.57° at 3GHz.

Ang (S41):

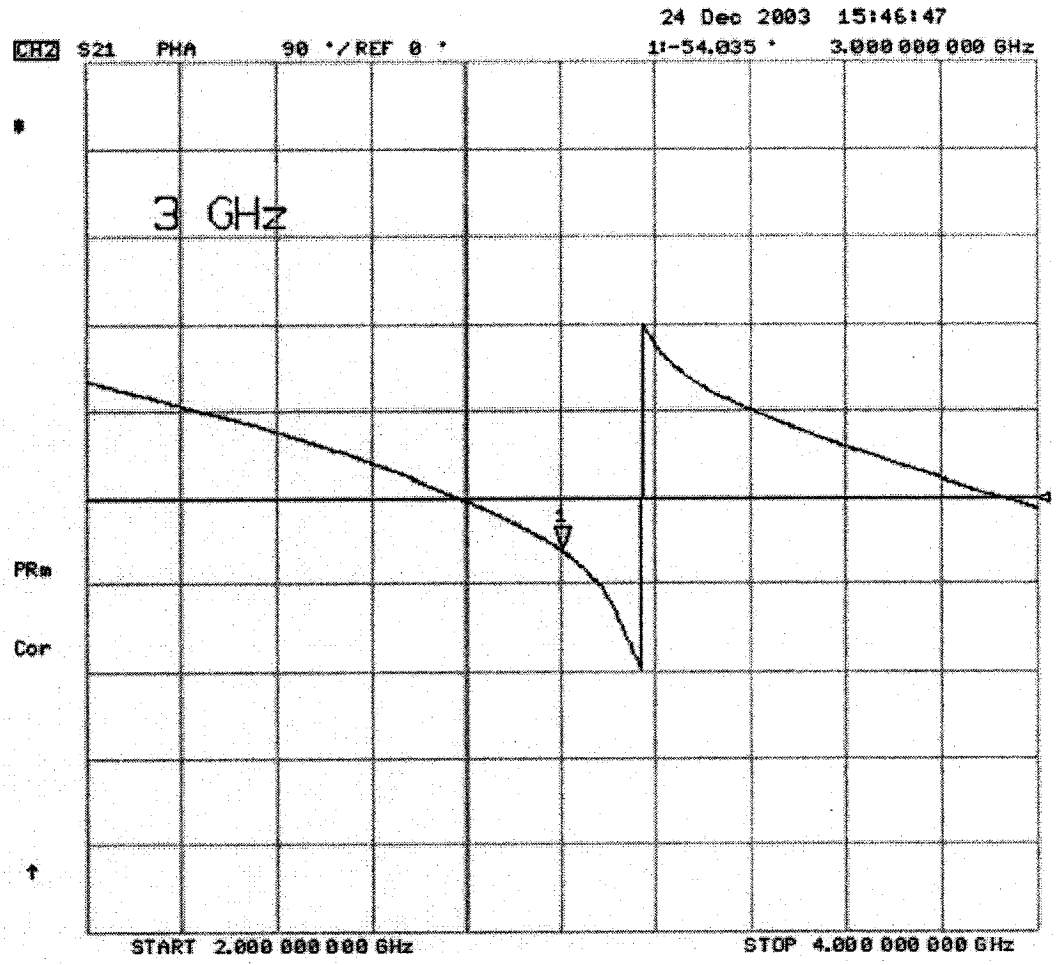

Figure 7.26: Serenade's bench measurements Phase Delay in the "Isolated" port (Ang(S41)) for the 3-dB 90° hybrid.

As can be seen in the above graph, the phase delay between ports 1 and 4, Ang(S41), is equal to -54.035° at 3 GHz.

Please note that the insertion loss and the phase delay introduced to the circuit from the SMA connectors soldered to the circuit board and the short 50Ω transmission lines have not been accounted for yet. They will be considered in the discussion section next.

The comparison between the simulation and bench results is discussed in the following section.

7.5 Discussion

The purpose of this section is to discuss and compare the simulation results obtained from PUFF ("*advanced*" model) and Serenade to their corresponding printed circuit boards' bench results. The graphs presented in this section are obtained from the simulation results and bench measurements for the hybrid coupler circuits presented in Sections 7.3 and 7.4 respectively.

Presented firstly are the frequency response plots obtained from PUFF, simulation and bench, for the "through" (S21) and "coupled" (S31) ports, shown in Figure7.27 and Figure7.28 respectively.

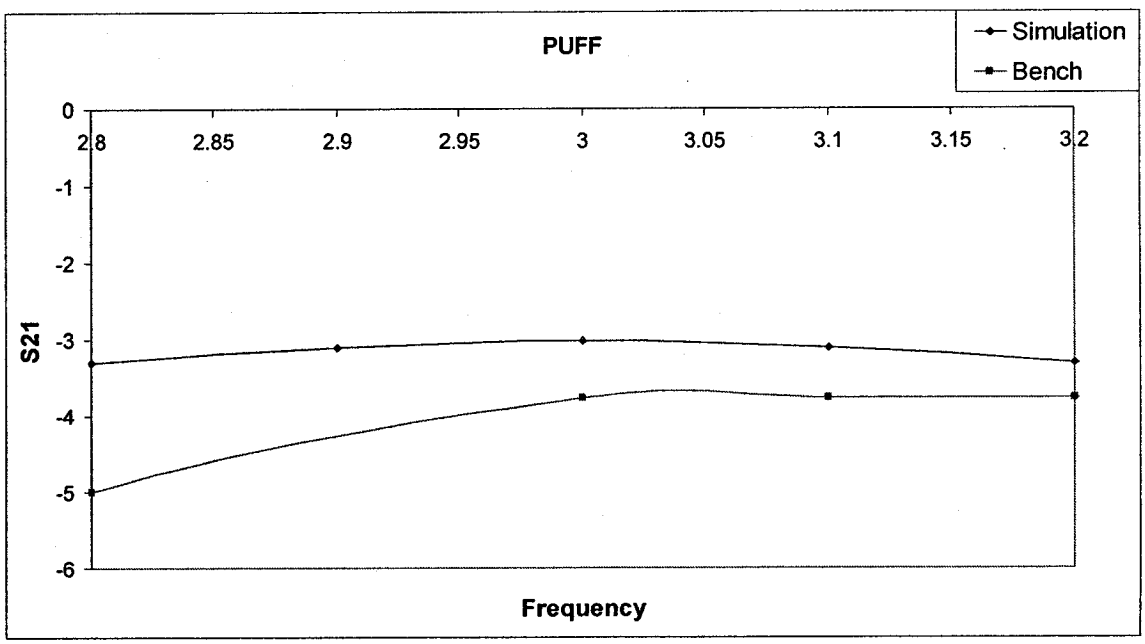

Figure7.27: PUFF's Hybrid Frequency Response for "Through" port simulation vs. bench.

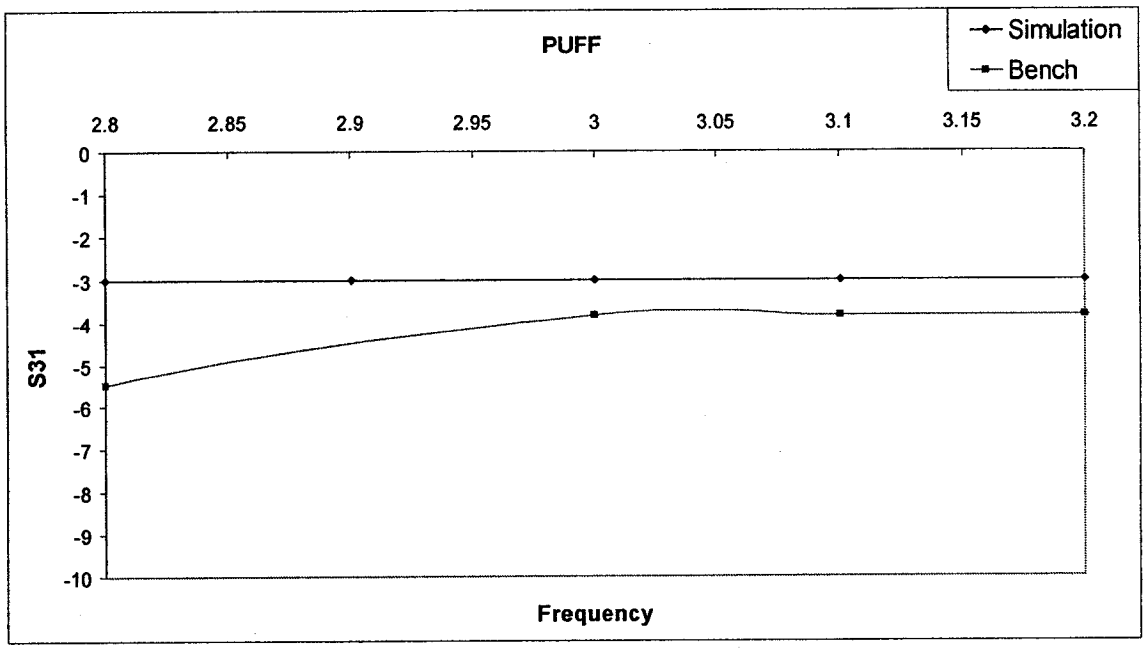

Figure7.28: PUFF's Hybrid Frequency Response for "Coupled" port simulation vs. bench.

Analyzing the frequency response plots in both Figure7.27 and Figrue7.28 of both the "through" and "coupled" ports (S21 & S31), the hybrid shows the correct 3dB split, however an additional loss on the order of 1 dB is also present. The measured insertion loss in the "through" arm (S21) is –3.767dB and the phase delay is 45°. Also, the measured insertion in the "coupled" arm (S31) is –3.51dB and the phase delay is -45°. The isolation between port 1 and port 4 (S41) is –23.37dB and the phase delay is -62°. A 50Ω (1.448mm wide), 5mm long transmission line is added at each of the four ports of the hybrid to allow for the SMA connectors to be soldered to the circuit board to facilitate bench measurements. This transmission line/SMA connector assembly adds extra insertion loss of -0.18dB and phase delay of -67.2° per side, which yields a total of -0.36dB insertion loss and -134.4° phase delay in each arm to the measurements. Taking

into account the added insertion loss, the total insertion loss in the "through" arm (S21) becomes -3.767dB - (-0.36dB) = -3.407dB, and in the "coupled" arm (S31) becomes -3.51dB - (-0.36dB) = -3.15dB. Also, the total phase delay in the "through" arm (Ang(S21)) becomes 45° + (-134.4°) = -89.4° and in the "coupled" arm (Ang(S31)) becomes -45° + (-134.4°) = -179.4°. Reviewing the total insertion loss values, it can be seen that the power imbalance between the two output arms is 3.407dB - 3.15dB which yields 0.103dB, which is a very reasonable for a measured hybrid. Comparing these numbers with the PUFF simulation data, we can see a difference of approximately 0.35dB in total insertion loss. Also, the phase delay relationship of the bench results to the simulation results is very comparable.

Presented secondly are the frequency response plots obtained from Serenade, simulation and bench, for the "through" (S21) and "coupled" (S31) ports, shown in Figure 7.29 and Figure 7.30 respectively.

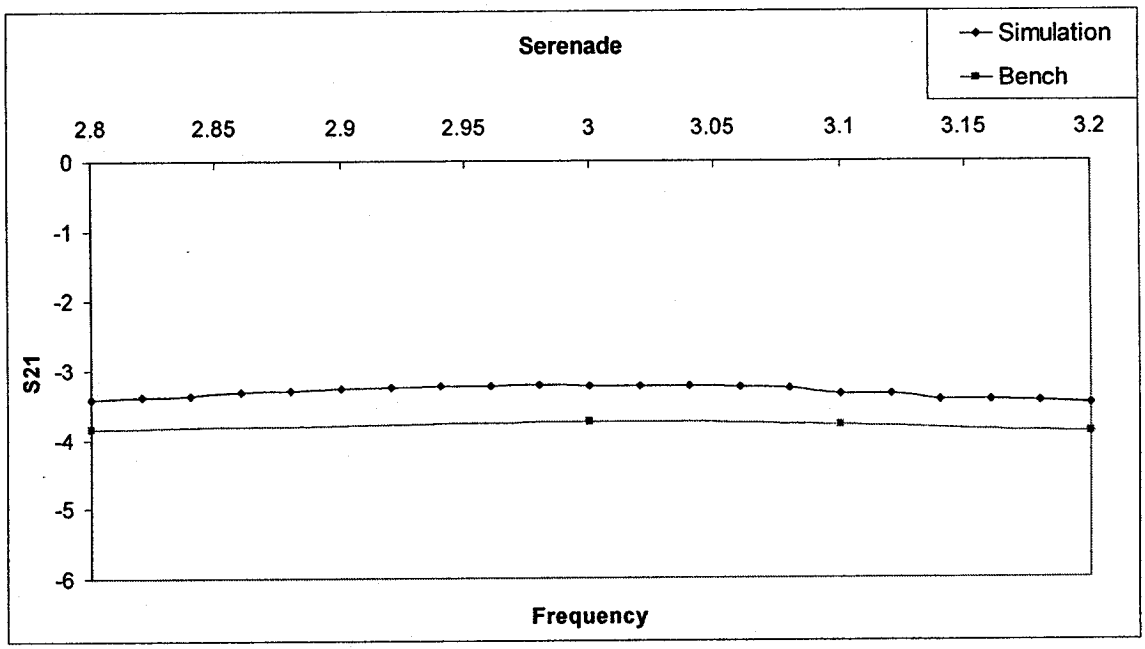

Figure7.29: Serenade's hybrid frequency response for "through" port simulation vs. bench.

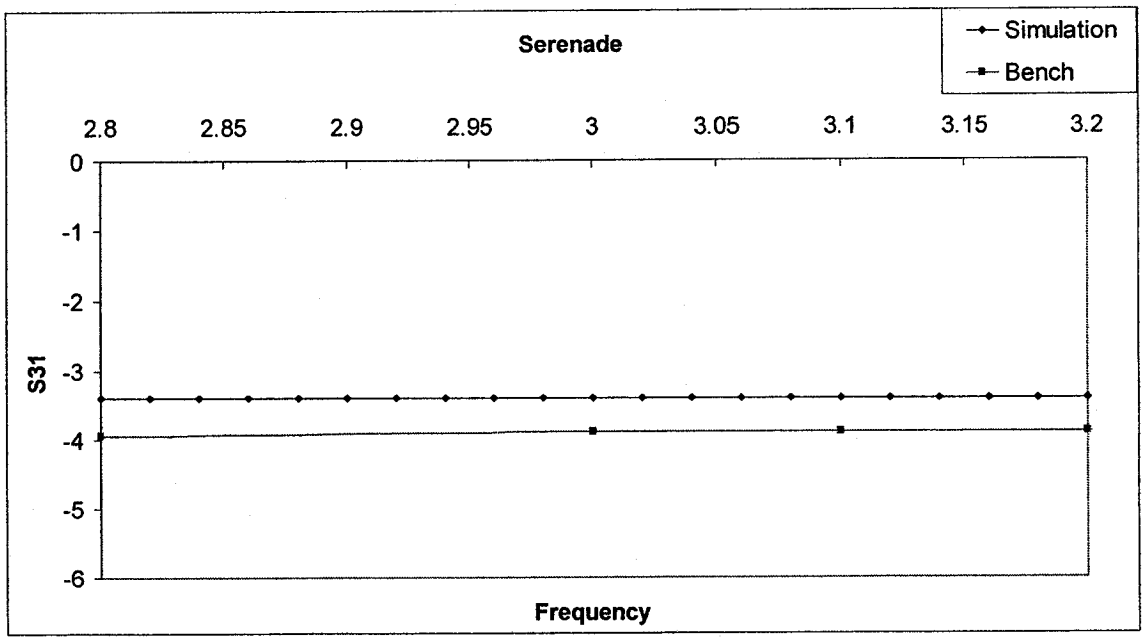

Figure 7.30: Serenade's hybrid frequency response for "coupled" port simulation vs. bench.

Analyzing the frequency response plots in both Figure 7.29 and Figure 7.30 of the "through" and "coupled" ports (S21 & S31), it can be easily seen that the bench results are very similar to the simulation response. The measured insertion loss in the "through" arm (S21) is –3.23dB and the phase delay is -86.36°. Also, the measured insertion loss in the "coupled" arm (S31) is –3.4dB and the phase delay is -176.43°. The isolation in the isolation arm (S41) is –32.5dB and the phase delay is -95.18°. From the Serenade circuit bench measurement graphs presented in Section 7.4.2. The measured insertion loss in the "through" arm (S21) is –4.125dB and the phase delay is 45° and return loss S22 of –16.97dB. Also, the measured insertion loss in the "coupled" arm (S31) is –3.41dB and the phase delay is -45° and return loss S33 of –15.79dB. The isolation between port 1 and port 4 (S41) is –22.17dB and the phase delay is -54° and return loss S44 of –16.97dB. Taking into account the added insertion loss and phase delay from the transmission line / SMA connector combination presented above, the total insertion loss in the "through" arm (S21) becomes –4.124dB – (-0.36dB) = -3.765dB, and in the "coupled" arm (S31) becomes -3.41dB - (-0.36dB) = -3.05dB. The total phase delay in the "through" arm Ang(S21) becomes 45° + (-134.4°) = -89.4° and in the "coupled" arm Ang(S31) becomes -45° + (-134.4°) = -179.4°. Reviewing the total insertion loss values, it can be seen that the power imbalance between the two output arms is 3.765dB – 3.05dB which yields 0.715dB, which is a little larger than the PUFF result. However, unlike PUFF, as can be seen in Figure 7.29 and Figure 7.30, both the simulation and bench frequency response of the "through" and "coupled" arms are extremely similar and do not exhibit a frequency shift. Comparing these numbers with the Serenade simulation

data, we can see a difference of approximately 0.545dB in power imbalance and 0.18dB total insertion loss in port 2 and 0.35dB in port 3.

In conclusion, as can be seen from the frequency response graphs and the discussion of both the insertion loss and phase delay, Serenade depicted less insertion loss and more balanced shape to the bench measurements than PUFF. These results are also an indication that the parasitic effects due to discontinuities and impedance mismatch are better accounted for in Serenade than in PUFF.

8. PATCH ANTENNAS

8.1 Theory

Patch antennas, also known as microstrip antennas, are rugged, lightweight, and low-cost antennas that are widely used in applications where size and weight are of prime concern, such as in the aerodynamic performance of aircraft and other vehicles. Much like a microstrip line, a patch antenna consists of a conducting metallic patch printed on a grounded substrate as shown in Figure 8.1 [60].

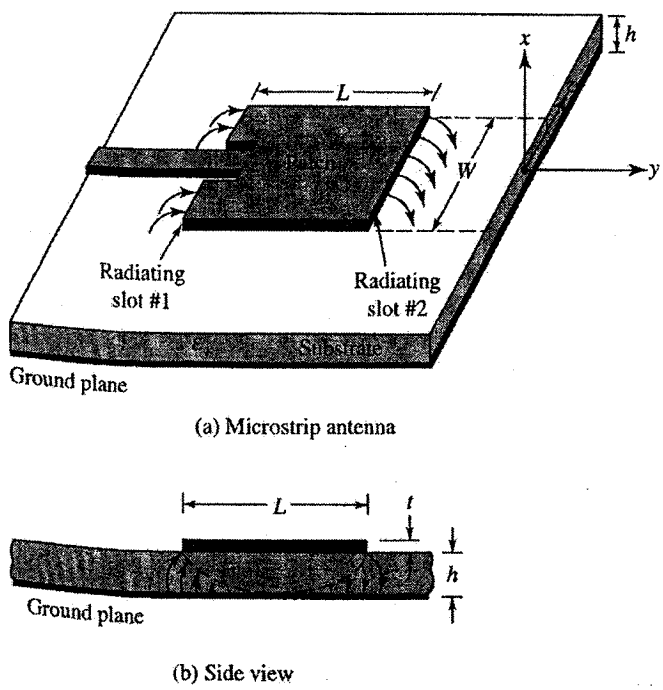

Figure 8.1: Patch antenna. (a) Overview. (b) Side view.

The quantities L, W, and t are the length, width, and thickness of the patch, respectively, and h assumes its usual role of substrate thickness. Such antennas are usually designed for broadside operation, but can be operated in endfire modes as well. In practice, $t \ll \lambda_0$, where λ_0 is the free-space wavelength; $h \ll \lambda_0$, usually $0.003\lambda_0 \le h \le 0.05\lambda_0$; the length is usually $\lambda_0/3 < L < \lambda_0/2$; and the substrate permittivity is usually $2.2 \le \varepsilon_r \le 12$. The radiating patch may assume many shapes (Figure 8.2 [61]), but the rectangular patch configuration, as illustrated in Figure 8.1, is by far the most common, and the one dealt with herein.

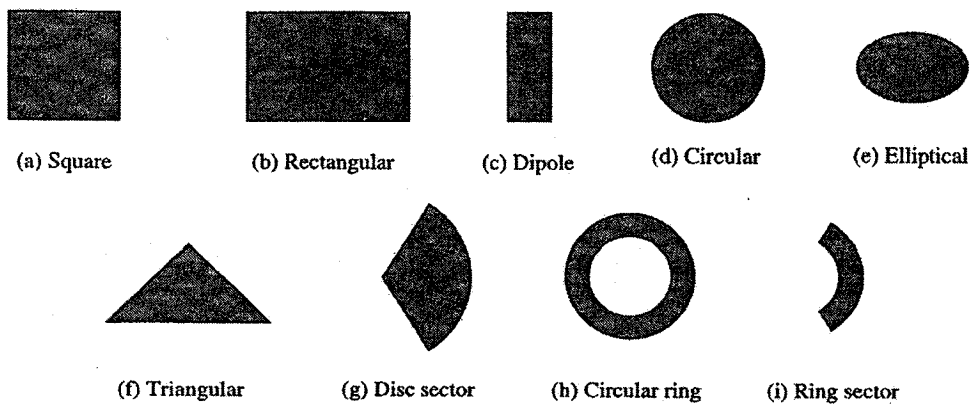

Figure 8.2: Various patch shapes.

8.1.1 Transmission-Line Model

A rectangular patch antenna can be modeled as two parallel, radiating slots, each having conductance G and susceptance B and separated by a low-impedance transmission line; Figure 8.3 [62] illustrates the geometry.

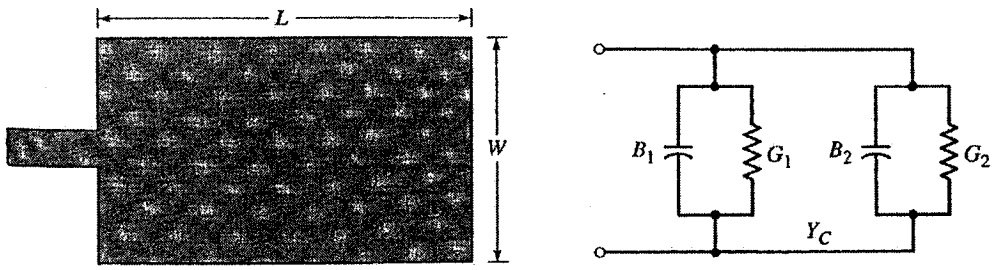

(a) Rectangular patch (b) Transmission model equivalent

Figure 8.3: Rectangular patch antenna and its equivalent transmission-line model.

Following the presentation in [63],

$G_{1,2}$ and $B_{1,2}$ are given by

$$G_{1,2} = \frac{W}{120\lambda_0}\left[1 - \frac{1}{24}(k_0 h)^2\right], \quad \frac{h}{\lambda_0} < \frac{1}{10} \tag{8.2.1a}$$

$$B_{1,2} = \frac{W}{120\lambda_0}[1 - 0636\ln(k_0 h)], \quad \frac{h}{\lambda_0} < \frac{1}{10}. \tag{8.2.1b}$$

where k_0 is the propagation constant for free space. The conductance may be alternatively expressed as

$$G_{1,2} = \frac{I_{1,2}}{120\pi^2} \tag{8.2.2a}$$

where

$$I_{1,2} = -2 + \cos(X) + XS_i(X) + \frac{\sin(X)}{X}, \quad X = k_0 W \tag{8.2.2b}$$

and $S_i(X)$ is the family of sine integrals. Asymptotic values for (8.2.2) are given by

$$G_{1,2} = \begin{cases} \frac{1}{90}\left(\frac{W}{\lambda_0}\right)^2 & W << \lambda_0 \\ \frac{1}{120}\left(\frac{W}{\lambda_0}\right) & W >> \lambda_0 \end{cases} \tag{8.2.3}$$

The resonant input resistance can be calculated by using

$$R_{in} = \frac{1}{2(G_{1,2} \pm G_{12,21})} \tag{8.2.4a}$$

where $G_{12,21}$, the mutual conductance, is given by

$$G_{12,21} \frac{1}{120\pi^2} \int_0^{\pi} \left[\frac{\sin\left(\frac{k_0 W}{2}\cos\theta\right)}{\cos\theta} \right]^2 J_0(k_0 L \sin\theta)\sin^3\theta d\theta . \tag{8.2.4b}$$

where J_0 is the Bessel function of the first kind.

The patch can be matched to a feed line of characteristic impedance Z_0 by recessing the feed junction a distance y_0 from the edge of the patch, as shown in Figure 8.4 (a) [64].

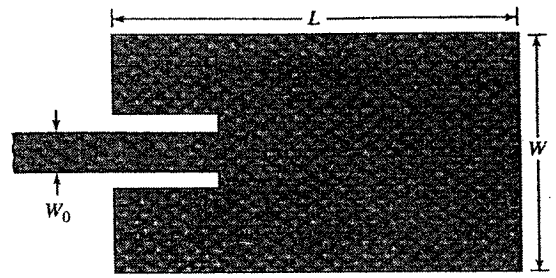

(a) Recessed microstrip-line feed

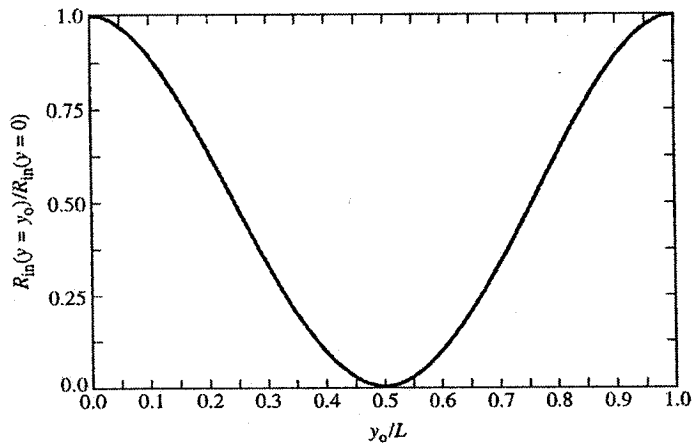

(b) Normalized input resistance

Figure 8.4: Line matching. (a) Recessed feed. (b) Variation of normalized input resistance with recess distance.

Equation (8.2.4a) gives the resonant input resistance as referenced to the first radiating slot of the equivalent circuit, i.e., as referenced to the feed without a recess; for the recessed geometry, the resistance is given by [65]

$$R_{in}(y = y_0) = \frac{1}{2(G_{1,2} \pm G_{12,21})}\left[\cos^2\left(\frac{\pi}{L}y_0\right) + \frac{G_{1,2}^2 + B_{1,2}^2}{Y_0^2}\sin^2\left(\frac{\pi}{L}y_0\right) - \frac{B_1}{Y_0}\sin\left(\frac{2\pi}{L}y_0\right)\right]. \quad (8.2.5a)$$

where $Y_0 = 1/Z_0$, and Z_0 is the characteristic impedance of the feed line. For most microstrips, $G_{1,2}/Y_0 << 1$ and $B_{1,2}/Y_0 << 1$, and 8.2.5a can be replaced with a simpler form

$$R_{in}(y = y_0) = \frac{1}{2(G_{1,2} \pm G_{12,21})} \cos^2\left(\frac{\pi}{L} y_0\right) = R_{in}(y = 0) \cos^2\left(\frac{\pi}{L} y_0\right). \qquad (8.2.5b)$$

Figure 8.4 (b) [66] on the previous page depicts a plot of the normalized input resistance as a function of the recess distance.

Effective Quantities and Dimensional Design

Just as there are effective quantities (width and dielectric constant) that take into account fringing effects and wave behavior for microstrip lines, such quantities also exist for patch antennas as shown in Figure 8.5 [67].

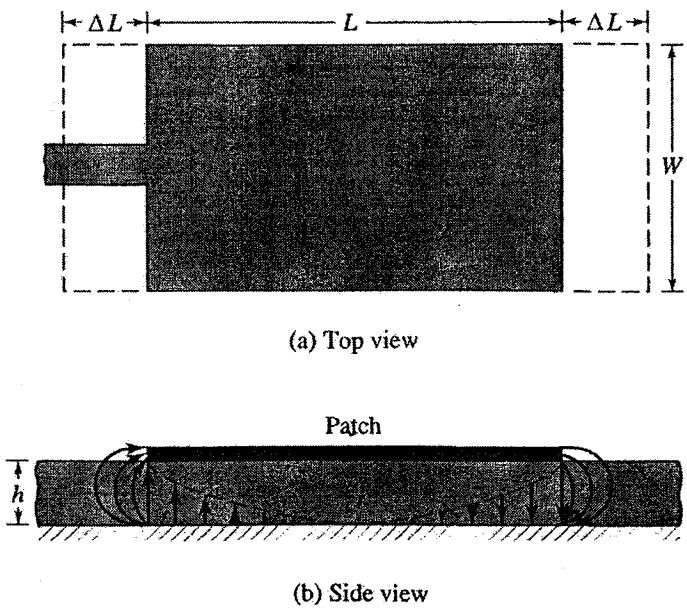

Figure 8.5: Physical and effective lengths of a rectangular patch antenna.

From Figure 8.5, the effective length, L_{eff}, is given by [68]

$$L_{eff} = L + 2\Delta L \tag{8.1.1a}$$

where the length extension, ΔL, is obtained from

$$\frac{\Delta L}{h} = 0.412 \frac{\left(\varepsilon_{eff} + 0.3\right)\left(\frac{W}{h} + 0.264\right)}{\left(\varepsilon_{eff} - 0.258\right)\left(\frac{W}{h} + 0.8\right)}. \tag{8.1.1b}$$

and ε_{eff}, the effective dielectric constant, can be determined as discussed in Chapter 2. Lastly, the following expressions may be used to determine the physical length and physical width of the patch:

$$L = \frac{1}{2f_r\sqrt{\varepsilon_{eff}}\sqrt{\mu_0\varepsilon_0}} - 2\Delta L = \frac{c_0}{2f_r\sqrt{\varepsilon_{eff}}} - 2\Delta L \tag{8.1.2a}$$

where $\frac{c_0}{2f_r\sqrt{\varepsilon_{eff}}} = \lambda/2$ and $2\Delta L$ is a correction factor for fringing effects.

and

$$W = \frac{1}{2f_r\sqrt{\mu_0\varepsilon_0}}\sqrt{\frac{2}{\varepsilon_r + 1}} = \frac{c_0}{2f_r}\sqrt{\frac{2}{\varepsilon_r + 1}}. \tag{8.1.2b}$$

where f_r is the required resonant frequency of the antenna.

The above design procedure and equations were followed to design the patch antenna to be studied in this work. The antenna is printed on the same circuit board material used for the previous circuits, Hitachi LX67 (ε_r=3.38, h=0.031"). Presented below are the obtained design dimensions:

Step 1: W

$$W = \frac{v_0}{2f_r}\sqrt{2/(\varepsilon_r + 1)} = 33.8mm,$$

Step 2: ε_{reff}

$$\varepsilon_{reff} = \frac{\varepsilon_r + 1}{2} + \frac{\varepsilon_r - 1}{2}\left[1 + 12\frac{h}{w}\right]^{-1/2} = 3.24,$$

Step 3: ΔL

$$\Delta L = h\left[0.412\frac{(\varepsilon_{reff} + 0.3)(\frac{w}{h} + 0.264)}{(\varepsilon_{reff} - 0.258)(\frac{w}{h} + 0.8)}\right] = 3.8mm,$$

Step 4: L

$$L = \frac{\lambda}{2} - 2\Delta L = \frac{c}{2\sqrt{\varepsilon_{reff}}f_r} - 2\Delta L = 20.2mm,$$

Step 5: L_e

$$L_e = L + 2\Delta L = \frac{\lambda}{2} = 27.78mm.$$

8.2 Simulations

In this chapter, the simulation results and the bench measurements of the microstrip patch antenna simulated in Serenade will be presented. PUFF cannot be used for antenna modeling because it is a transmission line model that cannot account for radiation effects.

8.2.1 Serenade Simulation Results:

The patch antenna dimensions obtained in the design stage were used in Serenade. Since there is no specific component available in Serenade to model a patch antenna, open-

ended distributed transmission lines (microstrip) were used instead to model the patch antenna. A matching network was designed and added to the patch antenna to optimize its input impedance and match it to 50Ω. Presented in Figure 8.6 is the patch antenna (with its matching network) simulated in Serenade.

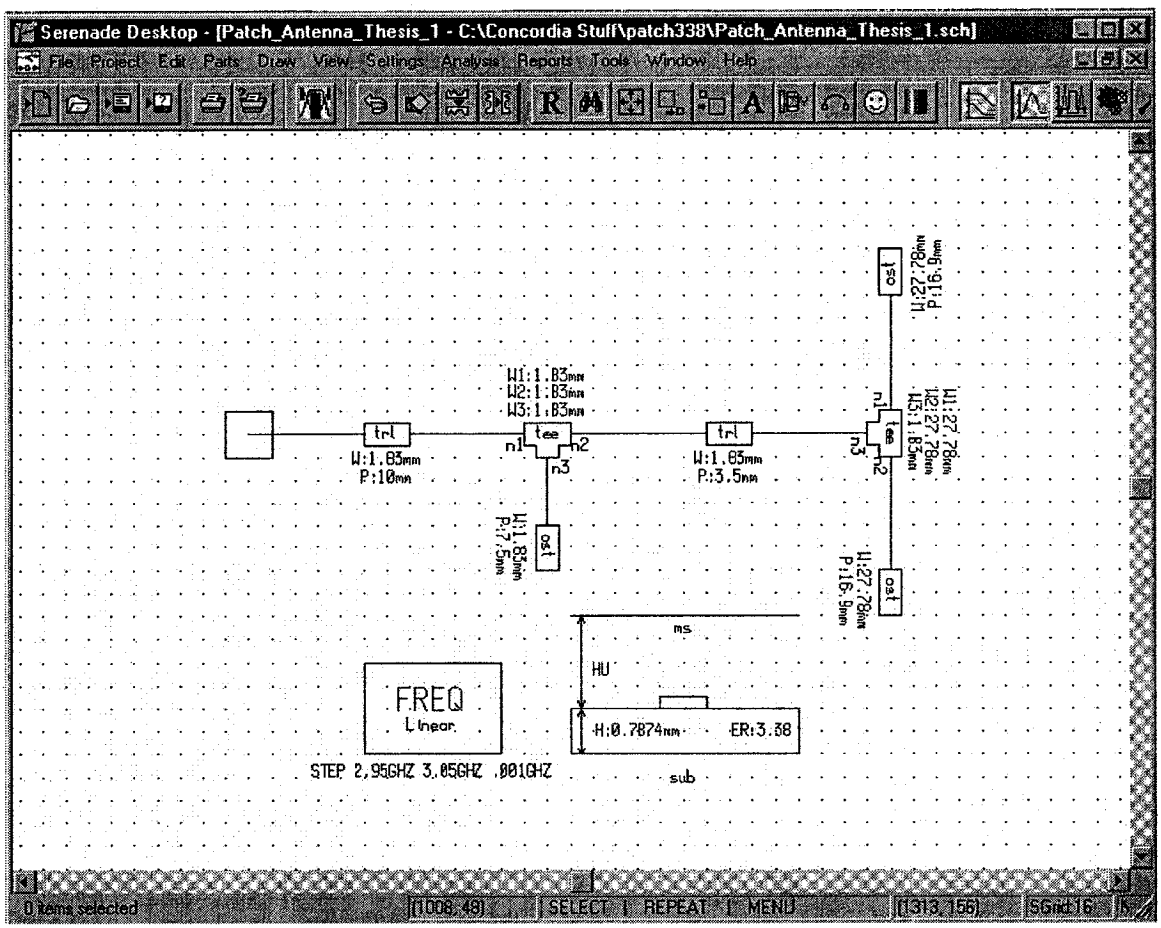

Figure 8.6: Rectangular patch antenna simulated in Serenade.

The measurements results will be presented in the next section.

Also, presented below in Figure 8.7 is the patch antenna input return loss.

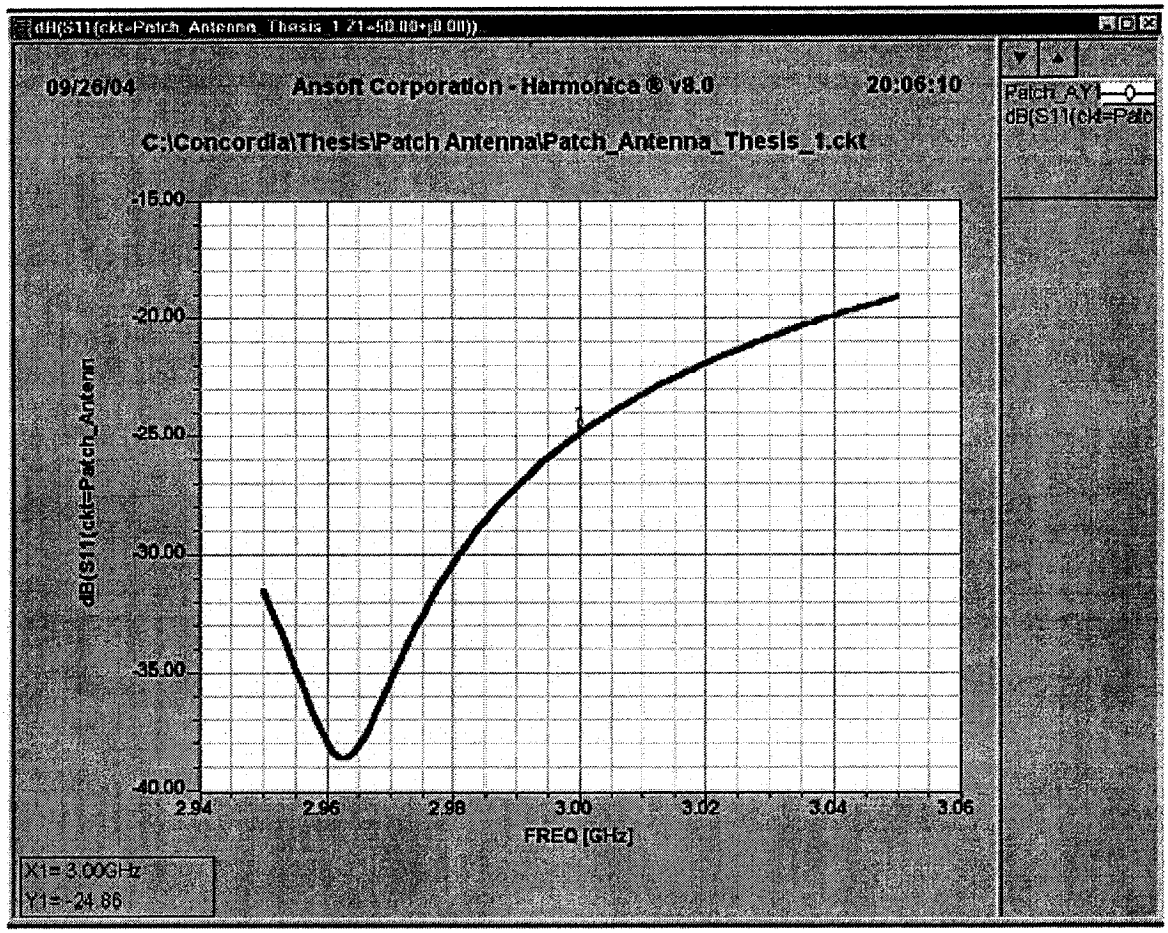

Figure 8.7: Patch antenna input impedance in rectangular format.

8.3 Measurements

Using the network analyzer 8720ES to measure the circuit on the bench, presented next are measurement results of the patch antenna. Figure 8.8 is a picture of the patch antenna. The purpose of the stub element is to optimize the input return loss at 2.96GHz. The little segments at the end of the stub element are placed to facilitate tuning for input return loss on the bench (if required).

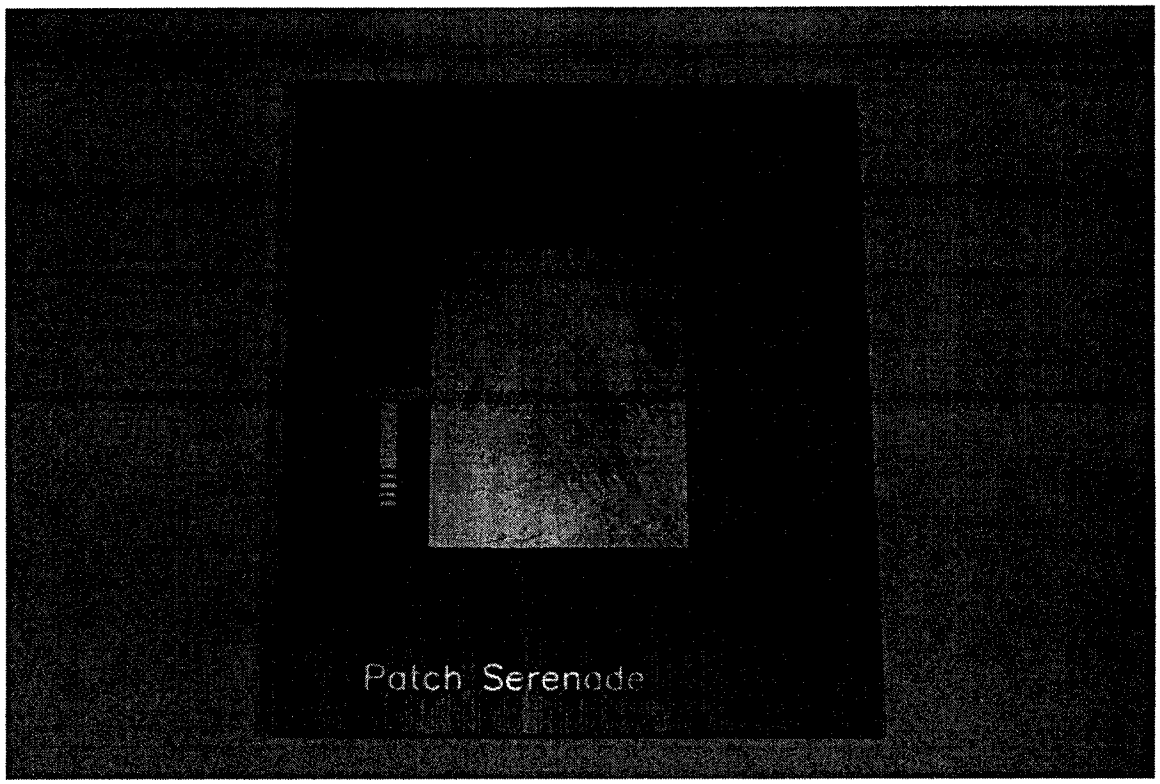

Figure 8.8: Picture of the Patch Antenna.

The bench measurements of the patch antenna simulated in Serenade are presented in this section. The patch was taped to the center of an aluminum ground plane with rolled off edges to minimize edge effects. The ground plane was one meter in diameter with a hole near the center to clear out for the antenna SMA connector.

Figure 8.9 shows the antenna input impedance in both Smith Chart and rectangular formats.

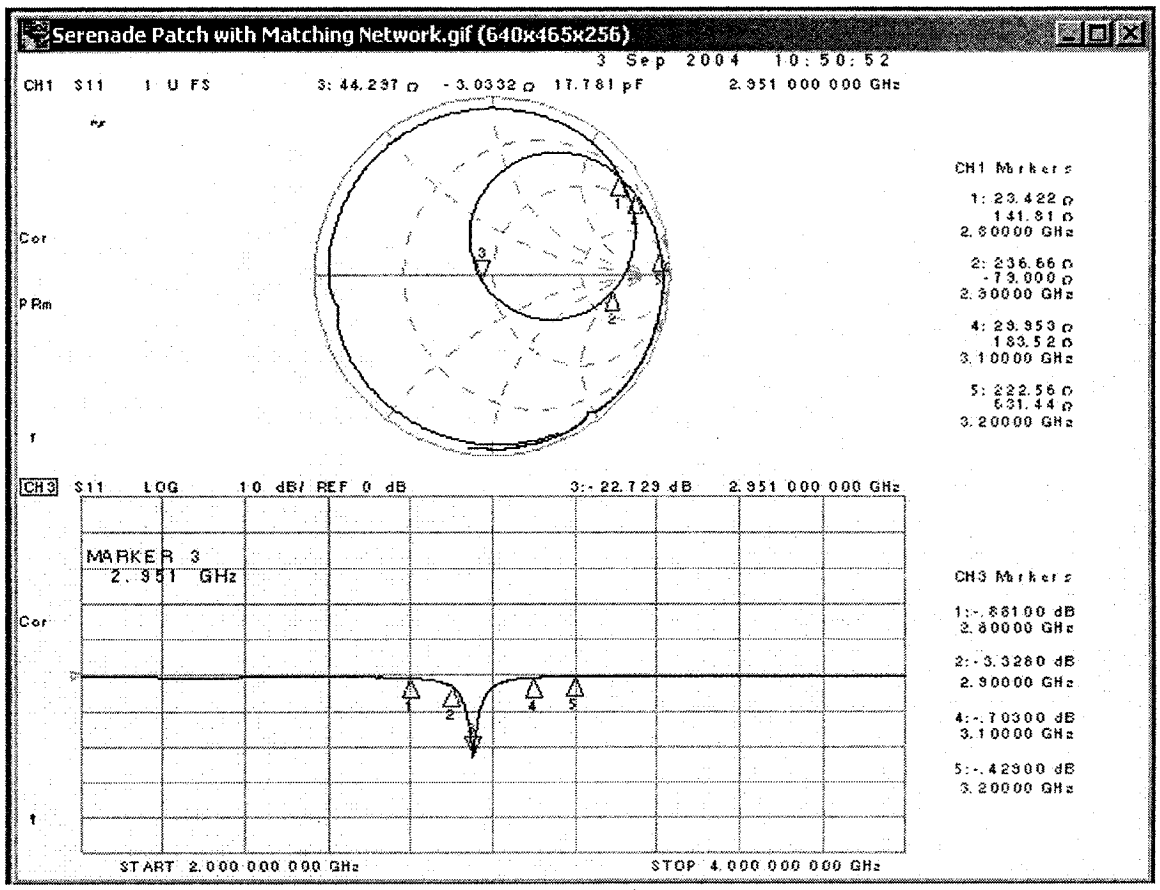

Figure 8.9: Input Impedance of the Serenade patch antenna with impedance matching network.

As can be seen from the figure above, the resonant frequency (marker 3, the closest to 50Ω and lowest input return loss, -22.7dB) is at 2.951GHz, which is a frequency shift of 49MHz (1.6%) from the intended design frequency f_r (3.0GHz). This shift in frequency will be discussed in the next section.

In order to measure the contribution of the antenna input impedance matching network, a measurement of the antenna was taken without the matching network. An SMA connector was installed directly at the patch edge. The results are shown in Figure 8.10 below.

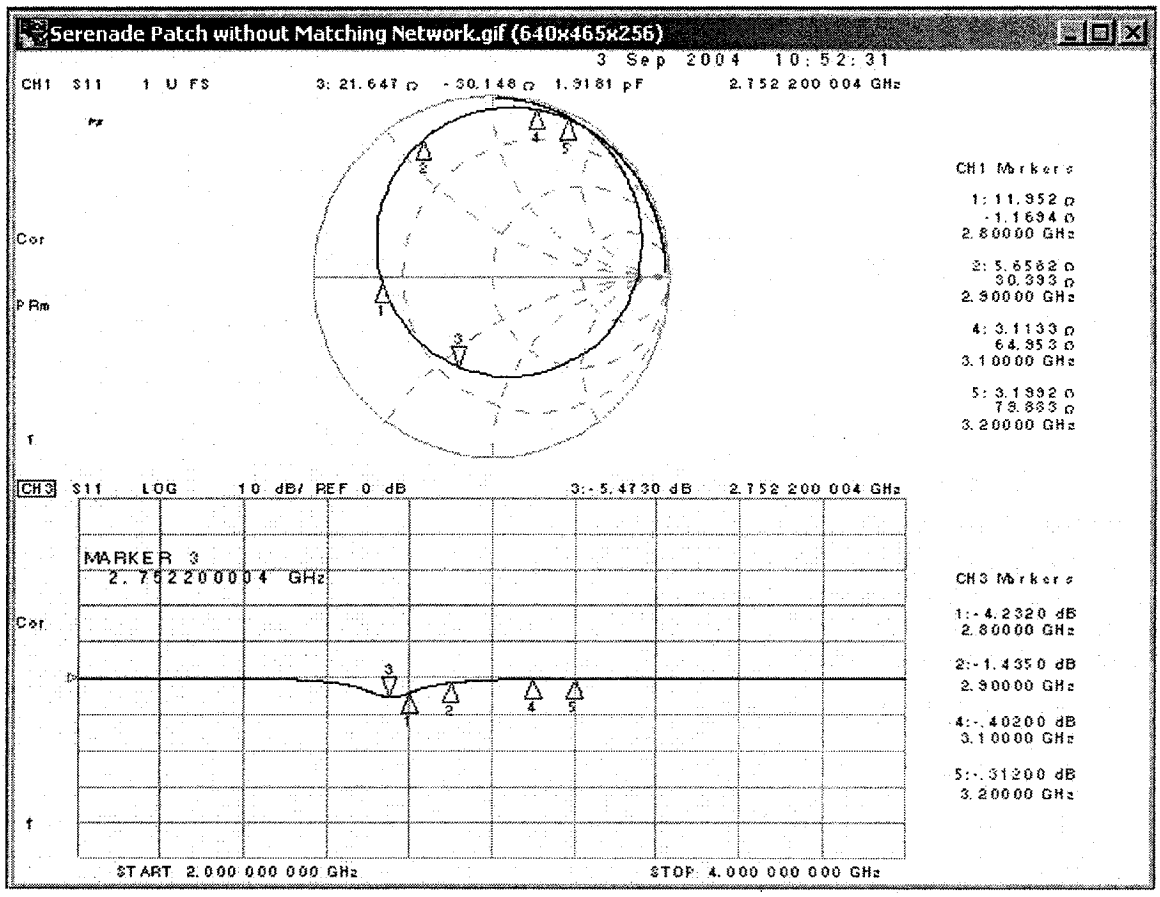

Figure 8.10: Input Impedance of the Serenade patch antenna without impedance matching network. The input reactance is zero at 2.8GHz.

As can be seen from the figure above, the resonant frequency (marker 1, the input reactance is zero, -4.232dB) is at 2.8GHz, which is a bigger shift of 200MHz from the intended design frequency f_r (3.0GHz), which is a bigger shift in frequency than with the presence of the matching network. This shift in frequency will also be discussed in Section 8.4.

8.4 Discussion

A rectangular patch antenna was designed at the design frequency f_r = 3.0GHz, following the "*patch antenna design recipe*" presented and discussed in Section 8.2 and printed on Hitachi LX67 (ε_r=3.38, h=0.031", 0.5oz) microstrip circuit board material. PUFF cannot be used for antenna modeling because it is a transmission line model that cannot account for radiation effects. Only Serenade was used to simulate the patch using the dimensions obtained in Section 8.2. As can be seen from the previous section, there were few significant differences between the simulation results and the bench measurements. These differences will be discussed in this section.

The simulation results were shown in Figure 8.7 (input return loss of –25dB @ 3.0 GHz). As can be seen, the input return loss at 3GHz is -25dB and less than -35dB at 2.96GHz. Also, from Figure 8.10, the "measured" resonance frequency (the input reactance is zero) is at 2.951GHz, which is a shift of 49MHz from the intended design frequency f_r (3.0GHz). The major influence of this frequency shift behavior is the difference in the ground plane size between the simulator and the bench measurement. Serenade presents an infinite ground plane under the microstrip transmission line whereas a 1-meter ground plane was used during measurements. Also, another substantial reason for this frequency shift phenomenon might come from the fact that the Serenade RF Designer is not a full wave simulator.

A measurement of the antenna without the matching network was shown in Section 8.3, in order to evaluate its contribution. An SMA connector was installed directly at the patch edge, and the results were shown in Figure 8.10 in Section 8.3. As can be seen, the input impedance matching was destroyed, as would have been expected. The input

impedance of a patch antenna at the antenna edge is high, in the range of 275Ω to 350Ω. This high impedance will cause higher reflection and the antenna input return loss would be higher.

9. CONCLUSION

In this thesis, the design and simulation of four microwave components were presented and studied. The four circuits were: Stepped-Impedance (*hi-Z, low-Z)* low pass filter, edge coupled-line band pass filter, 3-dB 90° hybrid and a rectangular patch antenna. The design center frequency was 3 GHz. These components were all passive and printed on MCL-LX-67Y microstrip dielectric material with dielectric constant of ε_r=3.38, loss tangent of tanδ=0.0009 and material thickness of 0.787mm from Hitachi Chemical Co. The two simulation software packages used in the design stage of the components were PUFF, which was originally designed for the students in the microwave circuits course at California Institute of Technology, and the student version of Serenade, a product of Ansoft. A comparison between the "*ideal*" model and the "*advanced*" model in PUFF was presented and discussed for the LPF, the BPF and the 3-dB 90° hybrid components individually. The results of the comparison showed virtually no difference or discrepancy in both the frequency response and return loss, which was the reason why only the circuit boards obtained from PUFF's "*advanced*" model were studied. Also, a comparison between the simulation results and the bench results of the individual circuits were presented and discussed. Both software packages predicted results that were relatively close to the bench measurements. The results of the low pass filter study in Chapter 5 showed that the microstrip transmission lines are more accurately modeled and the open-ended fringing effects are better accounted for with Serenade than in PUFF. Also, as shown in Chapter 6, the coupled microstrip lines in Serenade yielded more comparable results to the bench measurements than PUFF. A correction factor as

described in the PUFF manual has to be added in the PUFF simulation to account for the extra length caused by the fringing effects of open-ended lines. This extra step is not required in Serenade because the correction factor is built into the transmission line model. It was shown in Chapter 7 that the parasitic effects due to discontinuities and fringing effencts are better accounted for in Serenade. As discussed and presented in Chapter 8, PUFF cannot be used to model antennas and other radiating structures. However, the Serenade simulation results yielded in reasonable return loss (with impedance matching network). Further work could be done in the modeling, varying the dielectric constant, loss, and connector effects, to try and improve the comparison with measurements. For the cases studied in this thesis, Serenade results were closer than PUFF to the bench measurements. There are published results (in the PUFF manual) for circuits printed on dielectric constant of 10.2 that showed more agreeable results than were obtained in this study. The reasons for that would have to be explored further.

10. REFERENCES

[1] E. Yamashita, "Variational Method for the Analysis of Microstrip-Like Transmission Lines," IEEE Transactions on Microwave Theory and Techniques, vol. MTT-16, no. 8, pp. 529-535, August 1968.

[2] H. A. Wheeler, "Transmission-Line properties of a strip on a Dielectric Sheet on a Plane," IEEE Transactions on Microwave Theory and Techniques, vol. MTT-25, no. 8, pp. 631-647, August 1977.

[3] E. Hammerstad and O. Jensen, "Accurate Models for Microstrip Computer-Aided Design," IEEE Microwave Symposium, pp. 407-409, 1980.

[4] W. J. Getsinger, "Microstrip Dispersion Model," IEEE Transactions on Microwave Theory and Techniques, vol. MTT-21, pp. 34-39, January 1973.

[5] B. M. Neale and A. Gopinath, "Microstrip Discontinuity Inductances," IEEE Transactions on Microwave Theory and Techniques, vol. MTT-26, no. 10, pp. 827-831, October 1978.

[6] T. S. Chu and T. Itoh, "Generalized Scattering Matrix Method for Analysis of Cascaded and Offset Microstrip Step Discontinuities," IEEE Transactions on Microwave Theory and Techniques, vol. MTT-34, no. 2, pp. 280-284, February 1986.

[7] A. A. Oliner and K. S. Lee, "The Nature of the Leakage from Higher Modes on Microstrip Line," IEEE MTT-S Digest, pp. 57-60, 1986.

[8] Guillermo Gonzalez, *Microwave Transistor Amplifiers: Analysis and Design.* Englewood Cliffs, N.J.: Prentice-Hall, pp. 143-152, 1984.

[9] S. Wedge, R. Compton, D. Rutledge, "PUFF," (Computer Aided Design for Microwave Integrated Circuits, 1999). From: PUFF Distribution, Electrical Engineering M/S 136-93, California Institute of Technology, Pasadena, CA 91125.

[10] Ansoft Corporation, Harmonica Manual, "Harmonica Elements Library," 1999.

[11] Agilent Technologies, "Service Guide, 8753ET/ES", 2002.

[12] G. L. Matthaei, L. Young and E. M. T. Jones, *Microwave Filters, Impedance-Matching Networks, and Coupling Structures.* Artech House, 1980.

[13] S. Akhtarzad, T. Rowbotham and P. Johns, "The Design of Coupled Microstrip Lines," IEEE Transactions on Microwave Theory and Techniques, vol. MTT-23, no. 6, June 1975.

[14] R. Garg and I. J. Bahl, "Characteristics of Coupled Microstriplines," IEEE Transactions on Microwave Theory and Techniques, vol. MTT-27, no. 7, July 1979.

[15] M. Ramadan and F. Westgate, "Impedance of Coupled Microstrip Transmission Lines," Microwave Journal, 1971.

[16] J. Reed and G. J. Wheeler, "A Method of Analysis of Symmetrical Four-Port Networks," IRE Transactions on Microwave Theory and Techniques, October.

[17] H. Pues and A. Van de Capelle, "Accurate Transmission-Line Model for the Rectangular Microstrip Antenna," IEEE Transactions on Antennas and Propagation, vol. 131, pt. H, no. 6, pp. 334-340, Dec. 1984.

[18] E. O. Hammerstad, "Equations for Microstrip Circuit Design," Proc. Fifth European Microwave Conference, September, 1975.

[19] Guillermo Gonzalez, *Microwave Transistor Amplifiers: Analysis and Design.* Englewood Cliffs, N.J.: Prentice-Hall, p. 143.
[20] Gonzalez, p. 143.
[21] I. J. Bahl and D. K. Trivedi, "A Designer's Guide to Microstrip Line," Microwaves, May 1977.
[22] Guillermo Gonzalez, *Microwave Transistor Amplifiers: Analysis and Design.* Englewood Cliffs, N.J.: Prentice-Hall, p. 145.
[23] H. Sobol, "Extending IC Technology to Microwave Equipment," Electronics, March 1967.
[24] Guillermo Gonzalez, *Microwave Transistor Amplifiers: Analysis and Design.* Englewood Cliffs, N.J.: Prentice-Hall, p. 145.
[25] S. Wedge, R. Compton, D. Rutledge, "PUFF", (Computer Aided Design for Microwave Integrated Circuits, 1999), pp. 50-57.
[26] M. A. Murray-Lasso, "Black-Box Models for Linear Integrated Circuits," IEEE Trans. Educ., vol. E-12, pp. 170-180, Sept. 1969.
[27] V. A. Monaco and P. Tiberio, "Automatic Scattering Matrix Computation of Microwave Circuits," Alta Freq., vol. 39, pp. 59-64, Feb. 1970.
[28] H. A. Wheeler, "Transmission Line Properties of Parallel Wide Strip by a Conformal Mapping Approximation," IEEE Transactions on Microwave Theory and Techniques, vol. MTT-12, pp. 280-289, May 1964.
[29] H. A. Wheeler, "Transmission Line Properties of Parallel Strips Separated by a Dielectric Sheet," IEEE Transactions on Microwave Theory and Techniques, vol. MTT-13, pp. 172-185, March 1965.
[30] S. B. Cohn, "Problems in Strip Transmission Lines," IRE Trans. On Microwave Theory and Techniques, vol. MTT-3, pp. 119-126, March 1955.
[31] S. Akhtarzad, T. Rowbotham and P. Johns, "The Design of Coupled Microstrip Lines," IEEE Transactions on Microwave Theory and Techniques, vol. MTT-23, pp. 486-492, June 1975.
[32] S. Wedge, R. Compton, D. Rutledge, "PUFF," (Computer Aided Design for Microwave Integrated Circuits, 1999), pp. 1-9.
[33] E. J. Denlinger, "A Frequency Dependent Solution for Microstrip Transmission Lines," IEEE Transactions on Microwave Theory and Techniques, vol. MTT-19, no. 1, January 1971.
[34] D. Mirshekar-Syahkal and J. Brian Davies, "Accurate Solution of Microstrip and Coplanar Structures for Dispersion and for Dielectric Conductor Losses," IEEE Transactions on Microwave Theory and Techniques, vol. MTT-27, July 1979.
[35] R. A. Pucel, D. J. Masse and C. P. Hartwig, "Losses in Microstrip," IEEE Transactions on Microwave Theory and Techniques, vol. MTT-16, pp. 342-350, June 1968.
[36] T. G. Bryant and J. A. Weiss, "Parameters of Microstrip Transmission Lines and of Coupled Pairs of Microstrip Lines," IEEE Transactions on Microwave Theory and Techniques, December 1968.
[37] Agilent Technologies, "Service Guide, 8753ET/ES," 2002.
[38] David M. Pozar, *Microwave Engineering.* Addison-Wesley Publishing Company, 1990, pp. 502-503.
[39] Pozar, pp. 481-486.

[40] Pozar, pp. 481-486.
[41] Pozar, pp. 484-486.
[42] Pozar, pp. 503.
[43] G. L. Matthaei, L. Young and E. M. T. Jones, *Microwave Filters, Impedance-Matching Networks, and Coupling Structures*. Artech House, 1980.
[44] David M. Pozar, *Microwave Engineering*. Addison-Wesley Publishing Company, 1990, p. 485.
[45] Pozar, pp. 415-421.
[46] Pozar, p. 418.
[47] T. C. Edwards, "Foundations for Microstrip Circuit Design," J. Wiley, 1981, pp. 130-142.
[48] Edwards, p. 136.
[49] S. Akhtarzad, T. Rowbotham and P. Johns, "The Design of Coupled Microstrip Lines," IEEE Transactions on Microwave Theory and Techniques, vol. MTT-23, pp. 486-492, June 1975.
[50] T. G. Bryant and J. A. Weiss, "Parameters of Microstrip Transmission Lines and of Coupled Pairs of Microstrip Lines," IEEE Transactions on Microwave Theory and Techniques, December 1968.
[51] T. C. Edwards, *Foundations for Microstrip Circuit Design*. J. Wiley, 1981, p. 133.
[52] S. Akhtarzad, T. Rowbotham and P. Johns, "The Design of Coupled Microstrip Lines," IEEE Transactions on Microwave Theory and Techniques, vol. MTT-23, pp. 486-492, June 1975.
[53] T. C. Edwards, *Foundations for Microstrip Circuit Design*. J. Wiley, 1981, p. 138.
[54] David M. Pozar, *Microwave Engineering*. Addison-Wesley Publishing Company, 1990, pp. 183-186.
[55] Pozar, p. 513.
[56] Pozar, pp. 514-514
[57] Pozar, pp. 411-415.
[58] Pozar, p. 412.
[59] Pozar, p. 413.
[60] C. A. Balanis, *Antenna Theory, Analysis and Design*. J. Wiley and Sons, 1997, pp. 722-735.
[61] Balanis, p. 724.
[62] Balanis, p. 731.
[63] Balanis, pp. 731-734.
[64] Balanis, p. 735.
[65] Balanis, p. 734.
[66] Balanis, p. 735.
[67] Balanis, p. 729.
[68] Balanis, pp. 729-730.